Parameter identification of a vessel response model using onboard measurement data and nowcast wave spectra

Jasmijn de Jong

Master of Science Thesis
Offshore & Dredging Engineering

Parameter identification of a vessel response model using onboard measurement data and nowcast wave spectra

by

Jasmijn de Jong
4457587

Graduation Committee:

Dr. -Ing. Sebastian Schreier	Chair
Dr. Ir. Peter Naaijen	Daily supervisor
Ir. Mark Paalvast	Company supervisor

Delft University of Technology

Abstract

Operational optimization of vessels is valuable for the planning and execution of maritime operations. Accurate and efficient models to predict vessel motions are needed to make reliable operational decisions. The wave-induced vessel response can be modelled in terms of a Response Amplitude Operator (RAO) and a wave spectrum. Uncertainties related to the parameters that govern the RAO can significantly influence the reliability of the vessel motion prediction. To decrease these uncertainties, the maritime sector has realized the potential of using vessel motion measurements. As a result, it is envisioned that a vessel response model might include an identification module that searches for model parameters using measurements of responses to make a reliable prediction.

This study presents an identification procedure to handle the inherent uncertainties of vessel model parameters, aiming to improve vessel motion prediction. The identification procedure identifies the vessel's RAO by the measured response spectrum and now-cast wave spectrum, with the goal of finding the heave and roll natural frequencies. The natural frequencies provide information on the vessel's parameters. This is used to identify the parameters related to the mass distribution and damping of the vessel. These were found by minimizing a cost function, that quantified the difference between the measured and predicted response spectrum, using an optimization method. Identifiability analyses of the parameters were performed on two case studies.

For the first case study, a synthetic data set is created with the vessel response model to simulate the vessel motions. Tests were conducted with five different wave spectra and several vessel headings, constituting diversified scenarios. The RAO was identified by the measured response, the wave spectrum, and a sinusoidal function to describe the directional dependency of the RAO. Using the synthetic data set, the identification algorithm successfully identified the parameters with good agreement to their actual values.
The second case study involved the examination of parameter identification on real on-board vessel motion measurements. In most of the cases, the RAO could be identified from the measurements and the natural heave and roll frequency was found. The identified parameters resulted from the identification procedure and improved the vessel motion prediction compared to the initial prediction, but still, deviations remained. The identified parameters are verified against a different measured data set. The results show that the identified response spectra approach the measured responses, indicating that the identified parameters are reusable.

In summary, it was found that the parameters have a great influence on the output of the vessel response model. Therefore, it is essential to have a thorough understanding of the correct operational parameters for accurate motion prediction. The established identification procedure shows to be a good addition to existing vessel motion models to identify input parameters at relatively low computational cost.

Preface

Before you lies the thesis "Parameter identification of a vessel response model using onboard measurement data and nowacst wave spectra". This is the result of the 10 month graduation internship at MO4 as part of my master program Offshore Dredging Engineering at the TU Delft. With my graduation, an end has come to my student career which started in 2015 at the Mechanical Engineering faculty.

First of all, I would like to thank my colleagues at MO4 who helped me throughout my research and made it what it is today. From the first day, I felt welcomed and a member of the team. Without hesitation, I could approach anyone with burning questions on hydromechanics or Matlab. Every day, I went to work with great pleasure and excited to conduct my research, while secretly looking forward to the ping pong games during lunch break and drinks after work at the Wetering. Thanks Mark, my company supervisor, I could not have achieved this without your spiritual leadership and deep understanding of vessel motion dynamics. The freedom you gave me to frame my own research and support when I coped with difficulties were very valuable for me. And as chief happiness officer, I hope I ignited a spark to the MO4 team as well. Additionally, I want to thank Sjoerd, Joël and Olivier, the other (former) graduates at MO4 and Mocean. Our brainstorming sessions during lunchbreaks or boulder activities were not only useful but fun as well.

Secondly, I would like to thank Peter Naaijen, my daily supervisor and Sebastian Schreier, the chair of the committee. I am grateful for your willingness to be part of my thesis committee and the guidance with an academic point of view. Thank you for your patience during the progress meetings, the critical questions asked and the time you took to review my progress work. All the guidance has ensured that I gained new experiences in the research field.

And to the reader: I hope you enjoy your reading!

Jasmijn de Jong
Amsterdam, September 2022

Contents

List of Figures

List of Tables

NOMENCLATURE

Acronyms

CoF	Center of Floatation
CoG	Center of gravity
CTV	Crew Transfer Vessel
DDS	Decision Support System
DOF	Degree of freedom
EoM	Equation of Motion
KB	Center of Buoyancy
KG	Vertical coordinate of center of gravity
RAO	Response Amplitude Operator
SOV	Service Operation Vessel

Greek Symbols

θ	Direction
ζ_{a_n}	Wave amplitude
∇	Displacement
ω	Frequency
ρ	Density

Roman Symbols

A_{WL}	Waterplane area
B_{crit}	Critical damping term
B_{visc}	Viscous damping term
BM_l	Longitudinal metacentric radius
BM_t	Transversal metacentric radius
C_b	Block coefficient

C_w	Waterplane area coefficient
g	Gravitational acceleration constant
GM_l	Longitudinal metacentric height
GM_t	Transverse metacentric height
H_s	Significant wave height
H_{max}	Maximum wave height
I_l	Longitudinal moment of inertia
I_t	Transverse moment of inertia
I_{ii}	Moment of inertia
r_{ii}	Radii of inertia
T_p	Peak wave period

1

INTRODUCTION

In recent decades, the energy sector has seen significant development. In terms of installed capacity, offshore wind is rapidly growing, whereas the installation of new oil and gas facilities is decreasing. This shift impacts the type and duration of maritime activities that have to be carried out [20]. Such activities include transport to a wind farm location by transport vessels, installation by installation vessels, cable laying and trenching of the cables into the seabed by cable lay vessels and lastly, crew transfers for maintenance by Service Operation Vessels (SOV's) or Crew Transfer Vessels (CTV's). These offshore activities are performed by vessels that are costly in operation. Besides, in the future, wind farms will be located further offshore where rough weather and greater distances from shore make the turbines more difficult and expensive to access [38], [5]. Additionally, operational optimization of vessels is becoming highly important due to rising fuel costs and increased environmental constraints [36]. As a result, it is essential to reduce costs through efficient use of vessel fleets and maximum utilization of good weather periods to make offshore wind a competitive alternative [19]. This can be accomplished by introducing a digital twin during the decision-making process, which is a combination of using measured data and a model of the real physical asset [22]. Generally, this is a low-cost analysis to predict vessel behavior during operations based on knowledge of the environmental conditions.

This chapter covers the relevant background information to provide an understanding of critical topics discussed in this research. First, the state-of-the-art in defining operative limits of vessels will be discussed, followed by new applications and developments in the maritime industry. Finally, an overview of the complications surrounding the developments of digitization in the maritime industry will introduce the research gaps and consequential research questions.

1

1.1. RESEARCH BACKGROUND

1.1.1. VESSEL MOTION FORECASTING

Operative limits of vessels are currently defined in terms of maximum allowable metocean conditions. According to the definition of Det Norske Veritas (DNV) [10], maritime operations can be classified as either weather-restricted or weather-unrestricted, depending on the duration of the operation. Maritime operations with a duration less than 72 hours are typically defined as weather-restricted operations. Planning for these type of operations is made in terms of the workable weather window, known as workability. The workable weather window represents the duration of which the forecast sea states, typically characterized by the significant wave height (H_s) and peak period (T_p), are lower than the allowable sea states for an operation. This indicates that an operation can be executed safely and is generally referred to as *significant wave height limit* or H_s-*limit*.

Following the dynamic developments in the digital industry, the maritime industry is preparing for a future where the decision-making process of operations no longer requires the H_s-*limit*. The workability evaluation is gradually shifting to a more vessel-specific "motion limit" [12]. This is conceivable if a correlation between the considered vessel motion and the induced structural loads on the vessel can be established. The motion limit is obtained by determining a limiting motion (displacement, velocity, or acceleration) at a specific location on the vessel. A vessel motion prediction model can evaluate whether the established motion limit will be exceeded during operations based on expected environmental conditions.

This alternative method is believed to reduce risk and extend operational windows [30]. The decision to execute or postpone the operation can then be based on the predicted critical response instead of the forecast environmental parameters, H_s and T_p. Response prediction or forecasting of various sorts has been provided to numerous maritime operations since the 1980s [1]. The method proves to perform well, as the source of the wave predictions is a two-dimensional spectrum describing the sea-surface elevation as a function of frequency and propagation direction. A two-dimensional spectrum represents the real sea conditions generally better than a theoretical sea state. A theoretical sea state is usually a single peak spectrum which poorly represents wind sea and swell components and directional dispersion [9], [12]. Therefore, the motions computed with a two-dimensional spectrum induce a different motion of the vessel than those estimated during the design for a theoretical sea state with the same H_s, T_p and incoming direction [12].

1.1.2. SUPPORT BY VESSEL MOTION MEASUREMENTS

A successful decision support system (DSS) for operation optimization normally requires accurate vessel motion prediction. For decades, this has attracted a strong research interest. On the other hand, in recent years, vessels and offshore structures have been equipped with several types of sensors. These have increased the data available in the maritime sector and motivate decision-making through both vessel response modelling and measurement data. Measurement data with acceptable quality could be used to reduce the uncertainties of the response prediction.

Vessel response predictions are commonly subjected to two sources of error: error in the input of the metocean conditions or errors related to the vessel response model. Weather forecasts are usually fed into a model to obtain a vessel response prediction. Consequently, accurate weather forecasts can increase the reliability of the prediction. Therefore, research into weather forecast uncertainty has been studied widely [42], [4]. Determining how to evaluate weather forecast uncertainty and how to account for it when planning and conducting maritime activities has become a crucial subject of maritime industry [55].

From the point of view of maritime operations, one must accept the accuracy of the existing metocean prediction models, and focus on making the second source of error, the vessel response model, as correct as possible [30]. Thus, besides the weather forecast uncertainty, it is equally important to quantify and reduce the uncertainties associated with the vessel response model. The common approach to model wave-induced ship motions involves applying physical principles and results from model and full-scale experiments [36]. This is referred to as white-box modelling. Another approach to model ship dynamics is to use a black-box method. A black-box model is a mathematical model describing relations between input and output data for a given process or a system. For a ship motion model, the input is related to the metocean conditions and the output to the (measured) vessel response. The relations between input and output data are modelled and based only on experimental data to predict the vessel's behavior. This method does not require any prior knowledge about the system. The main disadvantage of the black-box modelling method is the high dependence on the data used to model the process.

Generally, vessel motion prediction models are white box models. Those models require knowledge of the characteristics or parameters of the vessel. It has been shown that uncertainties related to the parameters of the model can significantly influence the output of the model [21]. Thereby, these parameters are difficult to uniquely estimate for a ship under normal operational conditions without special experiments or equipment [37]. Therefore, applying a grey-box method to improve ship motion predictions has attracted research interest. The grey-box method is a combination of using detailed knowledge of the physics of the system to set up the initial problem and then using data to learn the remaining parameters or to update previous parameters. This method aims to incorporate the effects of physical phenomena which has been neglected in the white-box model using data from the system. This form of parameter identification has been studied widely and researchers addressed various challenges, which were discussed in the supporting literature review. This introduced the research gaps discussed in next Section.

1.2. Research gaps

To identify the primary gaps in existing parameter identification methods of vessel motion models, a thorough literature review was conducted. The most relevant contributors were covered, what consequently led to the research gaps discussed in this section. These research gaps will form the foundation of this study.

In short, current parameter identification algorithms are still at an early developing stage with many identified challenges towards industrial applications. Challenges for a robust parameter identification algorithm are:

- An algorithm should be developed that is not time-consuming and computationally inexpensive to make it attractive to use for the industry.
- All degrees of freedom of the vessel response should be included.
- The algorithm should be applicable to multiple vessels.

CHANGE OF LOADING CONDITION

In the long-term, vessel characteristics such as inertia distribution and even geometry are time-variant. During many critical maritime activities, such as heavy lifting and pipe laying, vessel loading conditions can change rapidly. As a result, the identified vessel's parameters based on available data prior to such procedures may not be adequate for direct application. It should be studied how to modify and predict vessel parameters for operations where the loading condition changes, resulting in an increase in the response prediction accuracy [21].

TYPE OF DATA USED FOR IDENTIFICATION

The most critical research gap and the one which will be the focus of this research is about considering the type of data used for identification. For the development of an algorithm, it is important to consider what data is usually available. Some studies showed good results when measurements of wave elevation were available or simulated. However, in real application, the instant elevations of waves are not always available onboard, which consequently limits the assessment of environmental loads. Wave spectra provided by weather forecast suppliers are easier to assess. Therefore a method has to be developed in which wave spectra, excluding information about phasing, is suitable for the identification process. For simplification, previous studies assumed a single peak Pierson-Moskowitz wave spectrum as input for the system [22], [23]. However, this does not accurately reflect the real sea conditions in terms of directional spreading and spectral form. Therefore, to realistically assess the real conditions, application of a two dimensional, multi-peak wave spectrum consisting of both wind sea and swell components might be needed. To make a realistic assessment, it was recommended to investigate many different sea states with different wave directions [51].

Besides the metocean input for the parameter identification, one should pay attention to the output of the system. Only few studies have used real onboard measurements as the output of the system, which are the wave-induced vessel motions [54]. Most studies only tested their parameter identification strategies on synthetic response data generated through computer programs [8], [48], [51], [22]. Therefore, it has to be studied whether an identification strategy can be developed which is applicable for real onboard measurements.

1.3. RESEARCH OBJECTIVES AND METHODOLOGY

As discussed earlier, it is envisioned that a digital twin system for decision support, might include an identification module that searches for model parameters using onboard vessel measurements of response. Hence, this research aims to reduce the uncertainty in vessel motion predictions. The main research objective of this thesis is summarized into the following:

> **Develop a parameter identification strategy to improve vessel motion predictions using nowcast wave spectra and onboard measurement data.**

1.3.1. RESEARCH QUESTIONS

A series of sub-questions is formed in order to frame the research and to get at the key objective:

1. Which parameter identification algorithm can be used to detect the correct values of the parameters of a vessel response model?
2. Do the identified parameters improve the predicted ship motion compared to the initial model output?
3. Is the parameter identification algorithm stable, robust, and applicable for real onboard motion measurements?

1.3.2. RESEARCH STRATEGY AND THESIS OUTLINE

This section provides the research strategy of this study and outlines which steps are taken to answer the research questions and to obtain the research objective. The strategy is comprised of various steps that are presented in a flowchart in Figure 1.1. Parameter identification is an iterative process where it is often necessary to go back and repeat earlier steps. This is illustrated with arrows in Figure 1.1. This section outlines the chapters in which the steps of the flowchart are discussed:

- **Step 1: Objective**
  The main focus of the research lies on the development of a parameter identification strategy that improves the predictions a vessel motion response model. The research objective is highlighted in the present chapter.

- **Step 2: Model**
  Next, the necessary background that is related to the calculation of the wave-induced vessel response is discussed in Chapter 2. This theory forms the background of the model to which the parameter identification will be applied to. Furthermore, Chapter 2 introduces the concept of parameter identification.

- **Step 3 and 4: Data gathering and examination**
  Step 3 is presented in Chapter 3 which elaborates on the various data sources that are available for this research. This includes metocean forecasts, vessel motion predictions and vessel motion measurements. The available data are evaluated based on a predetermined set of criteria in order to be suitable for identification, which is also discussed in Chapter 3.

1

- **Step 5: Parameter discussion**
  Step 5 discusses the parameters of the vessel response model, which will be identified in this research. It is indicated how the values of the parameters are currently obtained and how they are related to each other. The parameter discussion is covered in Chapter 4.

- **Step 6: Parameter identification selection**
  Next, the Chapters 5 and 6 elaborate on how the knowledge of the previous steps can be incorporated into the development of a suitable parameter identification procedure, which searches for the correct parameter values of the vessel response model.

- **Step 7: Parameter identification implementation**
  The implementation of the parameter identification according to two case studies will be covered in Chapters 7 and 8. Additionally, the results of case studies will be verified.

The goal of the identification procedure is an improved model with the identified parameters. In Chapter 9, the findings are discussed and conclusions are drawn that contribute to the answers of the research questions. Finally, recommendations for further research are provided.

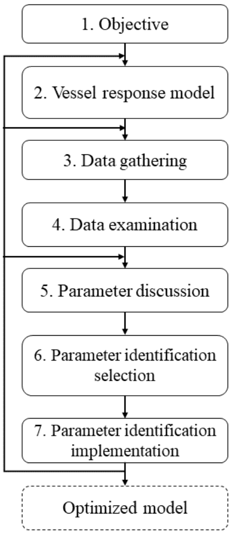

Figure 1.1: Research strategy

2

THEORETICAL BACKGROUND

2.1. INTRODUCTION

This chapter provides a brief overview of the theoretical background. As this research combines the fields of ship hydrodynamics and system identification, information of both are presented.

2.2. BACKGROUND SHIP MOTIONS

This Section seeks to give the essential background knowledge for frequency-domain analysis of the wave-induced vessel response and outlines the crucial input parameters to obtain the vessel motion response.

2.2.1. FREQUENCY DOMAIN ANALYSIS

Vessel motions can be analyzed in the time-domain or the frequency-domain [17]. It is assumed that vessel responses mainly have a linear behaviour to the sea state [47]. Therefore, it is acceptable to simplify the relation between wave elevation and the rigid body vessel motions by linearization of a transfer functions in the frequency domain [11]. Thus, if the wave spectrum is known, it is possible to calculate the vessel response spectrum. How the the vessel responses are evaluated in the frequency domain, is discussed in the following section.

2.2.2. WAVE ENERGY SPECTRUM

An irregular wave can be seen as the superposition of a series of sinusoidal waves. The wave elevation $\zeta(t)$ of a long-crested irregular sea, propagating along the positive x-axis, can be written as the sum of a large number of regular wave components, shown in Equation 2.1 [29].

$$\zeta(t) = \sum_{n=1}^{N} \zeta_{a_n} \cos(\omega_n t - \varepsilon_n) \tag{2.1}$$

2

in which, for each wave component n:

$$\begin{aligned} t &= \text{time} \\ N &= \text{number of components} \\ \zeta_{a_n} &= \text{wave amplitude (m)} \\ \omega_n &= \text{circular frequency (rad/s)} \\ \varepsilon_n &= \text{random phase angle (rad)} \end{aligned}$$

The variance in the amplitudes of these harmonic components is distributed throughout a frequency band to generate a wave spectrum, as shown in Figure 2.1. The wave spectrum is determined to describe the surface elevation of ocean waves and represents the irregular waves travelling across the ocean. The expression of Equation 2.1, a sum of a large number of harmonic wave components with variable periods, directions, amplitudes, and phases can be used to depict these irregular waves. The wave amplitude ζ_{a_n} can be expressed in a wave energy density spectrum $S_\zeta(\omega,\theta)$ with frequency component ω and direction component θ. This expression is defined by Equation 2.2.

$$S_\zeta(\omega,\theta)d\omega = \frac{1}{2}\zeta_{an}^2(\omega,\theta) \tag{2.2}$$

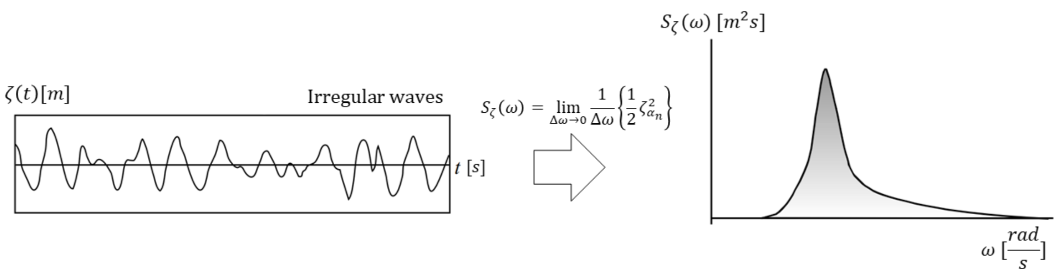

Figure 2.1: Surface elevation to wave spectrum, [29]

Figure 2.1 shows the conversion from the surface elevation as a function of time into the one-dimensional (1D) wave energy spectrum. However, waves travel towards the vessel from different directions, 1D wave spectrum does not cover this. By adding wave directionality, one obtains a 2D wave spectrum as shown in Figure 2.2.

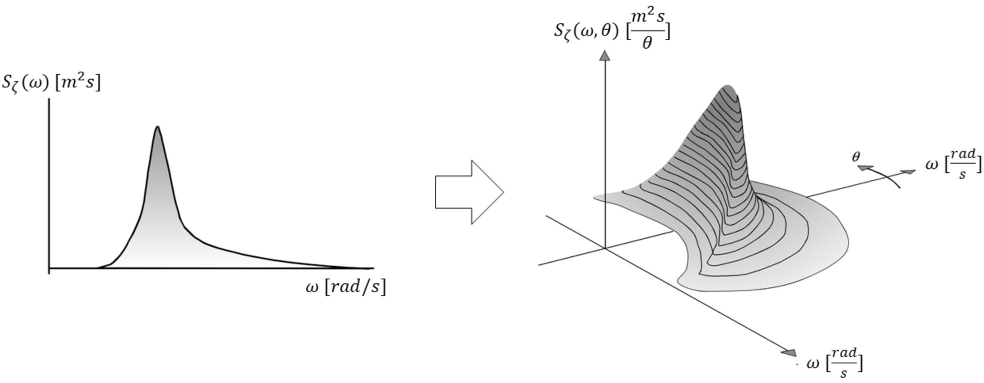

Figure 2.2: Directional wave spectrum, [29]

2.2.3. EQUATION OF MOTION

Vessels can experience motions that are defined by the six Degrees Of Freedom (DOF) shown in Figure 2.3. The six motion components are indicated as follows [29]:

- surge x: translation along the x-axis, positive in the positive x-direction
- sway y: translation along the y-axis, positive in the positive y-direction
- heave z: translation along the z-axis, positive in the positive z-direction
- roll ϕ : rotation around the x-axis, positive with starboard down
- pitch ϑ: rotation around the y-axis, positive with bow down
- yaw ψ: rotation around the z-axis, positive with bow to port

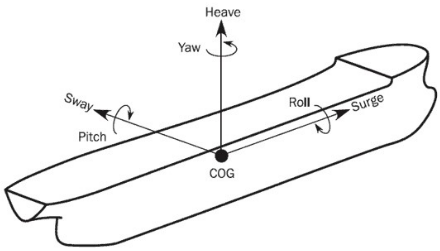

Figure 2.3: Notations and sign conventions for six DOF vessel motions

The vessel's motion response to incoming waves is determined by solving a set of differential equations, known as the "equation of motion" or EoM. The EoM for a vessel in six degrees of freedom where i,j = $\{x, y, z, \phi, \vartheta, \psi\}$, is shown in Equation 2.3.

$$\left((\mathbf{M}_{ij} + \mathbf{A}_{ij}(\omega))\ddot{\vec{\eta}}_j + \mathbf{B}_{ij}(\omega)\dot{\vec{\eta}}_j + \mathbf{C}_{ij}\vec{\eta}_j\right) e^{-i\omega t} = \mathbf{F}_i^{FK} e^{-i\omega t} + \mathbf{F}_i^{D} e^{-i\omega t} \tag{2.3}$$

2

in which:

$\ddot{\vec{\eta}}_j$	= translational (or rotational) acceleration vector
$\dot{\vec{\eta}}_j$	= translational (or rotational) velocity vector
$\vec{\eta}_j$	= translational (or rotational) displacement vector
$\mathbf{M}_{ij}$	= solid mass matrix
$\mathbf{A}_{ij}$	= hydrodynamic added mass matrix
$\mathbf{B}_{ij}$	= hydrodynamic damping matrix
$\mathbf{C}_{ij}$	= stiffness matrix
$\mathbf{F}_i^{FK}$	= Froude-Krylov forces or moments
$\mathbf{F}_i^{D}$	= diffraction forces or moments
ω	= frequency

The index pair i, j identifies the force contribution in direction i due to the motion of the system in direction j.

2.2.4. RESPONSE AMPLITUDE OPERATOR

The wave-induced vessel response can be modelled in terms of a Response Amplitude Operator (RAO) and a wave spectrum. The RAO acts as a transfer function between a wave spectrum and a vessel response spectrum and describes the linear relation between the input and the output [53]. The RAO is a function of both frequency and heading but also depends on a range of other factors including hull shape, loading condition and mooring or DP interaction. Equation 2.3 can be solved by finding the RAO for each degree of freedom of the vessel by superimposing η and the wave-loads. On the right-hand side of Equation 2.3, one finds the system's input being the wave-loads. The excitation load of a wave can be expressed as a linear relation between the wave amplitude, ζ_a, and the complex-valued transfer function for the excitation loads, $\hat{X}_a(\omega,\theta)$ [13]. This expression is shown in Equation 2.4.

$$\mathbf{F}_i e^{-i\omega t} = \zeta_a \hat{X}_a(\omega,\theta) e^{-i\omega t} \tag{2.4}$$

The complex notation of the body motions is introduced by:

$$\eta = \hat{\eta}_a e^{-i\omega t} \tag{2.5}$$

Substituting the Equations 2.4 and 2.5 into Equation 2.3 gives the solution of the EoM:

$$\left(-\omega^2(\mathbf{M}_{ij} + \mathbf{A}_{ij}(\omega)) + i\omega\mathbf{B}_{ij}(\omega) + \mathbf{C}_{ij}\right)\hat{\eta}_a = \zeta_a(\widehat{X}_a^{FK}(\omega,\theta) + \widehat{X}_a^{D}(\omega,\theta)) \tag{2.6}$$

Subsequently, dividing by ζ_a, the RAO is found and defined in Equation 2.7.

$$\mathrm{RAO}(\omega,\theta) = \left|\frac{\widehat{\eta}_a}{\zeta_a}\right| = \frac{\widehat{X}_a^{FK}(\omega,\theta) + \widehat{X}_a^{D}(\omega,\theta)}{-\omega^2(\mathbf{M}_{ij} + \mathbf{A}_{ij}(\omega)) + i\omega\mathbf{B}_{ij}(\omega) + \mathbf{C}_{ij}} \tag{2.7}$$

The RAO is a complex function in which the amplitude denotes the motion amplitude per unit wave amplitude and the phase of the RAO indicates the phase difference between the vessel motions and the waves.

2.2.5. WAVE-INDUCED VESSEL RESPONSE

Under the assumption of linear theory and stationary conditions, the wave-induced vessel response spectrum can be modelled in terms of a RAO and a wave spectrum. The steady-state responses induced by the wave system are given in Equation 2.8.

$$S_r(\omega,\theta) = |RAO(\omega,\theta)|^2 \cdot S_\zeta(\omega,\theta) \tag{2.8}$$

Where $S_\zeta(\omega,\theta)$ is the sea state energy density defined in Equation 2.2.

SPECTRAL RESPONSE MOMENT

Statistical relationships can be determined by computing the moments of the area under the spectrum [29]. For the spectral response moment m, the n^{th} order moment is given by Equation 2.9.

$$m_n = \int_0^{2\pi}\int_0^{\infty} \omega^n \cdot |RAO(\omega,\theta)|^2 \cdot S_\zeta(\omega,\theta) \cdot d\omega \cdot d\theta \tag{2.9}$$

This means that the m_0 is the area under the spectral curve. The significant displacement, velocity and acceleration $(x_{sig}, \dot{x}_{sig}, \ddot{x}_{sig})$ of a vessel can be derived according to:

$$x_{sig} = 2 \cdot \sqrt{m_0}, \qquad \dot{x}_{sig} = 2 \cdot \sqrt{m_2} \qquad \ddot{x}_{sig} = 2 \cdot \sqrt{m_4} \tag{2.10}$$

2.2.6. INPUT PARAMETERS

Several parameters govern the vessel response in terms of the RAO, which are the wave frequency (ω), the degree of freedom, the mass matrix (**M**), the added mass matrix (**A**), the damping matrix (**B**), the stiffness matrix (**C**) and the wave excitation forces (**F**). Usually, a diffraction-radiation analysis software tool can be used to compute the first-order wave exciting loads, added mass and radiation damping [35]. Here, it is assumed that the exact hull shape and draft are known. ANSYS AQWA is such a software analysis service which is an industry-grade tool that has been widely accepted over the past decades [40]. The definition of each matrix of the RAO will be discussed next.

- **M**; the mass matrix is defined by:

$$\mathbf{M} = \begin{bmatrix} \rho\nabla & 0 & 0 & 0 & 0 & 0 \\ 0 & \rho\nabla & 0 & 0 & 0 & 0 \\ 0 & 0 & \rho\nabla & 0 & 0 & 0 \\ 0 & 0 & 0 & I_{xx} & 0 & 0 \\ 0 & 0 & 0 & 0 & I_{yy} & 0 \\ 0 & 0 & 0 & 0 & 0 & I_{zz} \end{bmatrix} \tag{2.11}$$

  In Equation 2.11, ∇ denotes the displacement of the vessel, ρ denotes the water density and I_{ii} denote the moments of inertia. The mass matrix is a diagonal matrix since the off-diagonal terms, which represent inertial couplings within the system, are assumed to be relative small and therefore neglected [29]. The coupling terms are small if the center of gravity of the vessel aligns close to the body-fixed coordinate system. Additionally, the chosen axis system needs to be the main axis system, which is defined by coupling terms in the moments of inertia to vanish.

Displacement is a function of hull geometry and draft. Varying displacement will change the draft and could consequently change trim. Trim is the angle by which a vessel tilts relative to its baseline. If the waterline is not parallel to the vessel's baseline, the vessel trims. The trim is dependent on the vessel's loading condition.

Inertia is the quality of motion that causes a ship to resist a change in motion [25]. The moments of inertia are defined by the mass distribution of the vessel and not affected by the sea state or other external forces. The radii of inertia are derived from the moments of inertia by Equation 2.12:

$$r_{ii}^2 = \frac{I_{ii}}{\rho \nabla} \tag{2.12}$$

- $\mathbf{A}(\omega)$; the hydrodynamic added mass matrix is defined by:

$$\mathbf{A}(\omega) = \begin{bmatrix} a_{11}(\omega) & 0 & a_{13}(\omega) & 0 & a_{15}(\omega) & 0 \\ 0 & a_{22}(\omega) & 0 & a_{24}(\omega) & 0 & a_{26}(\omega) \\ a_{31}(\omega) & 0 & a_{33}(\omega) & 0 & a_{35}(\omega) & 0 \\ 0 & a_{42}(\omega) & 0 & a_{44}(\omega) & 0 & a_{46}(\omega) \\ a_{51}(\omega) & 0 & a_{53}(\omega) & 0 & a_{55}(\omega) & 0 \\ 0 & a_{62}(\omega) & 0 & a_{64}(\omega) & 0 & a_{66}(\omega) \end{bmatrix} \tag{2.13}$$

In Equation 2.13, $a_{ij}(\omega)$ denote the added mass terms for the force contribution in direction i due to the motion of the vessel in direction j. The added mass matrix is half-filled with zeros because the force-motion contribution in those directions is not coupled. This decoupling holds for vessels that are symmetric on port-starboard (i.e., the xy-plane). If this applies, the heave and pitch motions induce no transversal force due to the symmetry of the vessel [49]. This is similar for the longitudinal motions caused by an acceleration in direction $j = 2,4,6$. This study considers vessels that are symmetric on port-starboard and thus, for a vessel moving in six DOF, the added mass matrix consists of 18 components.

- $\mathbf{B}(\omega)$; the damping matrix defined is by:

$$\mathbf{B}(\omega) = \begin{bmatrix} b_{11}(\omega) & 0 & b_{13}(\omega) & 0 & b_{15}(\omega) & 0 \\ 0 & b_{22}(\omega) & 0 & b_{24}(\omega) & 0 & b_{26}(\omega) \\ b_{31}(\omega) & 0 & b_{33}(\omega) & 0 & b_{35}(\omega) & 0 \\ 0 & b_{42}(\omega) & 0 & b_{44}(\omega) & 0 & b_{46}(\omega) \\ b_{51}(\omega) & 0 & b_{53}(\omega) & 0 & b_{55}(\omega) & 0 \\ 0 & b_{62}(\omega & 0 & b_{64}(\omega & 0 & b_{66}(\omega) \end{bmatrix} \tag{2.14}$$

In Equation 2.14, $b_{ij}(\omega)$ denote the damping terms for the force contribution in direction i due to the motion of the vessel in direction j. In computing the damping matrix, diffraction programs make use of potential theory, which operates under the assumption that a fluid is ideal. This implies that the flow is expected to be nonrotational, incompressible, and inviscid. Therefore, the diffraction program only considers radiation damping terms and excludes viscous damping. Particularly for the roll motion, viscous damping might substantially be dominant in comparison to the potential damping component and therefore must be incorporated. This is because the critical roll motion near resonance might be extremely influenced by the estimated damping which could be significantly underestimated by the linear potential theory [23]. Therefore, additional viscous damping is added to include quadratic damping coefficients. The following Section describes how this is determined.

VISCOUS ROLL DAMPING

The viscous roll damping per sea state can be determined by stochastic linearization, so that the roll motion transfer function can represent a linear behavior. This method of linearization takes into account the response of the vessel in an irregular sea state.

Governing equations

The nonlinear 1DOF equation of motion for the roll motion is considered. The roll motion ϕ excited by some moment M is regarded as:

$$(I+a)\ddot{\phi}+b_1\dot{\phi}+b_2\dot{\phi}|\dot{\phi}|+c\phi=M \tag{2.15}$$

Where I is the ship inertia, a the added mass, b_1 and b_2 denote the linear and nonlinear damping coefficients and the c is the hydrostatic spring term. The damping moment thus is described as follows:

$$M_{damp}=b_1\dot{\phi}+b_2\dot{\phi}|\dot{\phi}| \tag{2.16}$$

In order to incorporate the nonlinear moment in a frequency domain approach, it needs to be linearized to the following form:

$$M_{damp}=(b_1+\hat{b_2}(\phi))\dot{\phi}=b_{eq}(\phi)\dot{\phi} \tag{2.17}$$

Where an equivalent linearized quadratic damping coefficient $\hat{b_2}(\phi)$ is found which can be added to the linear coefficient to find an equivalent damping coefficient (b_{eq}). This linearization needs to be carried out for each specific sea state response as the equivalent damping coefficient is a function of the roll angle.

Stochastic linearization

The integrals of the energy balance represent a time average over a period, or the arithmetic mean of Equation 2.17 is:

$$E[b_{eq}\dot{\phi}^2]=E[b_1\dot{\phi}^2+b_2\dot{\phi}^2|\dot{\phi}|] \tag{2.18}$$

It is generally assumed that the free surface elevation is Gaussian distributed with a zero mean. This means that the wave-induced roll motion can also be assumed

Gaussian with zero mean. Now the equation can be worked out with some general Gaussian moment rules:

For prediction in irregular seas, the stochastic linearization originally described by Kaplan is applied [31]. The result assumes both the input and output to be Gaussian distributed with a zero mean and minimizes the error between the linearized and actual system. This means that the wave-induced roll motion can also be assumed Gaussian with zero mean and therefore, the equivalent damping coefficient becomes:

$$b_{eq} = b_1 + \sqrt{\frac{8}{\pi}\sigma_{\dot{\phi}} b_2} \tag{2.19}$$

Where b_1 is the linear damping, $\sigma_{\dot{\phi}}$ is the root mean square roll velocity. For the other five DOFs, damping is predominantly linear and predicted well with radiation-diffraction analysis [40].

- **C**; the stiffness matrix is defined by:

$$\mathbf{C} = \begin{bmatrix} 0 & 0 & 0 & 0 & 0 & 0 \\ 0 & 0 & 0 & 0 & 0 & 0 \\ 0 & 0 & \rho g A_{\mathrm{WL}} & 0 & -\rho g A_{WL}(CoF - CoB) & 0 \\ 0 & 0 & 0 & \rho g \nabla GM_t & 0 & 0 \\ 0 & 0 & -\rho g A_{WL}(CoF - CoB) & 0 & \rho g \nabla GM_l & 0 \\ 0 & 0 & 0 & 0 & 0 & 0 \end{bmatrix} \tag{2.20}$$

In Equation 2.20, ρ denotes the water density, g denotes the acceleration due to gravity, A_{WL} denotes the vessel's waterplane area, CoF and CoB denote the longitudinal coordinates of the center of floatation and buoyancy and the GM_t and GM_l are the transversal and longitudinal metacentric heights. The terms $C(4,4)$ and $C(5,5)$ give the largest contribution in the stiffness matrix due to its dependence on ∇. Research found that the roll motion can be significantly influenced by GM_t and that GM_l mainly influences the pitch RAO at large wave periods [46]. The determination of the metacentric heights are discussed in more detail in Chapter 4.

- **F**; the wave excitation forces
The wave exciting forces and moments are produced by waves coming in on the restrained structure [29]. The wave excitation forces consist of two components, the Froude-Krylov forces (F_i^{FK}) and the diffraction forces, (F_i^D). The wave force terms are both frequency and heading dependent. These terms are usually computed by diffraction analysis software.

2.2.7. SUMMARY PARAMETERS

The results from the conducted literature review showed that previous research focused on different parameters. Some research focused on the hydrodynamic properties which are frequency dependent, these are the hydrodynamic coefficients of the added mass and radiation damping matrix as well as the wave excitation forces [8],[44],[45],[48]. The identified hydrodynamic parameters approached close to the parameters computed with a diffraction analysis software program, indicating that the program computes accurate hydrodynamic parameters [48]. Other research focused on the operational condition dependent and the permanent parameters, for example the mass terms and stiffness terms [21],[22],[23],[30],[51]. Since the hydrodynamic properties computed by radiation-diffraction software has been widely accepted over the past decades [40], the parameters that govern the vessel motion response model related to inertia distribution and viscous roll damping will be the focus of this research.

2.3. PARAMETER IDENTIFICATION

The fundamental background knowledge of wave-induced vessel motion models and the parameters that govern the vessel response were discussed in previous Section. When putting the vessel response model into practice, a challenge is that not all system parameters are known a priori. Here, parameter identification, a technique that may be used to improve the response model, can play an essential role. Parameter identification uses measurements of the real-world system to determine the unknown parameters. Theoretically, this may be achieved by analyzing data measured at the input and output of the system using parameter identification methods [41].

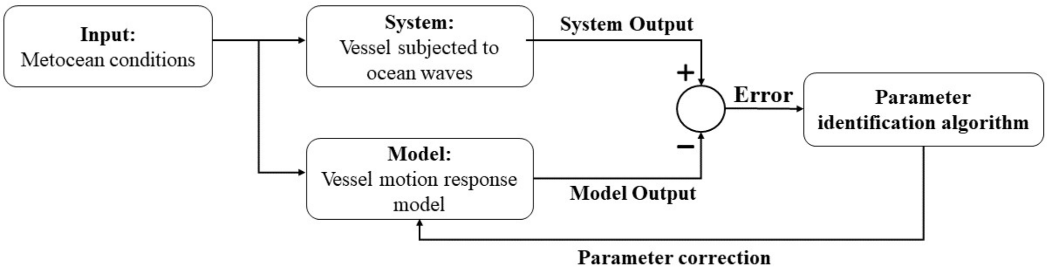

Figure 2.4: Parameter identification scheme

This can be approached by utilizing a parameter identification algorithm, which is schematically visualised in Figure 2.4. The Figure shows that parameter identification can be done using a mathematical model of the real-world system and adapting its parameters. The initial parameter values are estimated, for instance, based on some preliminary knowledge about the real-world system.

Parameter identification involves deducing the parameters of the vessel response model, whose governing equations of motion are known, from the excitation and response time history. For parameter identification of a system governed by Equation 2.8, it is assumed that the wave-induced vessel response are measured and the wave energy spectrum is known through a weather forecast or measurements. The task of parameter identification is to estimate the parameters of Equation 2.7, i.e., the coefficients of the RAO.

2.3.1. OPTIMIZATION

Optimization methods are used to solve parameter estimation procedures. Optimization is a tool to find the combination of inputs to achieve the best possible output subject to satisfying certain specified constraints and conditions. To make use of this tool, a cost function should be identified first, which is a quantitative measure of the performance of the system under study. The cost function $f(x)$ depends on certain characteristics of the system, called variables or parameters x. The cost function $f(x)$, is a function of x that will be minimized or maximized during the optimization process. A constraint function, denoted by c_i, may be applied to the parameters. The optimal set of parameters, x, is defined as the set for which the $f(x)$ is minimum or maximum. In the search for the minimum, repeated runs of $f(x)$ are carried out with systematic changes of the parameter values between the runs until convergence is obtained. In this research, the parameters will be identified through an optimization problem, this process is described in Section 6.4.1.

3

Overview of available data

3.1. Introduction

This chapter will elaborate on the various data sources available for this research. This includes the vessel motion predictions based on a physical model, metocean forecasts and vessel motion measurements. The available data establishes the project's framework and provides an indication of what can be accomplished. In addition, the available data type will be critical while deciding on the parameter identification method. Since this study seeks to combine different sources of data to improve the ship motion predictions.

3.2. Vessel response model

This research was conducted in collaboration with MO4. MO4 is a software company that delivers digital solutions to optimize offshore operations. One of their services is MO4 Forecasting. This is a vessel motion prediction tool that advises on vessel workability for operations in the coming hours or days. A vessel motion response model is set up as part of the MO4 forecasting service and has been running on several vessels. The model translates metocean spectral energy densities, supplied by meteorologists, into ship motions. To accomplish this, it employs physical models based on the theory presented in Chapter 2. Besides, the metocean spectral energy densities, the model requires a vessel specific RAO to compute the ship motions. The RAO is computed with hydrostatic coefficients and hydrodynamic data coefficients generated with ANSYS AQWA. Hydrostatic coefficients are determined based on the input of the vessel owner. Some are estimated (for instance radii of gyration), whilst others are better known from the vessel's stability booklet, for example the metacentric heights.

3.3. Vessel motion measurements

Another service of MO4 is the MO4 Analytics tool. This is a service that measures and visualizes the performance of offshore operations. MO4 outfits vessels with various sensors, one of which is a Motion Reference Unit (MRU) which measures the translational and rotational motions of a vessel. MO4 works with an SBG Ellipse-A MRU, that is often placed near the centre of gravity of the vessel. MO4 is currently looking into the possibility of comparing the quality of the motion predictions with the data of the MO4 Analytics tool. The initial incentive for this study is to investigate various options to use monitored data to improve motion predictions over the long term.

3.3.1. VESSEL

All the analyses in this research were performed with an offshore support vessel (OSV) as a case study. The OSV is the Acta Auriga from Acta Marine and is shown in Figure 3.1. The objective of Acta Marine is to improve the operability prediction of their OSV's in order to reduce the cost of their operations and therefore they use the MO4-system. The Acta Auriga has a length of 93.4 meter and a width of 18 meter.

Figure 3.1: Acta Auriga, [39]

This research will use motions measurements of the Acta Auriga from October and December 2021. The translational accelerations and angular velocities are measured by an MRU at a sample frequency of 40Hz.

3.3.2. REQUIREMENTS IDENTIFICATION DATA

To be suitable for identification data, the measured motion responses had to meet a set of specified requirements. The events meeting those requirements, are called "free-floating" events of the vessel. In this research, we are interested in the natural behaviour of the vessel since for the parameter identification process, the natural frequencies will be determined. Therefore, the identification of stationary and non-stationary behavior is of interest in time series analysis of the measurements. Identification of a free-floating events is done according to a set of established requirements, with the goal of capturing the natural behaviour of the vessel. The requirements for the free-floating events are:

- The vessel should not be connected to anything.
- A change in speed or heading changes the statistics of the steady state condition. Therefore:

  - The vessel should have a forward speed of less than 0.5 m/s.
  - The vessel must maintain a stable heading. The maximum allowable heading change is set at 3 deg.

- All of above described free-floating conditions must be maintained for at least a certain amount of time. The minimum record length is discussed in next section. Based on those calculations, the conditions should be preserved for at least 17 minutes.

3

3.3.3. SPECTRAL ANALYSIS

As discussed in Section 2.2.1, the vessel motions are computed in the frequency domain. An MRU has accelerometers and gyroscopes which has as raw output translation accelerations and rotational velocities of a vessel. All other outputs are post-processed real time and could contain processing errors. Therefore, for the translational motions, the accelerations are assessed and for the rotational motions, the velocities are assessed in this research. This was recommended by MO4 to prevent processing errors and thereby, in the past it was found that natural frequencies are better to observe in this output unit (acceleration for heave and velocity for roll). The necessity of finding natural frequencies will be discussed in Chapter 5. For the spectral analysis, the measured output of the system by the MRUs, which are translational accelerations and angular velocities, has to be transformed to the frequency domain. The MATLAB function fft (fast fourier transform) is used to create a spectrum from the measured time series [7]. fft computes the discrete Fourier transform (DFT) of of the measured signal $y(t)$ using a fast Fourier transform (FFT) algorithm.

The energy response spectrum of a measured signal cannot be directly created by the MATLAB function fft alone. This is because the MATLAB function fft transforms the input to output data in a two-sided spectrum with frequencies ranging from the negative half of the Nyquist frequency to the positive half of the Nyquist frequency. Therefore, to preserve the signal power and noise level, the fast Fourier transforms (FFT) are normalized by dividing each transform by the square root of the length of the original time-domain signal. Besides, to conserve the total power, all frequencies that occur are multiplied by a factor of 2. The derivation of the one-sided spectrum for the output signal y is given as follows:

$$
\begin{gathered}
\mathrm{L} = \mathrm{length(y)} \\
\mathrm{F} = \mathrm{fft(y)} \\
\mathrm{P2} = |\mathrm{F}|_{\overline{L}} \\
\mathrm{P1} = \mathrm{P2(1{:}L/2{+}1)} \\
\mathrm{P1} = 2 \cdot P1.^{2} \\
\mathrm{f} = \mathrm{Fs}^{*}\mathrm{(0{:}L/2)}_{\overline{L}} \\
\mathrm{P1} = \mathrm{P1}_{\overline{f(2)}}
\end{gathered}
$$

where P1 is the power density spectrum for the one-sided Fourier transform of signal y, f is the frequency and Fs is the sampling frequency.

The size of the transform when performing an FFT on a signal is equal to the number of frequency bins that will be created. Each bin represents the amount of energy present in the signal at that frequency. The frequency resolution is the difference in frequency between each bin, which limits the precision of the results [16]. From above described derivation of the one-sided energy spectrum, the frequency resolution can be determined by f(0)-f(1). The number of sampling points can be determined by analyzing the incoming wave frequency. An important point of attention is the required total duration of the measured time histories, to obtain proper spectral shapes and statistical values [29]. A record length equal to 100 times the largest expected single wave period in the irregular waves is often used as a safe standard. This study assessed metocean conditions with a wave period ranging from 4-10 s. The maximum wave period has been used to compute the minimum record length as follows:

$$\max T_p = 10s$$
$$N = \frac{100 * \max T_p}{60}$$
$$N = 16.67 \text{ minutes}$$

Thus, a minimum record length (N) of about 17 minutes is necessary to obtain the response spectrum. With a sample frequency of 40 Hz, the minimum length of the signal y = 40·1760 = 40800 samples. The frequency resolution follows from the number of sampling points. The response spectra of the measurements is smoothed using the MATLAB function smooth [34]. Smoothing is a method of reducing the noise within a data set. The smooth function allows to smooth data using the moving average method. A moving average filter smooths data by replacing each data point with the average of its neighboring data points within the specified span. This method is equivalent to lowpass filtering, with the smoothing response determined by the difference in Equation 3.1:

$$y_s(i) = \frac{1}{2D+i}(y(i+D) + y(i+D-1) + ... + y(i-D)) \tag{3.1}$$

where $y_s(i)$ is the smoothed value for the ith data point, D is the number of neighboring data points on either side of $y_s(i)$, and 2D+1 is the span which is the number of data points for calculating the smoothed value. The span was chosen to be 20, this is a default setting of MO4. This resulted that the frequency resolution of the energy density spectrum increased by a factor 20.

SIGNIFICANT MOTIONS

Besides the spectral analysis of the measured motions, the significant motions of the measurements are computed and can be compared to the predicted significant model by the model. The signification motion of the measurements are obtained by calculating the one-minute standard deviation $\hat{\sigma}_i$ of the measured signal $y_i(t)$. The standard deviation is determined by Equation 3.2.

$$\hat{\sigma}_i = \sqrt{\frac{\sum_{t=1}^{N_t} \left(\hat{y}_i(t) - \overline{y}_i\right)^2}{N_t - 1}} \tag{3.2}$$

$$\overline{y}_i = \frac{\sum_{t=1}^{N_t} \hat{y}_i(t)}{N_t} \tag{3.3}$$

where t denotes the time step for the number of time steps N_t and $\overline{y}_i$ is the sample mean and obtained by Equation 3.3. For the one-minute standard deviation, and a sample rate of 40 Hz, $N_t = 2400$ samples. The measured significant motion can be defined as:

$$x_{sig}^m = 2 \cdot \hat{\sigma}_i \tag{3.4}$$

3.4. WAVE INFORMATION

The MO4 vessel response model uses metocean conditions to evaluate the expected motions of the ship in each heading direction. Wave field data can be collected through forecast, hindcast, visual observation, or instrumental measurements [21]. Ideally, measurements of wave elevation and directions are always available, since this gives the most accurate representation of the sea state. However, to give upfront advise to their clients, MO4 employs weather forecasts as inputs to determine the metocean conditions. This source is always available and easy to access.

The weather forecasts are two-dimensional (2D) for every time step, therefore they provide spectral energy density per direction, and frequency. A disadvantage of utilizing wave spectra and evaluating the motions in the frequency domain, is that no information about the phasing between the waves and the vessel motion is provided. An example of a 2D wave spectrum is given in Figure 3.2. Wind generated waves can be classified into two basic categories: wind and swell seas [29]. Wind-dominated wave regimes tend to have shorter peak wave periods and propagate in different directions, whereas swell-dominated wave regimes tend to have longer peak wave periods and come from one direction. From Figure 3.2, it can also be noticed that the distinction between wind and swell can be captured, as well as directionality. Here wind seas are observed at a peak period around 5 s, where swell seas are observed at a peak period around 10 s. The accuracy of the vessel response model highly depends on the quality of the input 2D wave spectra. However, it is commonly understood that weather forecasts are inherently uncertain. Still, as discussed earlier, the focus of this research will be on making the vessel response model as accurate as possible and thereby trusting the weather forecasts.

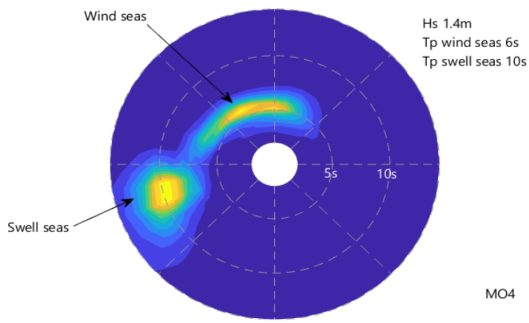

Figure 3.2: Example 2D wave spectral forecast, [40]

3.4.1. METOCEAN DATA SUPPLIERS

MO4 has worked with a variety of data providers in recent years to ensure accurate weather forecasts. In this study, the providers Infoplaza (NL) and DTN (NL) were employed. The weather forecasts are provided with different lead times. The lead time refers to the amount of time between the issuance of the forecast and the occurrence of the forecast. For weather forecasters, there are several global systems available, the most common of which are those from the European Centre for Medium-Range Weather Forecasts (ECMWF). MO4's external forecast providers receive data from sources as ECMWF and conduct their own analyses and interpretations on the results, which are then used to generate weather forecasts.

The Norwegian Meteorological Institute [42] investigated the accuracy of 2D wave spectra generated by the ECMWF at a North Sea location. The buoy and radar data were used to compare and validate the modelled 2D wave spectra. Wave data was gathered for the study over a three-year period, from 2014 to 2016. Furthermore, they have calculated idealized wave spectra by using empirical functions of Pierson-Moskowitz and JONSWAP in order to validate the ECMWF 2D wave spectra. The main findings were that the ECMWF model performs very well, especially in terms of the integrated parameters significant wave height and mean wave period. They also recommend to avoid using idealized spectra, such as JONSWAP or Pierson-Moskowitz, since they are only applicable in certain sea states. For the study, nowcast forecasts were validated, this means weather forecasts from 0 to 6 hours ahead. As a result of this study and in line with previous validation studies of MO4, the nowcast weather forecasts which MO4 receives, performs quite well and therefore will be utilized throughout this research.

3.5. DATA EXAMINATION FRAMEWORK

This section presents how all the previous discussed data is used to serve as input for the parameter identification process. This is depicted in Figure 3.3, showing a structural diagram for parameter identification.

On the left-hand side, the chart starts with system's input being the real metocean conditions to which the system is subjected. The system is a vessel subject to an external force (wave elevation). The vessel's translational and rotational responses are measured and processed. The processed measurements are measured energy response spectrum ($S^m_{r,i}$) for each degree of freedom i, discussed in Section 3.3.

On the right-hand side, the first block is the model's input which is a 2D wave spectrum representing the preassumed weather forecast, discussed in Section 3.4. The model output is a prediction of the response spectrum (S^p_r), based on the incoming weather forecast and the RAO (Section 3.2). The output error is the difference between the measured and predicted energy response spectra (S^m_r and S^p_r, respectively). This output error is used for parameter estimation, where parameters of the RAO are estimated by fitting the available measured data set with the goal of decreasing the output error. This is done by combining knowledge of the physics of the system to set up the initial prediction and then using data to learn the remaining parameters or to update previous parameters. The identified parameters are put back into the RAOs and the process repeats again, as shown in the diagram. Characteristics of the identification parameters will be discussed in next Chapter 4 and the parameter identification process will be explained in Chapter 6.

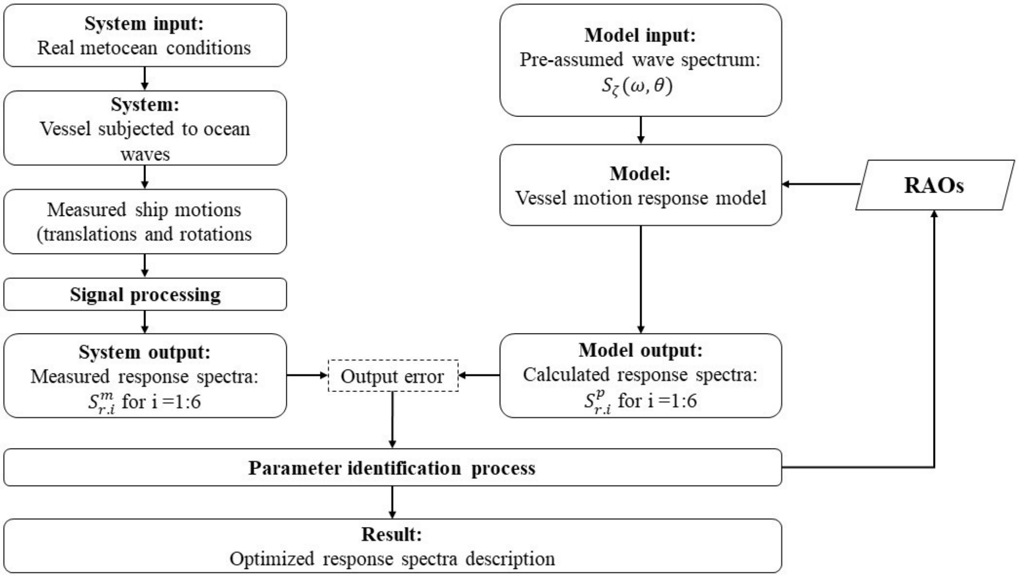

Figure 3.3: The structural diagram for parameter identification

4

Discussion of the parameters

4.1. Introduction

In this chapter, the identification parameters and other input parameters of the vessel response model are discussed. Chapter 2 showed that the vessel motion response model is a comprehensive numeric model and has a large number of parameters. The parameters that govern the vessel motion response model related to inertia distribution and viscous roll damping will be the identification parameters of this research. First, this chapter indicates how the values are currently obtained and how they relate to one another. Then, an attempt will be made to assign a lower and an upper limit for each parameter. This is required to avoid unrealistic parameter values during the identification process. The limits should reflect a reasonable and realistic uncertainty of the parameter values. The limits are based on preliminary knowledge of the origin of the parameters. Next, it is indicated which parameters affects which degrees of freedom by using the equation of the RAO (Equation 2.7). In addition to the identification parameters, this chapter will discuss other input parameters that are used to compute the output of the model, which are the waterplane area and added mass coefficients.

4.2. Identification parameters

The following section will discuss the identification parameters of *displacement*, *radii of inertia terms*, *metacentric heights* and *viscous roll damping*.

4.2.1. Displacement

The displacement is often obtained from the stability booklet of the vessel. The booklet offers detailed documentation of the loading conditions of the vessel. One can imagine that the vessel's mass varies a lot during the several phases of operation, for example during cable laying or as a result of the combustion of fuel. The varying mass will change the displacement, and consequently change the waterline and wet body surface. The stability booklets of the vessels offer a wide range of possible loading conditions and therefore possible values for the displacement with a corresponding draft. Hence, the uncertainty range for the displacement can be obtained from the stability booklet. For this study, the stability booklet of the Acta Auriga was available, and utilized to determine this range [24]. From the stability booklet, it was obtained that the displacement ranges from 5574 tonnes to 6986 tonnes. This means an uncertainty range of 11% with a mean of 6261 tonnes. Additionally, the stability booklet provides the draft which belongs to a certain displacement. The draft ranges from 5 m to 6 m for the possible range of displacement. The draft as function of the displacement is plotted in Figure 4.1. This relation will be used during the parameter identification process explained in Chapter 6.

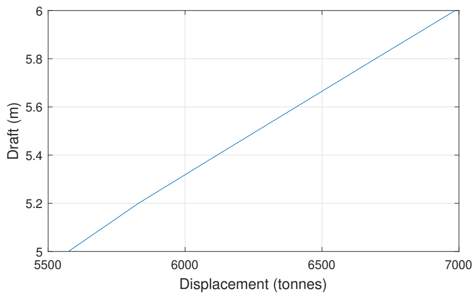

Figure 4.1: Draft as function of displacement

4.2.2. RADII OF INERTIA TERMS

Typically, the radii of inertia terms (r_{ii} or k_{ii}) are approximated by rule of thumb guidance. Various studies [18] suggest that the radii of inertia are dependent on the vessels beam B and length L, in the range of:

$$r_{xx} = 0.30 \text{ to } 0.40 \cdot B \qquad r_{yy} = 0.22 \text{ to } 0.28 \cdot L \qquad r_{zz} = 0.22 \text{ to } 0.28 \cdot L \tag{4.1}$$

The Acta Auriga has a length of 93.4 meter and a width of 18 meter. Therefore, the uncertainty ranges for the radii of inertia following from Equation 4.1 are:

$$r_{xx} = 6.3\text{m} \pm 17\% \qquad r_{yy} = 23.4\text{m} \pm 12\% \qquad r_{zz} = 23.4\text{m} \pm 12\% \tag{4.2}$$

4.2.3. METACENTRIC HEIGHT

The metacentric heights GM_t and GM_l directly determine the restoring moments for roll and pitch motions, as shown in Equation 4.3.

$$\begin{aligned} GM_t &= KB + BM_t - KG \\ GM_l &= KB + BM_l - KG \end{aligned} \tag{4.3}$$

Where KB is the centre of buoyancy, BM_t and BM_l are the transversal and longitudinal metacentric radii and KG is the vertical coordinate of the centre of gravity. This is illustrated in Figure 4.2.
A variation of vessel mass distribution will naturally lead to a variation of metacentric heights. The metacentric heights are usually obtained from the stability booklet of the vessel. For the Acta Auriga, the metacentric heights range according to:

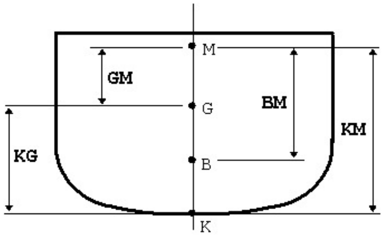

Figure 4.2: Ship's transverse stability, [3]

4

$$GM_t = 1.2\text{m} \pm 17\%$$
$$GM_l = 127\text{m} \pm 8.5\%$$

The metacentric heights depend on the displacement. Therefore, an displacement-dependency relation has been established for the parameter identification process. First, the metacentric radius is expressed as a function of the displacement, followed by an expression of the centre of buoyancy as a function of displacement.

The metacentric radius of a ship is the vertical distance between its center of buoyancy and metacenter. BM_t and BM_l are derived from dividing the moment of inertia of the waterplane by the displacement according to:

$$BM_t = \frac{I_t}{\nabla} \tag{4.4}$$
$$BM_l = \frac{I_l}{\nabla} \tag{4.5}$$

Where I_t and I_l are the transverse and longitudinal moments of inertia. According to Simpson's rules, the metacentric radii of a ship-shaped vessel can be approximated by following equations, [2]:

$$BM_t = \frac{C_w B^2}{12 T C_b} \tag{4.6}$$
$$BM_l = \frac{3 C_w L^2}{40 T C_b} \tag{4.7}$$

Where L is the vessel's length, B is the vessel's width, C_w is the waterplane area coefficient, T is the draft and C_b is the block coefficient. The C_w and C_b of the Acta Auriga are obtained from the stability booklet and range from 0.86 to 0.88 and 0.67 to 0.70, respectively. They depend of the displacement of the vessel [24], this is shown in Figure 4.3.
For ordinary ships, the centre of buoyancy (KB) can be obtained by using Morrish's formula, shown in Equation 4.8 [24].

$$KB = T - \frac{1}{3}(\frac{T}{2} + \frac{\nabla}{A_{WL}}) \tag{4.8}$$

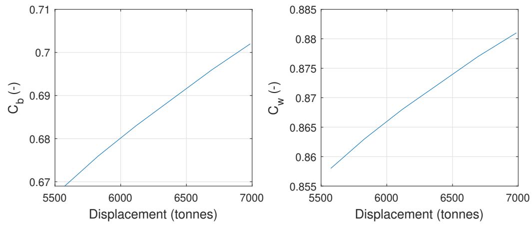

Figure 4.3: C_w and C_b as function of displacement

Where A_{WL} denotes the waterplane area. Substituting Equations 4.7 and 4.8 into Equation 4.3, the metacentric heights can be obtained by:

$$\begin{aligned} GM_t &= T - \frac{1}{3}(\frac{T}{2} + \frac{\nabla}{A_{WL}}) + \frac{C_w B^2}{12 T C_b} - KG \\ GM_l &= T - \frac{1}{3}(\frac{T}{2} + \frac{\nabla}{A_{WL}}) + \frac{3 C_w L^2}{40 T C_b} - KG \end{aligned} \tag{4.9}$$

The displacement and metacentric heights are linked via the calculation of the BM and KB. For the parameter identification process, this relation needs to be maintained which means that the displacement and metacentric heights can not be considered independently.

4.2.4. VISCOUS ROLL DAMPING

As discussed in Section 2.2.6, in addition to potential damping, viscous effects cause another type of damping. However, due to the complexity and non-linearity of wave and vessel responses, determining the amount of viscous damping is a difficult task. The vessel response model has two different approaches to derive the viscous roll damping term. It is either obtained by adding a fixed percentage of the critical roll damping to the potential damping term. Typically, a range of 2 – 16% of the critical damping is used. The critical damping of the vessel for the roll motion can be determined according to Equation 4.10:

$$B_{\text{crit}} = 2 \cdot \sqrt{(C_{4,4} \cdot M_{4,4})} \tag{4.10}$$

The other approach computes the viscous roll damping term using the Ikeda method [26]. Through this solving procedure, the model will generate multiple RAOs for various amounts of roll damping. The response calculation will then iterate to find the RAO with an amount of roll damping corresponding to the actual roll displacement. Stochastic linearization, discussed in Section 2.2.6, is performed to linearize the viscous damping per sea state. In this research, the first solving procedure of the viscous roll damping term is considered.

4.3. INFLUENCE PARAMETERS ON THE DEGREES OF FREEDOM

This Section discusses how uncertainty in the output of the input parameters affects the output of the vessel response model. As a result, one can predict which vessel motions are affected by which parameters and to what degree. By doing so, key information can be gathered regarding which degrees of freedom should be considered for the parameter identification strategy. As previously discussed, the Equation of the RAO is used to obtain information about the input parameters for the response in each degree of freedom:

$$\mathrm{RAO}(\omega,\theta) = \left|\frac{\widehat{\eta}_a}{\zeta_a}\right| = \frac{\widehat{X}_a^{FK}(\omega,\theta) + \widehat{X}_a^{D}(\omega,\theta)}{-\omega^2(\mathbf{M}_{ij} + \mathbf{A}_{ij}(\omega)) + i\omega\mathbf{B}_{ij}(\omega) + \mathbf{C}_{ij}} \tag{4.11}$$

Different parameters affect different RAOs in different ways. Varying the radii of inertia terms will influence RAOs for the corresponding rotational DOF, and the coupled translational DOF. Varying displacement will change draft and consequently change the waterline and wet body surface. These changes will lead to other possible changes on RAOs, depending on the hull geometry and mass distribution. The metacentric heights influence the RAOs for some specific DOFs, e.g. the GM_t affects the roll motion, and the GM_l affects the pitch motion. Damping plays an important role regarding the natural response periods. The influence of additional damping is significant for the RAOs where the resonance is dominated by its natural response, such as roll and heave. Table 4.1 summarizes which degree of freedom is affected by which specific parameter. This information is taken into account in the development of the identification strategy. The parameters which mostly affect one specific DOF will be identified with their corresponding DOF. This is due to the likelihood of finding information on these parameters in motion responses that are affected by that DOF. Additionally, the mean values of the parameters and the percentage of the parameters' uncertainty range is indicated in Table 4.1.

Parameter (**p**)	Symbol	DOF	Mean value	Uncertainty range
Displacement	∇	1-6	6261 tonnes	±11%
Radii of inertia for roll	k_{xx}	4	6.3 m	±17%
Radii of inertia for pitch	k_{yy}	5	23.4 m	±12%
Radii of inertia for yaw	k_{zz}	6	23.4 m	±12%
Transverse metacentric height	GM_t	4	1.2 m	±17%
Longitudinal metacentric height	GM_l	5	127 m	±8.5%
Viscous roll damping	B_{visc}	4	-	2–16% of critical damping

Table 4.1: Parameters for the identification procedure and their uncertainty range

4.4. ADDITIONAL PARAMETERS

Besides the selected identification parameters, other parameters serve the RAO and determine the output of the model. During the identification process, the precomputed added mass coefficient and waterplane area are used to determine the displacement, this procedure is elaborated on in Chapter 6. During this procedure, the precomputed added mass coefficient and waterplane area are kept fixed and are assumed to be correct. Therefore, to make this assumption, this section will discuss the dependence of the added mass coefficient and waterplane area on the displacement of the Acta Auriga.

4.4.1. WATERPLANE AREA

The waterplane area for the Acta Auriga is obtained from the stability booklet [24]. This document includes a table which presents the waterplane area for a certain displacement. It was found that the waterplane area not drastically changes (1385 - 1423 m^2) over the range of possible displacements. Figure 4.4 shows the dimensionless waterplane area for the possible range of displacements. The waterplane area is made dimensionless by dividing it by the maximum waterplane area (1423 m^2).

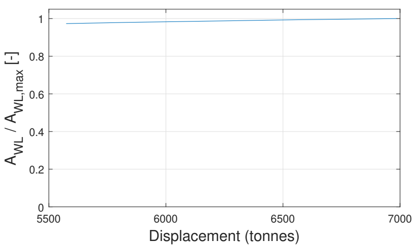

Figure 4.4: Variation of the dimensionless waterplane area as function of displacement

From the figure, it is shown that a change in displacement does not drastically affect the waterplane area of the Acta Auriga. This indicates a stable and low deadrise angle of the hull shape around the waterline. The deadrise angle of a vessel is the angle between the bottom of the vessel and a horizontal plane on either side of center keel. The mean of the possible waterplane area range is 1406 m^2 with an uncertainty of $\pm$1.35%.

4.4.2. ADDED MASS COEFFICIENTS

The added mass coefficient is obtained from a diffraction analysis. In Chapter 2 it was stated that for this research those precomputed values are assumed to be correct. The added mass coefficient is dependent on frequency. To investigate how strong that influence is, Figure 4.5 shows the added mass coefficient as a function of frequency. In this research, the added mass coefficients around at the natural frequency are of interest, this will be elaborated on in Chapter 5. In Section 5.6.1, it will be shown that the expected natural heave and roll frequency are around 1.03 rad/s and 0.48 rad/s, respectively. Therefore, the frequencies of Figure 4.5 range around the expected natural frequency. The added mass coefficients $a_{3,3}$ and $a_{4,4}$ are made dimensionless by dividing it by the maximum value of the coefficient. Figure 4.5 shows that added mass coefficients are relative constant over the range of frequencies.

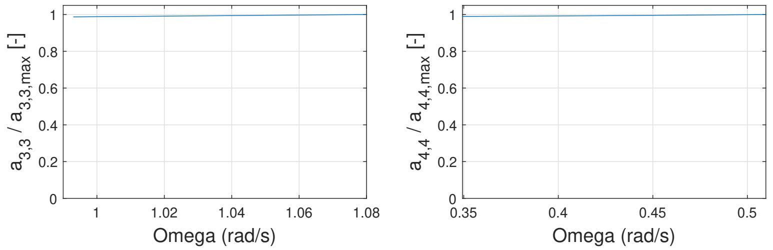

Figure 4.5: Variation of the dimensionless added mass coefficients as function of frequency

To investigate the influence of the displacement of the added mass coefficient, those coefficients are computed for three different possible displacements. The added mass coefficients for the expected heave natural frequency and roll natural frequency are plotted as a function of the displacement in Figure 4.6. The added mass coefficients $a_{3,3}$ and $a_{4,4}$ are made dimensionless by dividing it by the maximum value of the coefficients ($a_{3,3,max}$ = 7409 tonnes and $a_{4,4,max}$ = $5.67 \cdot 10^7$ kg·m^2).

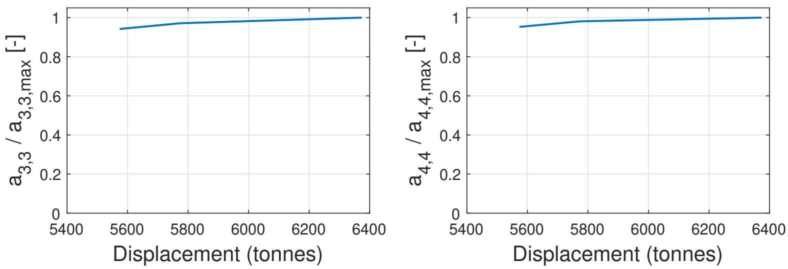

Figure 4.6: Variation of the dimensionless added mass coefficients as function of displacement

The figure shows that a change in displacement does not drastically affect the added mass coefficients of the Acta Auriga. The mean of the precomputed $a_{3,3}$-values is 7195 tonnes with an uncertainty range of ±3.0% and the mean of the precomputed $a_{4,4}$-values is $5.55{\cdot}10^7$ kg·m^2 with an uncertainty range of ±2.9%.

As a result, the mean of the waterplane area and added mass coefficients will be used during this research and possible deviations from this value are assumed to be small and not affecting the outcome of the calculations.

4.5. SUMMARY

This chapter provided a discussion about the identification parameters of this research. This information will be used to setup a suitable parameter identification procedure, which will be explained upcoming Chapters 5 and 6.

5

RAO IDENTIFICATION

5.1. INTRODUCTION

Chapter 3 gave an overview of the available data and resources for this research. Chapter 4 discussed the identification parameters and their uncertainty range. The analysis provides information regarding the degrees of freedom to be focused on during the parameter identification. A sub-step of the parameter identification process is the identification of the RAO from a measured vessel response spectrum and a wave energy spectrum. This chapter provides a detailed description of this procedure. The chapter is structured as follows: first, the purpose of the RAO identification is stated. Next, the mathematical problem of RAO identification is introduced. Thereafter, an approach to solving the mathematical problem is discussed. Finally, the implementation of the solving approach is described in a step-by-step format.

5.2. PURPOSE RAO IDENTIFICATION

The purpose of identifying the RAO is to obtain the heave and roll natural frequencies to use for the parameter identification process. The natural frequency of a system is the frequency at which oscillations are amplified significantly. It is important to have good understanding of the system's natural frequencies since excitation at these frequencies could create large displacements, which is often not desired [27]. In addition, the natural frequency of the system can provide information on the vessel's parameters. The natural frequency, ω_n, is obtained by Equation 5.1.

$$\omega_n = \sqrt{\frac{C}{M+a}} \tag{5.1}$$

where C is the stiffness property, M is the mass term and a is the added mass. Natural frequencies can be indicated by a local maximum in the response amplitude operator (RAO) at that frequency. At frequencies that are significantly higher than the natural frequencies, the transfer functions begin to decrease. At even higher frequencies, as the wavelengths become shorter than the length of the vessel, the RAOs typically begin to approach zero [29].

5.2.1. CHOOSE OF MOTIONS FOR IDENTIFICATION

Each degree of freedom that has a restoring force has an associated natural frequency. So, for a ship, there is a natural frequency in heave, roll, and pitch. The motions which are considered for the RAO identification procedure to obtain the natural frequency are the heave and roll motion.

The pitch natural frequency is not assessed. This was chosen since it is unlikely to pinpoint a clear peak in the pitch response spectrum or the identified RAO, as there is doubtful to be one. This is because the pitch motion for vessels is well damped due to large wave generation compared to the damping of the roll motion, which has relatively small damping.
This chapter will discuss how the RAO is identified, followed by the determination of the natural frequencies. The determined natural frequencies will be used for the parameter identification, this is discussed in Chapter 6.

5

5.3. THE MATHEMATICAL PROBLEM

This section describes the mathematical problem of this chapter. The wave-induced vessel response was discussed in Chapter 2, which showed that the steady-state responses are computed by Equation 5.2.

$$S_r(\omega,\theta) = |RAO(\omega,\theta)|^2 \cdot S_\zeta(\omega,\theta) \tag{5.2}$$

where, as described earlier, $S_r(\omega,\theta)$ and $S_\zeta(\omega,\theta)$ are respectively the energy response spectrum of the vessel and the profile of incoming waves at different angle θ, at a certain frequency ω. The RAO is also depended on both frequency and direction.

Chapter 3 presented the available data of this research, which are $S_r(\omega,\theta)$, from onboard measurements, and $S_\zeta(\omega,\theta)$, provided by weather forecast suppliers. Therefore, the RAO in Equation 5.2 is assumed as the unknown in this mathematical problem. The aim of this chapter is to determine the RAO, given the data of $S_r(\omega,\theta)$ and $S_\zeta(\omega,\theta)$.

5.4. SOLVING METHOD

This section presents a solving method proposed by Bonaschi et al. [15] to solve the mathematical problem described in previous section. This problem is a classical inverse problem: determining a physical law from experimental data [32]. Due to the inverse nature of the problem, establishing a RAO based on measured responses is fraught with several challenges. For instance, it is difficult to account for the dependence of the RAO on both frequency and direction when determining the RAO. To overcome this problem, Bonaschi et al. proposed to decouple the RAO in a frequency-direction relation shown in Equation 5.3.

$$|RAO(\phi,\omega)| = D(\phi) \cdot F(\omega) \tag{5.3}$$

Where $D(\phi)$ and $F(\omega)$ are functions of the direction and the frequency, respectively. This expression allows to consider dependency on ω and ϕ separate, and simplifies the calculations. Using the decoupled relation of Bonaschi et al. [15], Equation 5.2 can be simplified according to Equation 5.4.

$$F(\omega) = \sqrt{\frac{S_r(\omega)}{\int_0^{360} D(\phi)^2 \cdot S_\zeta(\omega,\phi)\, d\phi}} \tag{5.4}$$

In this equation, it is assumed that the directional dependency function $D(\phi)$ is trusted and that the frequency dependent function $F(\omega)$ is to be derived from the measured response and wave spectrum. The derivation of the directional function $D(\phi)$ and implementation of the method will be discussed in next section.

5.5. Directional function $D(\phi)$

5

This section elaborates on how an expression for the directional function $D(\phi)$ from previous section is obtained. The directional function $D(\phi)$ can be obtained by examining directional trends of predetermined RAOs of the Acta Auriga. In this research, the identification of the heave and roll RAOs will be considered, the reason for this was explained in Section 5.2. Therefore, to obtain the directional function, the heave acceleration RAO and roll velocity RAO are obtained with an initial set of parameters. The amplitude of those RAOs are plotted in a three-dimensional surface plot as function of frequency and direction depicted in Figure 5.1.

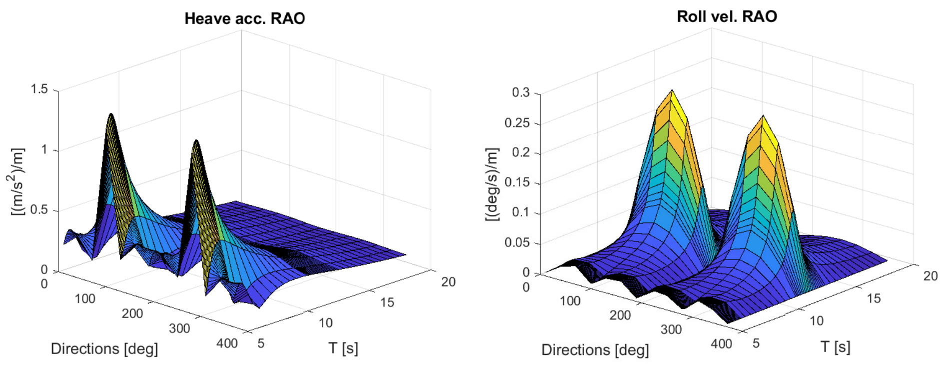

(a) Heave RAO

(b) Roll RAO

Figure 5.1: Heave and roll RAO amplitudes for frequency and direction

From the RAOs, a trend can be observed and an estimate of the $D(\phi)$ function can be derived. The graph has a sinusoidal shape on the x-axis, which represents the direction in degrees. This can be further illustrated in Figures 5.2 and 5.3. The left plot of Figure 5.2 shows the RAO amplitude as a function of direction, where each line is a cross section of Figure 5.1 for a different value for T. The right plot of the figure shows the normalized RAO amplitude. The y-axis in the figure have been normalized such that the amplitude of all the graphs lie between 0-1, this is done since it is easier to observe the common sinusoidal shape. The normalization has been done according to Equation 5.5:

$$x_{\text{normalized}} = \frac{x - x_{\text{min}}}{x_{\text{max}} - x_{\text{min}}} \tag{5.5}$$

where $x_{\text{normalized}}$ is the normalized RAO amplitude for a direction, x is the RAO amplitude for a direction, x_{min} is the minimum RAO amplitude and x_{max} is the maximum RAO amplitude. Figure 5.3 also illustrates this for the roll motion.

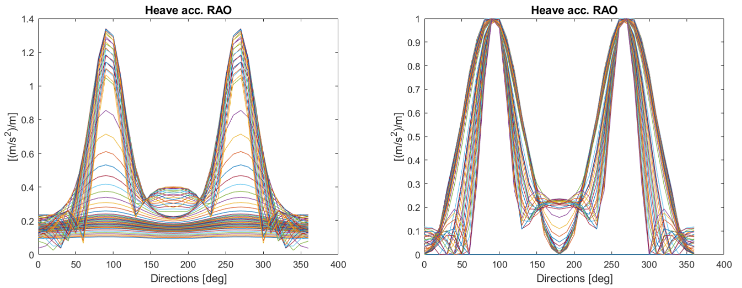

(a) Heave acceleration RAO (b) Normalized heave acceleration RAO

Figure 5.2: Heave RAO amplitudes as a function of direction for different T

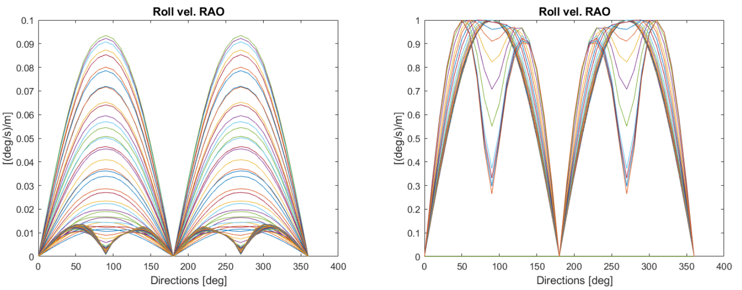

(a) Roll velocity RAO (b) Normalized roll velocity RAO

Figure 5.3: Roll RAO amplitudes as a function of direction for different T

From Figures 5.2 and 5.3, the maximum amplitude of the directional shapes is found in beam directions (90 and 270 deg) and gradually decreases in head directions (0 and

180 deg). This is not unexpected since the heave and roll motions are often caused by waves moving perpendicular to the direction of motion of the ship. Yet, some graphs of Figure 5.3 show the opposite behaviour. This is for periods of $T < 6$s. However, the periods of interest are around the natural period, which was discussed in Section 5.2. The roll natural period of the Acta Auriga for the set of parameters is 13 s. Therefore, to obtain the directional shape function of the roll RAO, the periods of $T < 6$s are not considered. The directional shape function for the heave and roll RAO will be obtained by a fitted function approximating the directional descriptions of the Figures 5.2 and 5.3. The shape for the heave directional function appears to be steeper than the roll directional shape. For both the heave and roll motions, the directional shape of the RAO is determined by a sinusoidal function to the power p, where p is a parameter describing the steepness/smoothness of the curve. In addition, to make $F(\omega)$ in Equation 5.4 represent the 1D energy response spectrum, normalization of $D(\phi)$ is required such that the integral over $D(\phi)$=1. As a result, the directional function $D(\phi)$ can be expressed in the following form:

$$D(\phi) = a \cdot |\sin(\phi)|^p \tag{5.6}$$

The coefficient p is found by using the method of least squares and fitting the RAO data of Figures 5.2 and 5.3 to the function of Equation 5.6 with the coefficient p. The least-squares method minimizes the summed square of residuals. The residual for the i^{th} data point r_i is defined as the difference between the function $D(\phi) \cdot F(\omega)$ and the RAO amplitude for each T. The result of the fitting process is an estimate of the model coefficients p for the heave en roll directional functions and are listed in Table 5.1. The directional function of the heave acceleration and roll velocity for the determined values of p are plotted in Figure 5.4.

	p
Heave	2.01
Roll	0.83

Table 5.1: Values of p for directional function

For these p-values the coefficient a of Equation 5.6 is determined such that $\int_0^{360} D(\phi)\, d\phi = 1$. The coefficients a for the heave en roll directional functions and are listed in Table 5.2.

	a
Heave	0.32
Roll	0.25

Table 5.2: Values of a for directional function

The expression of $D(\phi)$ considerably simplifies the task of identifying the RAO. Since the response spectra of the vessel and waves are known, $F(\omega)$ remains the only unknown in Equation 5.4. Assuming that the directional information obtained from the precomputed RAOs is trusted, the problem unknowns are reduced for each frequency and sea state.

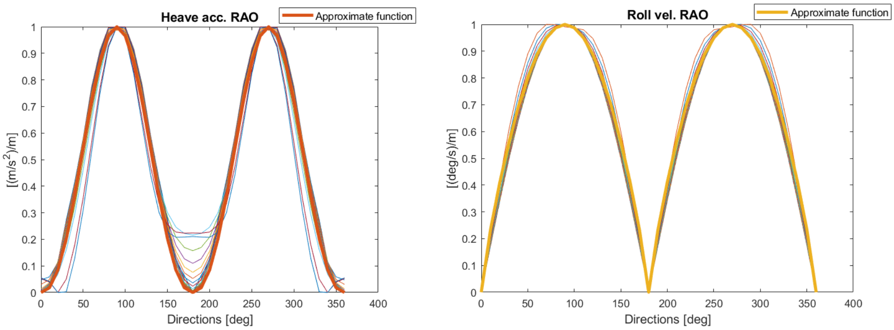

(a) Heave directional shape RAO (b) Roll directional shape RAO

Figure 5.4: Directional functions for heave and roll

5.6. IMPLEMENTATION OF THE SOLVING METHOD

This section discusses the implementation of the identification method to obtain an expression for the RAO according to a step-by-step plan. This section also describes how the natural frequency is found from the identified RAO. With the prior information of the Acta Auriga, an expected natural frequency can be determined. This is useful to find the natural frequency from the identified RAO, as it enables a targeted search. Since multiple peaks could be present in the identified RAO, a search range to detect the natural roll and heave frequency within this range is established. The search range is determined is next section.

5.6.1. DETERMINATION UNCERTAINTY SEARCH RANGE

The search range of the natural frequency for the Acta Auriga is determined according to the uncertainty related to the input parameters which determine the natural frequency. The search range is established for the heave and roll motion.

HEAVE

The heave natural frequency is obtained from Equation 5.7. The input values of the parameters of Equation 5.7 and their uncertainty range are listed in Table 5.3. Chapter 4 showed that each parameter has a certain uncertainty range. With these uncertainty ranges, an uncertainty range for the natural frequencies is determined.

$$\omega_{n3} = \sqrt{\frac{C_{3,3}}{M_{3,3} + a_{3,3}}} = \sqrt{\frac{\rho g A_{\mathrm{WL}}}{\nabla \cdot \rho + a_{3,3}}} \tag{5.7}$$

With Equation 5.7 and Table 5.3, the expected natural frequency is computed including the associated uncertainty range, shown in Equation 5.10. The uncertainty range of the natural frequency is determined by the rules of uncertainty determination [52]. Accordingly, for the heave natural frequency, the search range is set to be between 0.95 - 1.11 rad/s and the uncertainty is ±7.7% with respect to the mean.

Parameter	Value	Uncertainty range	Unit	Uncertainty percentage
A_{WL}	1406	19	m^2	$\pm$1.35%
∇	6261	638	tonnes	$\pm$11%
$a_{3,3}$	7195	216	tonnes	$\pm$3.0%

Table 5.3: Input parameter for natural heave frequency determination

$$\omega_{\text{n3}} = 1.03 \ \frac{\text{rad}}{\text{s}} \pm 7.7\% \tag{5.8}$$

Roll

In similar manner, the roll natural frequency is obtained from Equation 5.9 and the input values of the parameters and their uncertainty range of the equation are listed in Table 5.4.

5

$$\omega_{\text{n4}} = \sqrt{\frac{C_{4,4}}{M_{4,4} + a_{4,4}}} = \sqrt{\frac{\rho g \nabla GM_t}{k_{xx}^2 \rho \nabla + a_{4,4}}} \tag{5.9}$$

Parameter	Value	Uncertainty range	Unit	Uncertainty percentage
GM_t	1.2	0.2	m	$\pm$17%
∇	6261	638	tonnes	$\pm$11%
k_{xx}	6.3	5.2	m	$\pm$17%
$a_{4,4}$	$5.55{\cdot}10^7$	$1.61{\cdot}10^6$	$kg*m^2$	$\pm$2.9%

Table 5.4: Input parameter for natural roll frequency determination

The expected natural frequency is computed including the associated uncertainty range, shown in Equation 5.10. Accordingly, for the roll natural frequency, the search range is set to be between 0.36 - 0.59 rad/s and the uncertainty is ±24% with respect to the mean.

$$\omega_{\text{n4}} = 0.48 \ \frac{\text{rad}}{\text{s}} \pm 24\% \tag{5.10}$$

5.6.2. Step-by-step plan

Next, a step-by-step plan as well as an example are presented to show the implementation of the proposed RAO identification procedure.

1. Obtain identification data
   First, wave and response spectra need to be obtained, which serve as identification data for the solving method. The requirements of the vessel's response spectra were specified in Section 3.3.2. A wave spectrum and response spectrum are used as input for the identification process. Those are plotted in Figure 5.5. Note that the 1D wave spectrum on the left hand side is plotted in the Figure, whereas

the method computes the directional independent RAO with a two-dimensional spectrum (directionality of wave spectrum included), shown in Equation 5.4. The heave and roll response spectra of this example is created with the wave spectrum and a presumed RAO. The input parameters of the RAO are assumed to be the "true" parameters. This RAO is referred to as "true RAO" in this chapter. The goal of the RAO identification is to infer the natural frequency of the "true RAO".

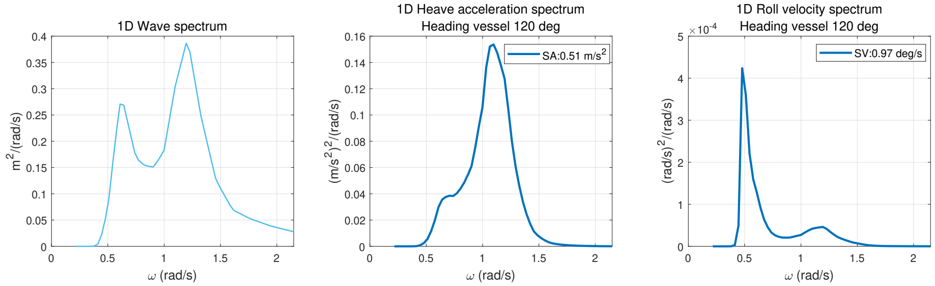

Figure 5.5: 1D wave spectrum and heave and roll response spectra - 17/10/2021

5

2. Compute expected natural frequency
   Next, the expected natural frequency of the system prior to the identification procedure is computed, discussed in Section 5.6.1. The heave and roll natural frequency are computed with an initial set of assumed parameters according to Equations 5.7 and 5.9, respectively.

3. Select search range
   If the identified RAO contains numerous peaks, it must be determined which peak corresponds to the system's natural frequency. The precomputed natural frequencies and corresponding uncertainty range from previous step are used to indicate a search range. The lower and upper bound of the search range followed from the determined uncertainty range of the precomputed natural frequency in previous section. A peak in this search range will be assigned to identified natural frequency.

4. Determine directional function $D(\phi)$
   Subsequently, the directional function $D(\phi)$ must be determined for the ship's RAOs. The heave and roll directional functions for the Acta Auriga were computed in Section 5.5.

5. Identify RAO
   With the response spectrum, the wave energy spectrum and the directional function, an direction independent expression for the RAO can be found according to Equation 5.4. The method has been applied to identify the heave and roll RAO from the spectra of Figure 5.5. The results are plotted in Figures 5.6 and 5.7. The search range is indicated with a dotted line. The identified $F_{heave}(\omega)$ and $F_{roll}(\omega)$ are indicated in blue. The heave and roll RAO followed from multiplying $F(\omega)$ by $D(\phi)$ (Equation 5.3) and are indicated in orange for the main wave direction. The

true heave acceleration and roll velocity RAOs are indicated in dashed lines for different wave directions.

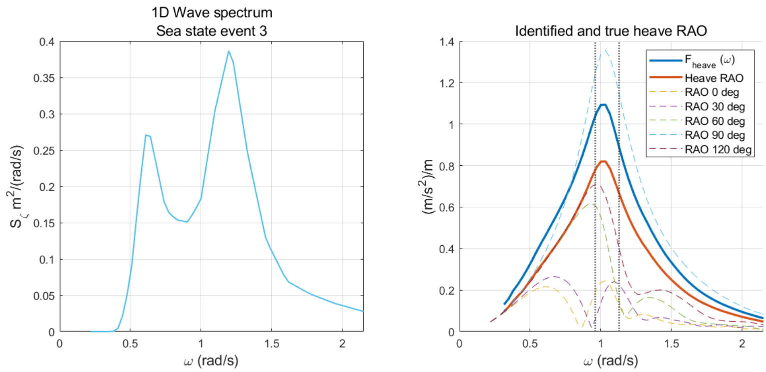

Figure 5.6: 1D Wave spectrum and identified and precomputed RAOs

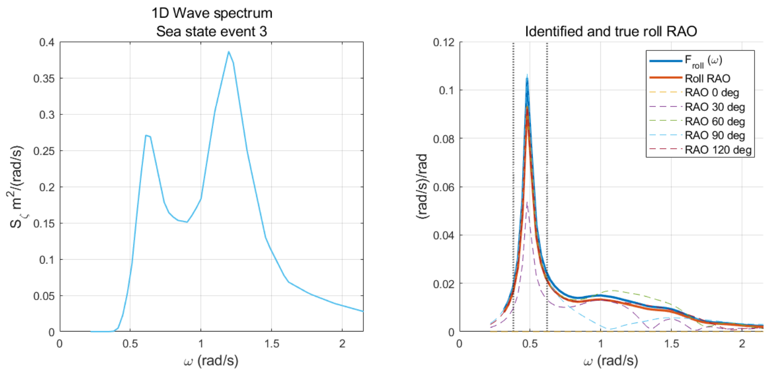

Figure 5.7: Wave and response spectrum

6. Determine natural frequencies
   The natural response frequency ω_n is found at the frequency linked to the observed peak of the identified RAO (i.e. $\max(F(\omega_n))$. Only maxima in the established search range are considered.

7. Take the mean among multiple identified natural frequencies
   Finally, the procedure is repeated for several wave and response spectra, measured on the same day. The final natural frequency follows from taking the mean among the obtained results. The process of identifying the RAO at several cases, determining the natural frequency from each of these instances, and then averaging it out throughout all reduces the problem's reliance on a single observation. This makes the process less susceptible to errors of single observations.

The identified RAO, obtained from discussed procedure, should work quite well given there is wave energy in the frequency band of interest. If a part of a RAO is not accounted for by the wave climate, it is impossible to deduce information about the RAO in that frequency band from the measured vessel responses. Besides, the wave spectrum used in this research is a nowcast wave spectrum and this prediction contains inherent uncertainties. This must be taken into account in the identification process and therefore, expected RAO and wave spectrum should be investigated prior to the process. It is important to understand how well the solving method identifies the RAO from the available data. On the other hand, it is important to analyze to which extent the identified RAO is data-dependent. Therefore, to the test the proposed procedure and analyze its performance, two case studies are conducted. The case studies are discussed in Chapters 7 and 8, after presenting the whole parameter identification procedure in Chapter 6.

6

PARAMETER IDENTIFICATION

6.1. INTRODUCTION

Chapter 5 showed how the RAO can be identified from the available data sources of this research, consisting of measured vessel response energy spectra and nowcast wave energy spectra. From the identified RAO, the system's heave and roll natural frequencies could be determined. This chapter elaborates on how the knowledge of previous chapters can be incorporated to develop a suitable parameter identification procedure, which searches for the correct parameter values of the vessel response model. The development of this procedure is comprised of various steps that will be detailed in this chapter.

6.2. PARAMETER IDENTIFICATION PROCEDURE SELECTION

This Section elaborates on the parameter identification procedure. The procedure is selected based on the literature review and the available data. The parameters to be identified were determined in Chapter 2 and can be found in Table 4.1. Each parameter is categorized and for each category a different identification strategy is considered. Figure 6.1 depicts the parameter identification procedure.

Certain considerations were taken into account during the procedure's development. This entailed considering the order in which the various parameters should be determined and the motion responses that should be taken into account. Rather than identifying all of the unknown parameters at once in a large estimation, it is more time-efficient to start by finely adjusting certain degrees of freedom of the vessel model. The identification procedure incorporates physical formulas as well as an optimization technique.

- The physics-based approach was used to discover characteristics of the system by observing the system's natural frequencies, this is described in Sections 6.3 - 6.3.2.
- The optimization approach will be discussed further in the following Section 6.4, which will be followed by an explanation of the blocks of Figure 6.1.

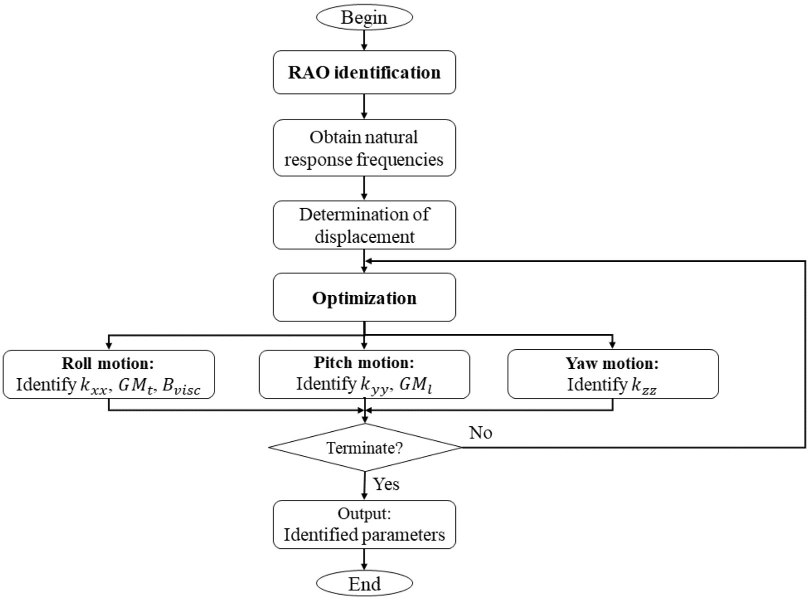

Figure 6.1: Proposed parameter identification procedure

6.3. RAO IDENTIFICATION AND SYSTEM'S NATURAL FREQUENCIES

The procedure of Figure 6.1 starts by identifying the RAOs from the measured vessel response spectra and nowcast wave spectra. This is done by using a decoupled frequency-direction relation for the RAO. From the identified RAOs, the natural frequencies for heave and roll (ω_{n3}, ω_{n4}) could be found. The natural frequencies are found at the frequency linked to a maximum of the identified RAO. This procedure was discussed in Chapter 5 and is useful since the natural frequency of the system can provide information on the vessel's parameters. How the natural frequencies are utilized to determine certain parameters is elaborated on in upcoming Sections 6.3.1 and 6.3.2.

6.3.1. DETERMINATION OF DISPLACEMENT WITH NATURAL HEAVE FREQUENCY

The first parameter identification is focused on identifying the displacement of the vessel. Since the displacement influences the response in all degrees of freedom, this is the most important parameter to identify and therefore identified first in the procedure. The heave natural frequency depends on the mass and stiffness properties of the system, stated in Equation 6.1.

$$\omega_{\mathrm{n3}} = \sqrt{\frac{C_{3,3}}{M_{3,3} + a_{3,3}}} = \sqrt{\frac{\rho g A_{\mathrm{WL}}}{\nabla \cdot \rho + a_{3,3}}} \tag{6.1}$$

The theory discussed in Chapter 2 stated that $C_{3,3} = \rho g A_{\mathrm{WL}}$ and $M_{3,3} = \nabla \cdot \rho$. As a result, the first term of Equation 6.1 could be rewritten in the second term. Subsequently, since the heave natural frequency was obtained from the RAO identification procedure, it is possible to determine the displacement of the vessel. The displacement can be determined by rewriting Equation 6.1 into Equation 6.2.

$$\nabla = \frac{(\rho g A_{WL}) - (\omega_{n3}^2 a_{3,3})}{\omega_{n3}^2 \rho} \tag{6.2}$$

This equation can only be used to calculate the displacement if the other parameters, added mass and waterplane area, can be trusted and assumed to be accurate. The dependence of those parameters on the displacement was discussed in Section 4.4.1 and 4.4.2. It was found that those parameters to not drastically change for a variation of the displacement.

6.3.2. DETERMINATION OF ROLL RADIUS OF GYRATION WITH NATURAL ROLL FREQUENCY

From Chapter 4, it was shown that the displacement, k_{xx}, GM_t and B_{visc} have a influence on the roll response. While the displacement has already been identified in the procedure described in Section 6.3.1, the roll motion will be used to identify the k_{xx}, GM_t and B_{visc}.

6

Here, as the natural roll frequency has been identified from the measured roll spectrum (Chapter 5), this knowledge assist to identify the remaining roll parameters. The roll natural frequency is calculated using Equation 6.3 [29].

$$\omega_{\mathrm{n4}} = \sqrt{\frac{C_{4,4}}{M_{4,4} + a_{4,4}}} = \sqrt{\frac{\rho g \nabla GM_t}{k_{xx}^2 \rho \nabla + a_{4,4}}} \tag{6.3}$$

k_{xx} can be expressed in terms of GM_t by rewriting Equation 6.3 into Equation 6.4 and assuming that the other parameters of the equation, the displacement and ω_{n4} are correctly identified by the previous steps of the procedure. The added mass coefficient $a_{4,4}$ was shown to be relative constant for a variation of displacement in Section 4.4.2. Thus, the k_{xx} can be expressed according to Equation 6.4:

$$k_{xx} = \sqrt{\frac{\nabla g GM_t - \omega_{n4}^2 a_{4,4}}{\nabla g \omega_{n4}^2}} \tag{6.4}$$

The equation shows how k_{xx} and GM_t relate to one another. During the identification process, this relation will be maintained and clever knowledge of the physical system is used while identifying the parameters. This is considered by changing parameter GM_t which consequentially determines k_{xx} while respecting the relation. While evaluating the optimization algorithm, this relation may lead to decreased computation time and better agreement for the true parameters than leaving the constraint out. This is because the GM_t will serve as identifiable parameter, and k_{xx} will follow from each variation of GM_t.

6.4. PARAMETER IDENTIFICATION BY OPTIMIZATION

Identification of model parameters by comparing and adjusting simulated results to measured data with an optimization algorithm is a well-known procedure for different applications [28]. As discussed in 2.3.1, generally an objective function is defined to assess the agreement of the model results with the measured data. The optimization algorithm then adjusts the model parameters to better fit the measurements by minimizing the objective function. Since the displacement is determined with the natural heave frequency, discussed in Section 6.3.1, the optimization algorithm will identify the remaining identification parameters, k_{xx}, k_{yy}, k_{zz}, GM_t, GM_l and B_{visc}. This section is structured as follows: first, the objective function is defined. Next, the optimization technique that evaluates the objective function and searches for the model parameters is described. In addition, the stopping criteria of the optimization algorithm are listed. Finally, the implementation of the optimization is discussed.

6.4.1. DEFINING THE COST FUNCTION

Section 2.3.1 discussed that the model parameters can be inferred by optimizing a cost function $f(\mathbf{x})$. The output error between the measurement and the model prediction was depicted in Figure 3.3. The minimization of the output error will be accomplished by estimating the model parameters through an optimization. The cost function is expressed in Equation 6.5 and computes the normalized root mean square error between the measured and the predicted energy response spectrum. The root mean squared error (RMSE) is the square root of the mean of all error squares. This cost function has been chosen since the use of RMSE is widely employed and is regarded as an excellent error measure for numerical predictions [6]. The RMSE is normalized by dividing it by the maximum value minus the minimum value of the measured response spectrum. The RMSE is normalized to facilitate the comparison between the different degrees of freedom of the vessel. The cost function is defined as:

$$f(\mathbf{x}) = \frac{\sqrt{\frac{\sum_{n=1}^{N}\left(S^m_{r,i}(\omega)-S^p_{r,i}(\omega,\mathbf{x})\right)^2}{N}}}{\max(S^m_{r,i}(\omega))-\min(S^m_{r,i}(\omega))} \tag{6.5}$$

where $S^m_r(\omega)$ and $S^p_r(\omega,\mathbf{x})$ denotes the measured and predicted energy response spectrum of the vessel for parameter variation $\mathbf{x}$ and for each degree of freedom i. A value of zero of the cost function would indicate a perfect fit to the data therefore, the objective of the optimization is to minimize the cost function. Equation 6.5 shows that the differences of the measured and predicted response spectrum are found by taking the differences at a particular frequency. Therefore, to properly use Equation 6.5, the measured response data is interpolated to the frequencies of the predicted response data. By synchronizing the frequencies, the measured and predicted response spectra can be subtracted from each other easily.

6.4.2. OPTIMIZATION TECHNIQUE

An optimization technique was necessary to select for the minimization. Various algorithms are described in the literature as solutions to optimization problems [30], [33],

[45], [54]. For this study, the optimization technique was selected according to a certain set of objectives:

- The algorithm should be able to estimate multiple parameters simultaneously
- The algorithm should not be time consuming
- The algorithm should always convergence to the global minimum, independent of the initial starting values of the parameters

Based on these criteria, the optimization method of [33] which applies the Nelder-Mead algorithm is selected for the identification process. This algorithm is implemented in the "fminsearch" function from the MATLAB optimization toolbox. This function finds the minimum of a scalar function of several variables. The Nelder-Mead algorithm [50], does not require function gradients or Hessian for its minimization algorithm. MATLAB is used to run the simulations, change the parameters, and compute the cost function.

This algorithm is selected since it finds the minimum of an unconstrained multivariable function using a derivative-free method. Hence, multiple parameters can be identified simultaneously. Additionally, since it does not use numerical or analytic gradients, making the method computationally inexpensive compared to the gradient-based methods of [30], [45] and [54]. The Nelder-Mead algorithm was chosen as the optimization method for its flexibility and simplicity. The working principle of the Nelder-Mead algorithm is presented in Appendix 9.4. Lastly, it was important to ensure that the algorithm found the global optimum. Through the optimization, a large number of local minima may be present and the computation process could be highly dependent on the initial starting values of the parameters [43]. In this thesis, the process to ensure global minima is handled by executing the algorithm from several initial starting points. It was found that the algorithm converged to the same global minimum, independent of the initial starting values. This suggest that the optimization problem is convex. Those results are shown in Appendix 9.4.

In addition, it could be of relevance to impose bounds on each parameter. This could counteract unrealistic values of final results. Therefore, each parameter was assigned a lower and an upper limit before running the algorithm. The limits should reflect a reasonable uncertainty of the parameter values, this was determined in Chapter 4.

6.4.3. STOPPING CRITERIA

The optimization function begins from an initial guess, iterates according to a given update scheme, and finishes when a stopping criteria is met. This section will elaborate on the predefined stopping criteria containing certain tolerances of the algorithm. A tolerance is typically a threshold that, when exceeded, halts the iterations of the algorithm. The stopping criteria were based on the sensitivity analysis of [51]. The following criteria are applied during the identification process:

- TolX is a lower bound on the size of a step between the parameter variable (x_i) and the next parameter variation, meaning the difference of ($x_i - x_{i+1}$). If the algorithm attempts a smaller step than TolX, the process is terminated. This criterion varied depending on the parameter. For the radii of inertia TolX was 0.01 m. For the metacentric heights was typically around 0.5% of the initial starting value.
- TolFun is a lower bound on the change in the value of the cost function during a step. If $|f(x_i) - f(x_{i+1})| <$ TolFun, the process is terminated. The TolFun value was set to 0.001.
- MaxIter is a bound on the number of solver iterations. One iteration takes approximately one minute, therefore, MaxIter was set to 30, resulting in a maximum computation time of 30 minutes. This was chosen to meet the requirement of the algorithm to be not time consuming.

6.4.4. IMPLEMENTATION OF THE ALGORITHM

The identification of the model parameters is accomplished by applying the optimization algorithm to predicted and measured response spectra. From Figure 6.1, it can be noticed that the identification of the parameters are assigned to different degrees of freedom. Therefore, the response spectra of different degrees of freedom are evaluated to identify different parameters. The DOF and the related parameters are listed below:

6

- **Roll motion**
  The roll motion response spectrum will be evaluated with the optimization algorithm to identify the k_{xx}, GM_t and B_{visc}. The optimal set of parameters k_{xx}, GM_t and B_{visc}, is defined as the set for which the cost function is minimum. While modifying the set of possible parameter values, previous knowledge of the parameters GM_t and k_{xx} should be maintained:
  - GM_t
    As discussed in Section 4.2.3, the displacement and metacentric heights are related to one another via the calculation of the BM and KB. For the parameter identification process, this relation needs to be maintained which means that the displacement and metacentric heights can not be considered independently. The relation between the displacement, GM_t and other parameters is stated in Equation 6.6.

$$GM_t = T - \frac{1}{3}\left(\frac{T}{2} + \frac{\nabla}{A_{WL}}\right) + \frac{C_w B^2}{12 T C_b} - KG \tag{6.6}$$

    Here, the displacement has already been identified, explained in Section 6.3.1. With the displacement, the corresponding draft (T), C_w and C_b can be determined using Figures 4.1 and 4.3. Thus, the remaining unknown in Equation 6.6 to obtain the GM_t is the KG. Therefore, the optimization algorithm identifies the GM_t by evaluating the cost function for different values of KG.
  - k_{xx}
    The k_{xx} is related to the GM_t, this was discussed in Section 6.3.2. For the search of the minimum of the cost function, modifying parameter GM_t will

consequentially determine k_{xx} while respecting the relation established in Equation 6.4.

- **Pitch motion**
  From Chapter 4, it was concluded that the displacement, k_{yy} and GM_l mainly have a strong influence on the pitch response of the vessel. Therefore, the parameters k_{yy} and GM_l are identified by applying the optimization algorithm to the measured and predicted pitch response spectrum.

  - GM_l
    The displacement and GM_l are also related to one another via the calculation of the BM and KB. In similar manner as for the GM_t determination, the remaining unknown of Equation 6.7 is the KG. Therefore, the optimization algorithm identifies the GM_t and GM_l by evaluating the cost function for different values of KG.

$$GM_l = T - \frac{1}{3}\left(\frac{T}{2} + \frac{\nabla}{A_{WL}}\right) + \frac{3C_w L^2}{40TC_b} - KG \tag{6.7}$$

  Since for both the roll and pitch motion, the correct value of KG must be found, the optimization is applied by evaluating both motions through the cost function. The optimization algorithm searches for KG which provides the parameters GM_t and GM_l matching both the roll and pitch motions best. Consequently, the cost functions to find the parameters k_{xx}, k_{yy}, GM_t, GM_l and B_{visc} is defined as:

$$f_{\text{roll}}(\mathbf{x}) = \frac{\sqrt{\frac{\sum_{n=1}^{N}\left(S_{r,4}^{m}(\omega)-S_{r,4}^{p}(\omega,\mathbf{x}_1)\right)^2}{N}}}{\max(S_{r,4}^{m}(\omega)) - \min(S_{r,4}^{m}(\omega))} \tag{6.8}$$

$$f_{\text{pitch}}(\mathbf{x}) = \frac{\sqrt{\frac{\sum_{n=1}^{N}\left(S_{r,5}^{m}(\omega)-S_{r,5}^{p}(\omega,\mathbf{x}_2)\right)^2}{N}}}{\max(S_{r,5}^{m}(\omega)) - \min(S_{r,5}^{m}(\omega))} \tag{6.9}$$

  where $\mathbf{x}_1 = k_{xx}, GM_t$ and B_{visc} and $\mathbf{x}_2 = k_{yy}$ and GM_l.

- **Yaw motion**
  From Chapter 4, it was concluded that only the displacement and k_{zz} had a strong influence on the yaw response. In addition, the parameter k_{zz} is identified by applying the optimization algorithm to the measured and predicted yaw response spectrum. Therefore, the cost function to find the parameter k_{zz} is defined as:

$$f_{\text{yaw}}(\mathbf{x}) = \frac{\sqrt{\frac{\sum_{n=1}^{N}\left(S_{r,6}^{m}(\omega)-S_{r,6}^{p}(\omega,\mathbf{x}_3)\right)^2}{N}}}{\max(S_{r,6}^{m}(\omega)) - \min(S_{r,6}^{m}(\omega))} \tag{6.10}$$

  where $\mathbf{x}_3 = k_{zz}$

6

It should be mentioned that running the optimization algorithm for the cost functions defined in Equations 6.8, 6.9 and 6.10, can be executed simultaneously to identify the parameters. The updated value of the cost function $f(\mathbf{x})$ can be compared to the first evaluation of the cost function. Consequently, it can be determined whether the identification led to improvement.

7

Case study 1

7.1. Introduction

This chapter presents the first case study of this research. The proposed parameter identification strategy is tested on a collection of synthetic data. This allows the identification procedure to analyze the performance of the procedure before applying it to actual measurements. This chapter is structured as follows: first, the case set-up is defined, including characteristics of the vessel and metocean conditions. Thereafter, the results of the analysis are shown and discussed.

7.2. Simulation setup - Synthetic data

Synthetic data sets are generated through computer programs, instead of being composed through the measurements of real-world events. The purpose of a synthetic data set is to serve as a stand-in for real operational data sets. Therefore, a synthetic data set is created with the vessel response model to simulate vessel motions measurements. This has several advantages, including decreasing noise when utilizing sensitive measured data and knowing the real input parameters, which are impossible to achieve with measured data. By doing so, the identified parameters can be compared to the true values. If the method performs well, it can be applied to real measurements. The analysis is performed with the Acta Auriga as vessel for the case study.

The synthetic data set are response spectra and are created with a wave spectrum and a RAO. The input parameters of the RAO are assumed to be the "true" parameters. The goal of the identification strategy is to find these values, listed in Table 7.1. The motion responses are calculated of the synthetic data set for a specific location on the vessel. The location of calculated responses is chosen to be at the location of the MRU of the Acta Auriga, which was placed at [x=40.8 m, y=0 m, z= 12.1 m] w.r.t. the baseline of the vessel.

Parameter (**p**)	Symbol	Value	Unit
Displacement	∇	6261	tonnes
Radii of gyration for roll	k_{xx}	6.48	m
Radii of gyration for pitch	k_{yy}	23.35	m
Radii of gyration for yaw	k_{zz}	23.35	m
Transverse metacentric height	GM_t	1.2	m
Longitudinal metacentric height	GM_l	127	m
Viscous roll damping	B_{visc}	5	% of crit. damping

Table 7.1: True parameters values for the synthetic data set

7.2.1. INITIAL PARAMETERS

Before running the identification algorithm, an initial prediction of the vessel response was made with initial parameters as input for the model. Two test cases are set up and the results of each will be discussed. In the first test case, the displacement is underestimated and the radii of gyration terms and metacentric heights followed from the lower bound of the uncertainty range. The viscous roll damping is underestimated. This case is referred to as Test case 1. In the other test case, the displacement of the vessel is overestimated and and the radii of gyration terms and metacentric heights followed from the upper bound of the uncertainty range. This case is referred to as Test case 2. The initial starting parameters of both cases are shown in Table 7.2.

Parameter (**p**)	Symbol	Test case 1	Test case 2	Unit
Displacement	∇	5574	6986	tonnes
Radii of gyration for roll	k_{xx}	5.4	7.2	m
Radii of gyration for pitch	k_{yy}	20.5	26.1	m
Radii of gyration for yaw	k_{zz}	20.5	26.1	m
Transverse metacentric height	GM_t	1	1.4	m
Longitudinal metacentric height	GM_l	115	139	m
Viscous roll damping	B_{visc}	3	8	% of crit. damping

Table 7.2: Initial parameters values for two test cases

7

7.2.2. METOCEAN CONDITIONS

The synthetic measured data is generated with different sea states as an input. The peak period T_p of the sea states varied from 4-10 s. The sea states are referred to as Events 1-5 and are shown in Figure 7.1. The wave energy spectra originate from weather forecasts from the 2nd of December until the 13th of December 2021 provided by Infoplaza. The weather forecasts are obtained for a location in the North Sea, 120 km off the east coast of England. An effort was made to obtain a diverse scenario in selecting the sea states from the available data. For instance, Event 3 depicts a sea state with wind and swell seas. Here, the wind waves peak lies around T_p = 6s and the swell waves peak around T_p = 10s. Vessel headings of 30, 60, 90, 120, 150 deg in which at 0 degree, the vessel bow is heading north.

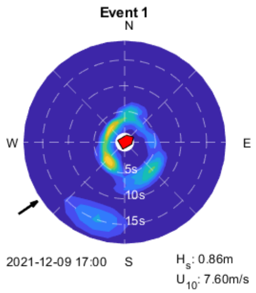

(a) Event 1: $T_p = 4s$

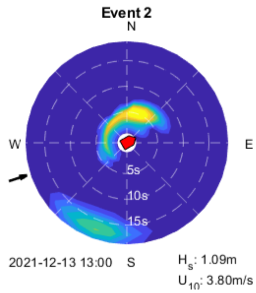

(b) Event 2: $T_p = 6s$

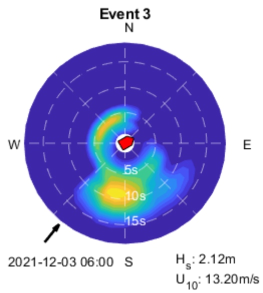

(c) Event 3: $T_p = 10s$

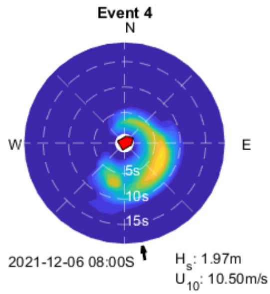

(d) Event 4: $T_p = 8s$

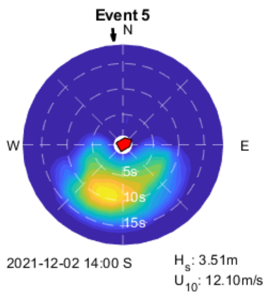

(e) Event 5: $T_p = 10s$

Figure 7.1: Wave spectra Event 1-5

7.3. RESULTS

7.3.1. FIRST EVALUATION COST FUNCTION

First, the cost function $f(x)$ from Equation 6.5 is evaluated to determine the initial deviation between measured and predicted responses. This function computes the quadratic error between the measured and predicted energy density spectrum for each DOF and for both test cases. The mean values of $f(x)$ among the chosen sea states and vessel headings for each DOF associated to the initial parameters are shown in Table 7.3. For further illustration, the response spectra for sea state Events 3 and direction 30 deg are shown in Figures 7.2 and 7.3 for Test case 1 and 2. As discussed in Section 3.3.3, for the translational motions, the acceleration response spectra are assessed and for the rotational motions, the velocity response spectra are assessed. From the figures, it can be noticed that the parameter values of Test 1 cause an overprediction of the generated output and the parameter values of Test case 2 provide an underprediction of the generated output compared to the true spectra.

DOF	$f(x)$ Test case 1	$f(x)$ Test case 2
Surge	0.109	0.063
Sway	0.337	0.088
Heave	0.037	0.037
Roll	0.448	0.127
Pitch	0.115	0.072
Yaw	0.156	0.109
Sum all DOF	1.201	0.496

Table 7.3: Evaluation of cost function for test case 1 and 2

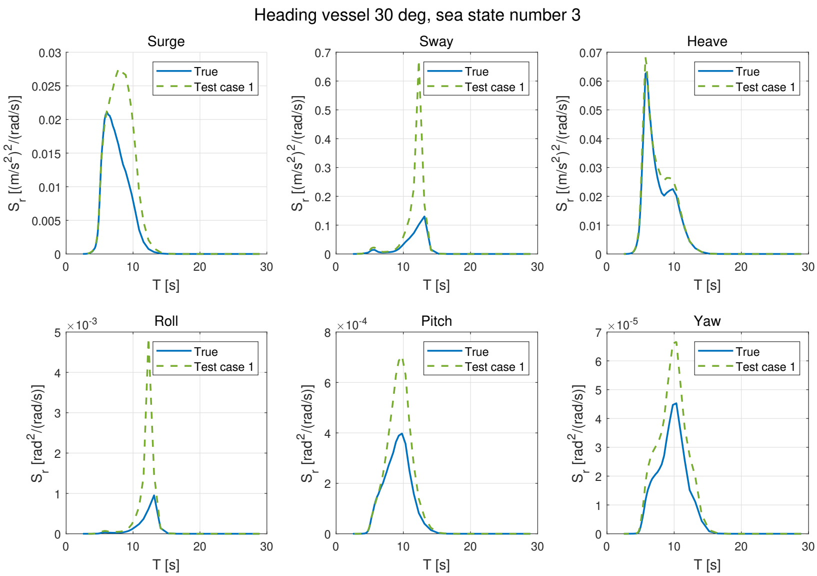

Figure 7.2: Comparison response spectra for the synthetic response and the initial prediction test case 1 computed for Event 3 ($T_p = 6s$ and $10s$) and direction 30 deg

7

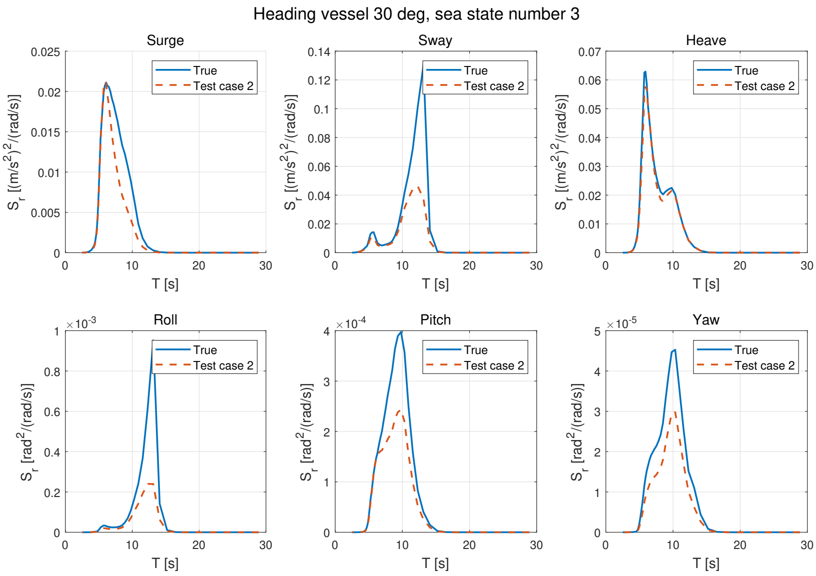

Figure 7.3: Comparison response spectra for the synthetic response and the initial prediction test case 2 computed for Event 3 ($T_p = 6s$ and $10s$) and direction 30 deg

7.3.2. RAO IDENTIFICATION

This section presents the results of the RAO identification. The procedure to identify the RAO was discussed in Chapter 5. The RAO is identified by using the directional shape, the vessel response and wave energy spectrum. As discussed in Chapter 5, the RAO identification procedure has been followed for the heave and roll motion. The wave input for the corresponding vessel responses are the five described sets of sea states presented in Section 8.2.1.

As an example, Figures 8.5 and 8.6 show the 1D wave spectrum and the synthetic heave and roll response spectra for sea state Event 3 for vessel heading 60 and 150 deg. The significant acceleration and significant velocity are indicated in the legend of the figures as well by the abbreviation "SA" and "SV", respectively. Those are obtained by Equation 2.10, discussed in Section 2.2.5.

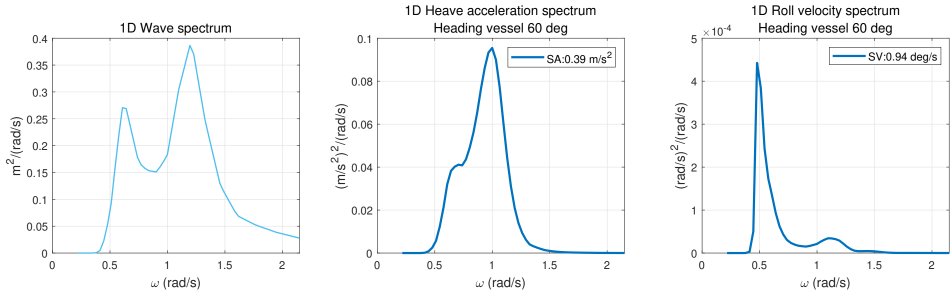

Figure 7.4: 1D wave spectrum and heave and roll response spectra of sea state event 3 and vessel heading 60 deg

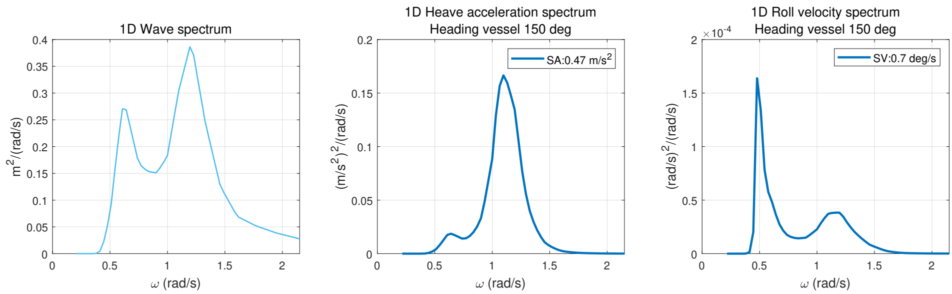

Figure 7.5: 1D wave spectrum and heave and roll response spectra of sea state event 3 and vessel heading 150 deg

From the data of Figures 7.4 and 7.5, the heave acceleration RAO and roll velocity RAO has been identified and are shown in Figures 7.6, 7.7, 7.8 and 7.9. The RAO obtained from the wave and response spectra is referred to as "identified RAO" and the true RAO, known from the synthetic data set, is referred to as "true RAO" in this chapter. In the left plot of the figures, the wave spectrum is shown. In the right plot of the figures, the identified RAO is shown as well as the true RAOs for different wave directions.

The RAO is identified with a decoupled frequency-direction relation (Chapter 5). Here, the directional dependency function $D(\phi)$ is trusted and that the frequency dependent function $F(\omega)$ is to be derived from the measured response and wave spectrum. The identified $F_{heave}(\omega)$ and $F_{roll}(\omega)$ are plotted in Figures 7.6, 7.7, 7.8 and 7.9 and are indicated in blue. The heave and roll RAO followed from multiplying $F(\omega)$ by $D(\phi)$ (Equation 5.3) and are found the main wave direction, indicated in orange. The wave direction

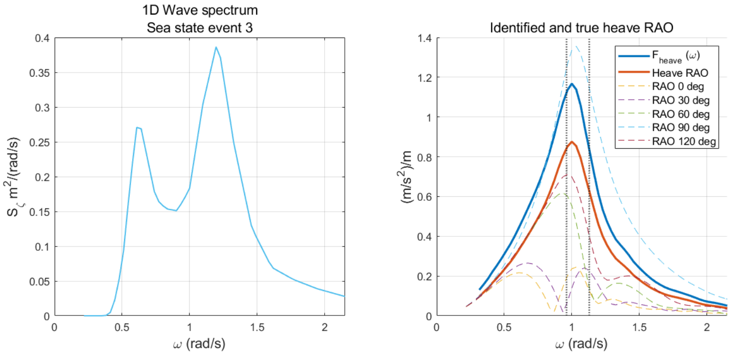

Figure 7.6: 1D wave spectrum and identified and true heave acceleration RAO for sea state event 3 and vessel heading 60 deg

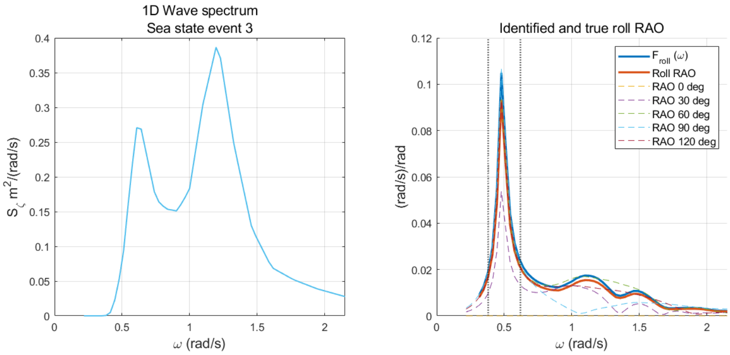

Figure 7.7: 1D wave spectrum and identified and true roll velocity RAO for sea state event 3 and vessel heading 60 deg

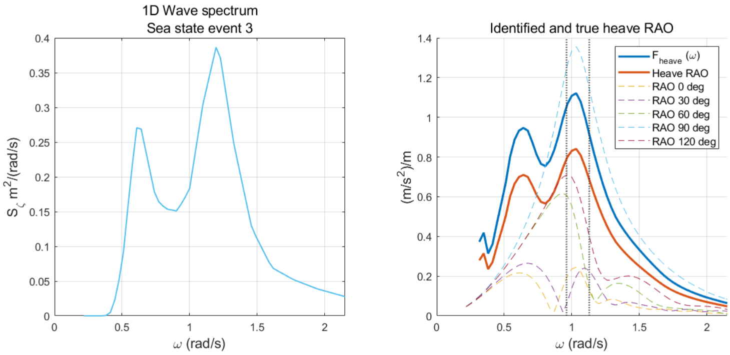

Figure 7.8: 1D wave spectrum and identified and true heave acceleration RAO for sea state event 3 and vessel heading 150 deg

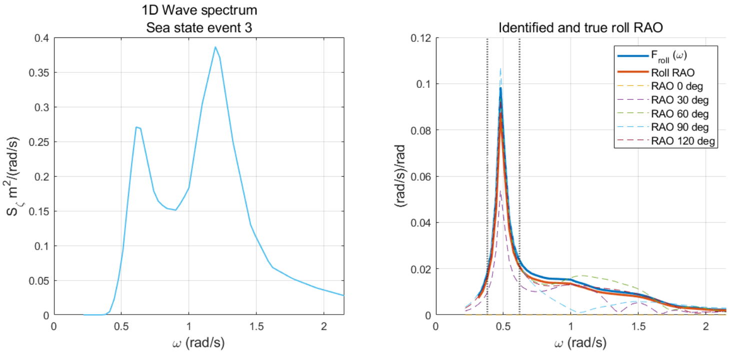

Figure 7.9: 1D wave spectrum and identified and true roll velocity RAO for sea state event 3 and vessel heading 150 deg

The identified RAO seems to approach the true RAO's quite well. From Figures 7.6, 7.7, 7.8 and 7.9, it is shown that the true heave acceleration and roll velocity RAOs, indicated in dashed lines, differ due to different directions of the incoming waves. In Figure 7.6, the identified RAO shapes agrees perfect with the true RAO but the energy is overestimated. This may be due to the fact that the identified RAO is direction independent as it is obtained from a response spectrum and a two-dimensional wave spectrum, with waves approaching the vessel in several directions. Therefore, the identified RAO cannot be directly compared to the true RAOs. Though a peak in the identified RAO could be observed, which is the goal of the identification process. The examination of the natural frequencies from the identified RAO is discussed in next section.

NATURAL FREQUENCIES

The natural heave and roll frequencies are determined from the identified RAOs. The natural frequencies are obtained by observing a peak in the RAO. For the roll motion, this is a straightforward procedure since often one clear peak is visible. For the heave motion, the search for the natural frequency peak had to be specified more, since multiple peaks could be present in the identified RAO, for example in Figure 7.8.

Therefore, prior knowledge of the system was used to indicate a search range in which the heave and roll natural frequencies are expected to be found. The search range was determined in Section 5.6.1. The frequency with belongs to a maximum of the identified RAO in the established search range will be associated to the identified natural frequency. This range is depicted with a dashed line in Figures 7.6, 7.7, 7.8 and 7.9. The true heave and roll natural frequency are retrieved from the synthetic data set and are 1.037 and 0.481 rad/s, respectively. The determined natural frequencies are listed in Tables 7.4 and 7.5. The final natural roll and heave frequency are derived by the mean of all the observed natural frequencies among the chosen sea states.

The results for all the sea state events and vessel headings are depicted in Tables 7.4 and 7.5. The last row and column give the mean of a direction or the sea state. In a few cases, the search algorithm was not able to find a peak in the heave RAO in the specified search range. Therefore, some boxes in Table 7.4 are left empty. Additionally, the true heave and roll natural frequencies (ω_n) are listed in last row of the table.

	30 deg	60 deg	90 deg	120 deg	150 deg	Mean all deg	Unit
Event 1	-	1.032	0.967	1.000	1.065	1.013	rad/s
Event 2	-	1.000	1.032	1.032	1.000	1.008	rad/s
Event 3	1.032	1.032	1.032	1.032	1.032	1.034	rad/s
Event 4	1.032	1.000	1.000	1.032	1.000	1.032	rad/s
Event 5	1.032	1.000	1.000	1.032	1.000	1.013	rad/s
Mean 1-5	1.013	1.032	1.013	1.006	1.019	**1.016**	rad/s
True value						**1.018**	rad/s

Table 7.4: Observed heave natural frequency

	30 deg	60 deg	90 deg	120 deg	150 deg	Mean all deg	Unit
Event 1	0.481	0.481	0.481	0.481	0.481	0.481	rad/s
Event 2	0.481	0.481	0.481	0.481	0.481	0.481	rad/s
Event 3	0.481	0.481	0.481	0.481	0.481	0.481	rad/s
Event 4	0.481	0.481	0.481	0.481	0.481	0.481	rad/s
Event 5	0.481	0.481	0.481	0.481	0.481	0.481	rad/s
Mean 1-5	0.481	0.481	0.481	0.481	0.481	**0.481**	rad/s
True value						**0.481**	rad/s

Table 7.5: Observed roll natural frequency

The identified RAOs are quite pragmatic for intended research interest: to observe a local maxima around the expected natural frequency. It can be seen that a good agreement between the identified natural frequencies and the real natural frequencies known from the synthetic data set, were found using the identified RAOs.

Especially for the roll motion, the identified natural frequencies showed consistent results for every sea state and vessel heading, which agreed with the true natural roll frequency. For the heave motion there were still small differences in the identified natural frequencies. This could be because the true heave RAOs of Figures 7.6 and 7.8 also do not show a peak at the same frequency, while for the roll motion it does. Resonances are usually marked by a local maximum in the response amplitude operator (RAO). Though, resonance does not always appear at the natural frequency [29]. When determining the natural frequency, the right hand side of the equation of motion is zero, while when determining the resonant frequency, the right hand side of the equation of motion contains the frequency-dependent wave loads. Therefore, both the natural frequency and the frequency-dependent wave loads determine the resonant frequency. For the roll motion, the frequency-dependent wave loads differ little for different wave directions and are relatively small compared to the stiffness coefficient. Therefore, the resonant frequency of the roll RAO is pretty stable for different directions. On the other hand, for the heave motion the frequency-dependent wave loads are giving a relatively larger contribution in determining the resonance frequency and differ more per direction compared to the roll motion. Therefore, the heave RAOs differs more for different directions in terms of peak frequency and amplitude.

Despite the small differences of the observed heave natural frequency from Table 7.4, taking the mean of all values still gives an estimate of the natural frequency close to the correct value.

DISPLACEMENT DETERMINATION

Next, the displacement is determined according to Equation 7.1.

$$\nabla = \frac{(\rho g A_{\mathrm{WL}}) - (\omega_{\mathrm{n3}}^2 a_{3,3})}{\omega_{\mathrm{n3}}^2 \rho} \tag{7.1}$$

The input parameters of Equation and 7.1 the identified displacement are listed in Table 7.6. The observed natural heave frequency resulted from the analysis of previous Section. The waterplane area and added mass coefficient were determined in Section 4.4. The final natural heave and roll frequency are derived by the mean of the observed natural frequencies among the chosen sea states and vessel headings, indicated in bold in Tables 7.4 and 7.5. It was shown that the waterplane area and added mass coefficients do not drastically change over a range of different displacements. The waterplane area for the initial displacement is listed in Table 7.6. Additionally, the identified and true displacement are given in the Table.

Parameter	Value	Unit
Waterplane area	1406	m^2
Added mass $a_{3,3}$	7302	tonnes
True ω_{n3}	1.037	$\frac{rad}{s}$
Identified ω_{n3}	1.017	$\frac{rad}{s}$
True displacement	6261	tonnes
Identified displacement	**6376**	**tonnes**

Table 7.6: Input for displacement calculation

From Table 7.6, it can be noticed that a small deviation of the identified natural frequency compared to the true natural frequency (0.20 %) leads to a deviation of the calculation of the displacement compared to the true displacement of (1.67 %).

7.3.3. OPTIMIZATION RESULTS

The following section presents the results of the optimization algorithm. The objective of the optimization procedure is to identify the parameters k_{xx}, k_{yy}, k_{zz}, GM_t, GM_l and B_{visc}. Implementation of the optimization procedure was detailed in Section 6.4.4. The displacement determined in the previous Section has been utilized for the identification of the remaining parameters.

DOF 4 AND 5 - k_{xx}, k_{yy} GM_t, GM_l AND B_{visc}

For the identification of parameters k_{xx}, GM_t and B_{visc} the measured roll response spectrum is utilized. For the identification of parameters k_{yy} and GM_l the measured pitch response spectrum is utilized.

As discussed in Section 6.4.4, the optimization algorithm evaluates the roll and pitch response spectra simultaneously, since the metacentric heights GM_t and GM_l both depend on the vertical coordinate of the centre of gravity. Therefore, the optimization algorithm identifies the GM_t and GM_l by evaluating the cost function for different values of KG. The GM_t, GM_l and vertical coordinate of the centre of gravity KG are related by Equation 6.6. The input parameters for the Equation followed by the determination of the displacement and are given in Table 8.5.

Parameter	Value	Unit
Identified displacement	6376	tonnes
Draft (T)	5.57	m
C_w	0.87	[-]
C_b	0.69	[-]

Table 7.7: Parameters for calculation GM_t and GM_l

In addition, as described in Section 6.4.4, the radius of gyration roll k_{xx} and GM_t are related by Equation 6.3. If the optimization algorithm modifies the GM_t, the k_{xx} is calculated with Equation 7.2. The input parameters for the Equation are given in Table 8.6.

7

$$k_{xx} = \sqrt{\frac{\nabla g GM_t - \omega_{n4}^2 a_{4,4}}{\nabla g \omega_{n4}^2}} \tag{7.2}$$

Parameter	Value	Unit
Identified displacement	6376	tonnes
Added mass $a_{4,4}$	$5.55 \cdot 10^7$	$kg * m^2$
Observed ω_{n4}	0.481	$\frac{rad}{s}$

Table 7.8: Parameters for calculation k_{xx}

Evaluating the optimization algorithm has identified the parameters $k_{xx}, k_{yy}, GM_t, GM_l$ and B_{visc}. For each sea state and vessel heading, the cost function is evaluated for a certain set of parameters. The parameters belonging to the minimum cost function value and thus the final identified parameters are given in Table 7.9.
The identified parameters differ little with the true parameters. This may be due to a deviation of the identified displacement compared to the true displacement.

DOF 6 - k_{zz}

In addition, the parameter k_{zz} is identified by the optimization algorithm using the yaw response spectra of the synthetic data set. The parameters of the final iterations, and

	Initial Test case 1	Initial Test case 2	Identified Test case 1	Identified Test case 2	Unit
k_{xx}	5.40	7.20	6.46	6.43	m
k_{yy}	20.5	26.1	23.15	23.15	m
KG	7.45	7.10	7.25	7.26	m
GM_t	1	1.40	1.18	1.19	m
GM_l	115	139	124.4	124.4	m
B_{visc}	3.00	8	5.26	5.21	% of critical damping

Table 7.9: Comparison of initial and identified parameters: $k_{xx}, k_{yy}, GM_t, GM_l$ and B_{visc} for Test case 1 and 2

hence the final identified k_{zz} are listed in Table 7.10.

	Initial Test case 1	Initial Test case 2	Identified Test case 1	Identified Test case 2	Unit
k_{zz}	20.50	26.10	23.35	23.35	m

Table 7.10: Comparison of initial and identified parameters: k_{zz} for test case 1 and 2

7.3.4. FINAL EVALUATION OF COST FUNCTION AND IDENTIFIED PARAMETERS

The results of the parameter identification procedure are given in Table 7.11. The percentage difference between the true and the identified values of both test cases is depicted in the table as well. The initial and final values of the cost function $f(x)$ are depicted Table 7.12. In addition, the response spectra for Event 3 and vessel heading 30 and 60 are shown in Figures 7.10 and 7.11. This case study examined if the identification strategy is suitable for parameter identification. By knowing the true values of the synthetic data set, the identified parameters can be directly compared to the identified ones.

From Table 7.11 it is shown that using multiple wave spectra and vessel headings in the identification process, led to good results. Some of the identified parameter values differ a little from the true values. This is likely due a higher value of identified displacement, which was the first identified parameter. The identified displacement was used to identify the remaining parameters. Therefore, the remaining parameters differ slightly to the true ones, for example the viscous roll damping percentage has to be higher to counteract the too high value of the displacement. However, those deviations are small and the identified parameters still approach to the true values. Therefore, the strategy is applied to a second case study in which real onboard motion measurements are used. The setup and results are discussed in next chapter.

Parameter (**p**)	True	Identified Test case 1	Identified Test case 2	Unit	% difference Test case 1	% difference Test case 2
∇	6261	6376	6376	tonnes	1.67 %	1.67 %
k_{xx}	6.48	6.43	6.44	m	0.77 %	0.61 %
k_{yy}	23.35	23.15	23.15	m	0.86 %	0.86 %
k_{zz}	23.35	23.35	23.35	m	0 %	0 %
GM_t	1.20	1.18	1.19	m	1.67 %	0.83 %
GM_l	127	124.4	124.6	m	2.05 %	1.89 %
B_{visc}	5.00	5.26	5.21	% of critical damping	5.2 %	4.2 %

Table 7.11: Initial and identified parameters for Test case 1 and 2

DOF	Initial $f(x)$ Test case 1	Initial $f(x)$ Test case 2	Final $f(x)$ Test case 1	Final $f(x)$ Test case 2
Surge	0.109	0.063	0.008	0.009
Sway	0.337	0.088	0.010	0.011
Heave	0.037	0.037	0.007	0.007
Roll	0.448	0.127	0.002	0.009
Pitch	0.115	0.072	0.008	0.003
Yaw	0.156	0.109	0.008	0.008
Sum all DOF	1.201	0.496	0.043	0.048

Table 7.12: Initial and final evaluation of cost function for Test case 1 and 2

7

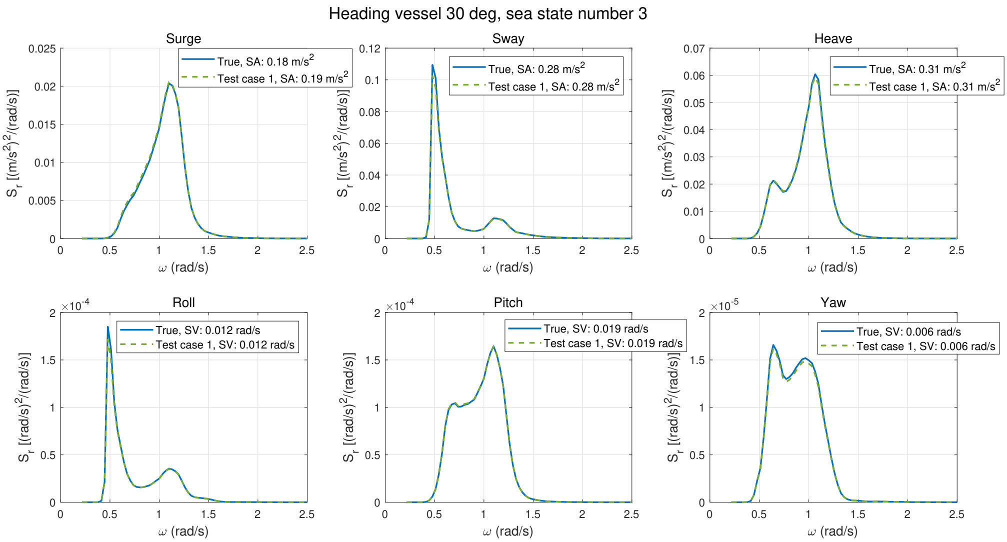

Figure 7.10: Comparison of the synthetic and identified response spectra for test case 1 computed for Event 3 ($T_p = 6s$ and $10s$) and vessel heading 30 deg

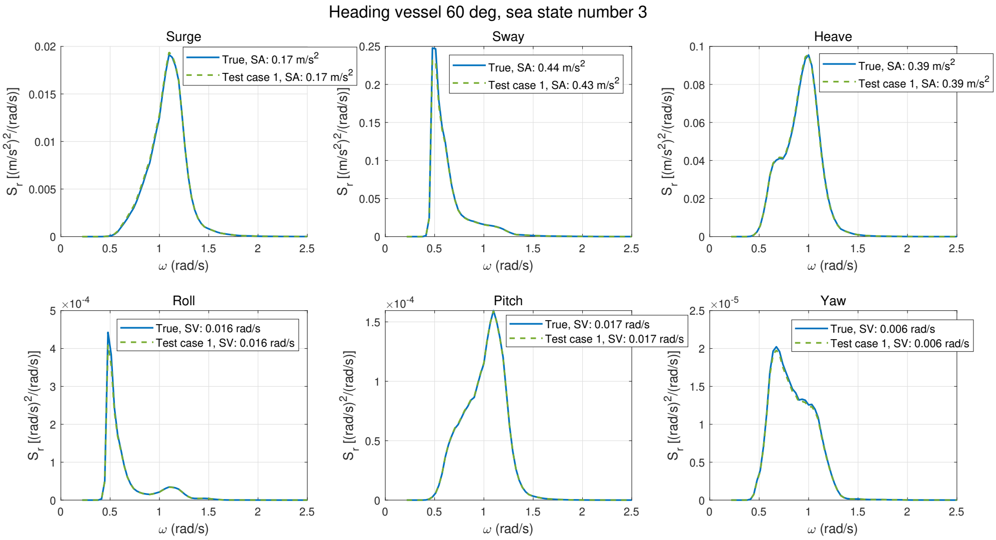

Figure 7.11: Comparison of the synthetic and identified response spectra for test case 1 computed for Event 3 ($T_p = 6s$ and $10s$) and vessel heading 60 deg

8

CASE STUDY 2

8.1. INTRODUCTION

In the previous chapter, the parameter identification procedure was tested on a synthetic data set. By knowing the true parameters of the data set, it could be investigated whether the procedure identifies the correct parameters. In this chapter, a second case study is discussed, which has the purpose of investigating whether it is possible to apply the parameter identification procedure to real onboard measurement data. First, the setup for this second case is defined, including the initial input parameters of the vessel, metocean conditions and information regarding the measurements. Thereafter, the results of the identification procedure are shown and the identified parameters are verified against a second measurement data set.

8.2. CASE SETUP

The analysis was performed on the same vessel as in the previous case study, the Acta Auriga. Before running the identification algorithm, an initial prediction of the vessel's response was made with initial parameters as input for the model. The responses are calculated for the location of the MRU. The MRU was placed near the centre of gravity at [x=40.8, y=0, z= 12.1] w.r.t. the baseline of the vessel. A set of initial parameters have been chosen and are listed in Table 8.1.

Parameter (**p**)	Symbol	Value	Unit
Displacement	∇	6274	tonnes
Radii of gyration for roll	k_{xx}	6.48	m
Radii of gyration for pitch	k_{yy}	23.35	m
Radii of gyration for yaw	k_{zz}	23.35	m
Transverse metacentric height	GM_t	1.2	m
Longitudinal metacentric height	GM_l	127	m
Viscous roll damping	B_{visc}	5	% of crit. damping

Table 8.1: True parameters values for the synthetic dataset

8.2.1. MEASURED DATA

The measured data which is suitable for identification was described in in Section 1.3.2. The identification procedure is applied to "free-floating" events to identify the selected parameters. This case study assesses the performance of the identification procedure of two days. First, the identification procedure is applied to the measured responses of the 17^{th} of October 2021, in which four free-floating events occurred. The significant wave height of that day was between 0.98 and 1.29 m. The other day that is assessed is the 12^{th} of November, in which 6 free floating events occurred and the significant wave height was higher, between 1.6 and 2.0 m. First, the results of the 17^{th} of October 2021 will be discussed in detail, to show step-by-step the working principle of the identification procedure. Next, only the final results, improvements and interpretation of measurement day 2, the 12^{th} of November will be presented

8.3. RESULTS - 17/10/2021

This section shows the results of the identification procedure applied to measured data of the 17^{th} of October. The identified parameters are verified for measurements of the 16^{th} of October.

8.3.1. METOCEAN CONDITIONS

A timeline of the 17^{th} of October 2021 and the measured events are depicted in Figure 8.1. The metocean conditions during those events were retrieved from a nowcast weather report provided by Infoplaza. The sea states, in the form of 2D wave spectra, are shown in Figure 8.2. The free-floating events will be referred to as Measurement events 1-4.

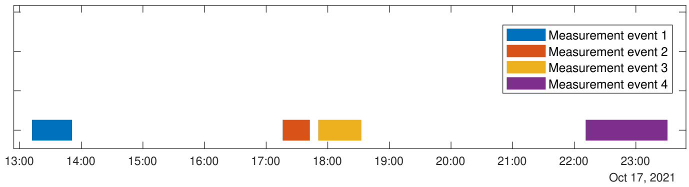

Figure 8.1: Timeline Measurement events 1-4 - 17/10/2021

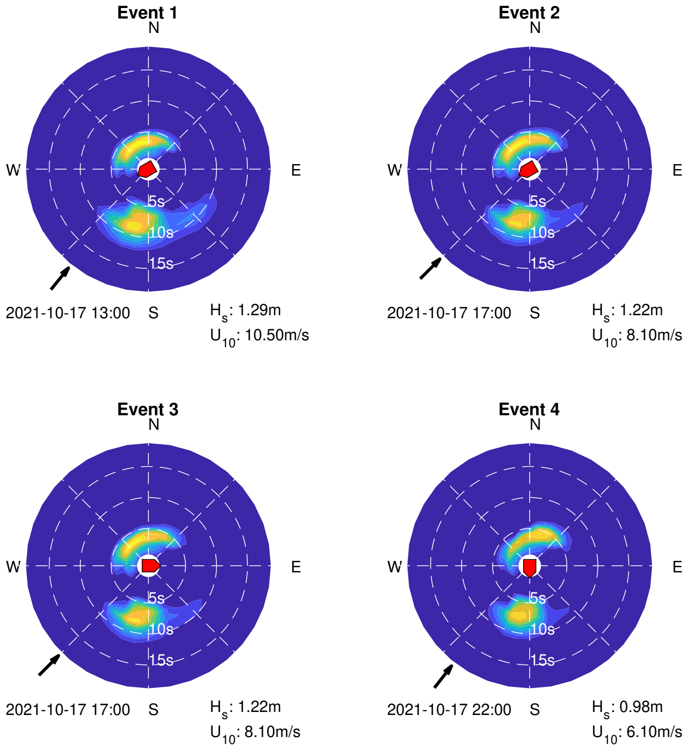

Figure 8.2: 2D wave spectra for Measurement events 1-4 - 17/10/2021

Wind and swell seas are observed during the Measurement events. It can be observed that the sea states remain relatively constant throughout the day in terms of significant wave height and peak periods. The significant wave height was between 0.98 and 1.29 m. The wind seas are observed at a $T_p = 4s$, the swell seas are observed around $T_p = 10s$.

8.3.2. FIRST EVALUATION COST FUNCTION

The measured translational accelerations and angular velocities by the MRU of Measurement events 1-4 are transformed to the frequency domain using Fourier transformation, discussed in Section 3.3.3. The response spectra are predicted by the vessel response model for Measurement events 1-4 using the initial parameters from Table 8.1 and the wave spectra of Figure 8.2. The initial deviations between both response spectra are computed by evaluating the function $f(x)$ of Equation 6.5. The mean of $f(x)$ among Measurement events 1-4 for each DOF are shown in Table 8.11. For further illustration, the measured and initially predicted response spectra for Measurement event 2 and 3 are shown in Figures 8.3 and 8.4. The significant acceleration and significant velocity are indicated in the legend of the figures as well by the abbreviation "SA" and "SV", respectively. By comparing the significant motions, it is possible to determine whether the initial prediction and measurement were significantly off. The computation of the significant motions of the measurements was discussed in Section 3.3.3.

In the figures, the blue solid line represents the response spectrum obtained from the measurements. The green dotted line represents the predicted response spectrum, determined by the model and the initial parameters. From the figures, it can be observed that the surge motion is highly underpredicted compared to the measurements. The heave motion prediction agrees the most among all the DOF. The parameter identification procedure aims to find parameters fitting the measured response spectra better than the initial prediction. The results will be discussed in the following sections.

DOF	$f(x)$
Surge	0.34
Sway	0.21
Heave	0.18
Roll	0.26
Pitch	0.22
Yaw	0.22
Total	1.44

Table 8.2: Evaluation of cost function for Measurement event 1-4 and initial prediction

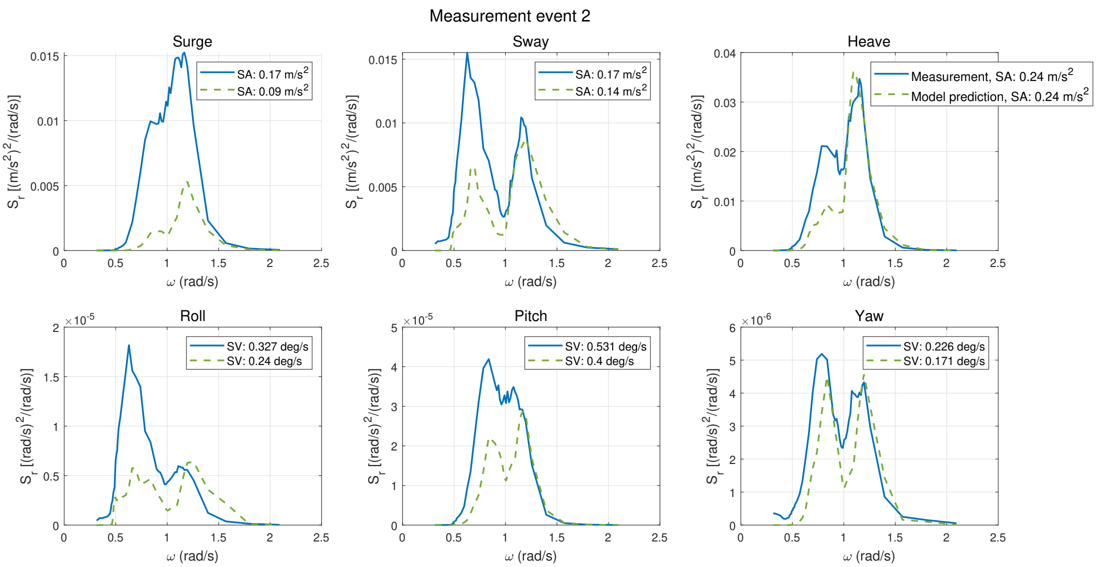

Figure 8.3: Comparison of the response spectra for the measurement and the initial prediction computed of Measurement event 2 - 17/10/2021

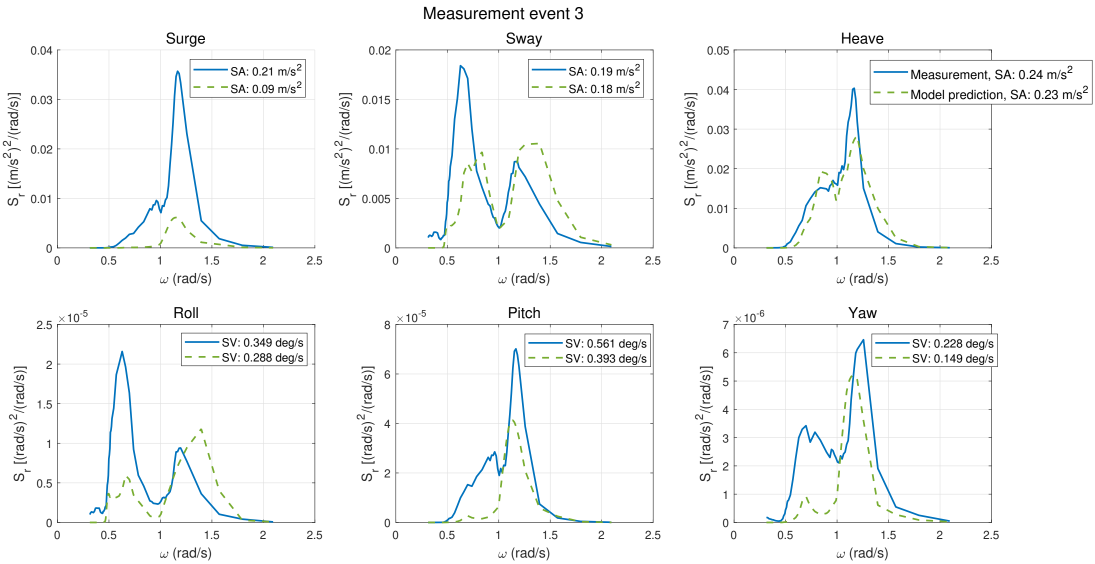

Figure 8.4: Comparison of the response spectra for the measurement and the initial prediction computed of Measurement event 3 - 17/10/2021

8.3.3. RAO IDENTIFICATION

This section presents the results of the RAO identification. Similar as described in Section 7.3.2, the RAO is identified using the directional shape, the vessel response and wave energy spectrum. The RAO identification procedure, described in Chapter 5, has been followed for the heave and roll motion for each of the Measurement events 1-4. As an example, figures 8.5 and 8.6 show the 1D wave spectrum and the measured heave and roll response spectra for Measurement events 1 and 2.

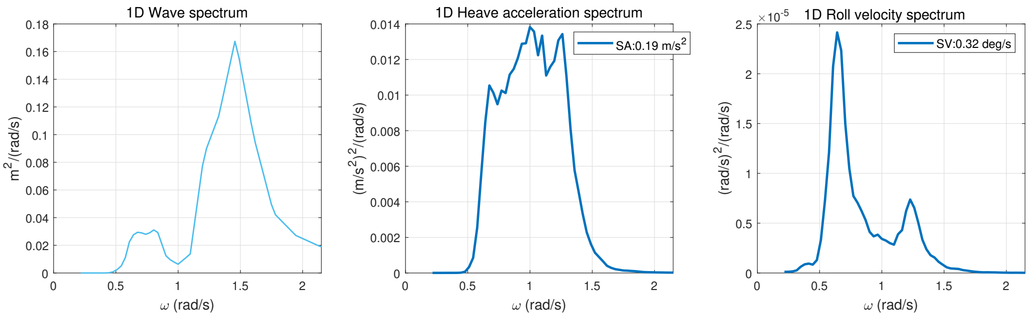

Figure 8.5: 1D wave spectrum and heave and roll response spectra of Measurement event 1 - 17/10/2021

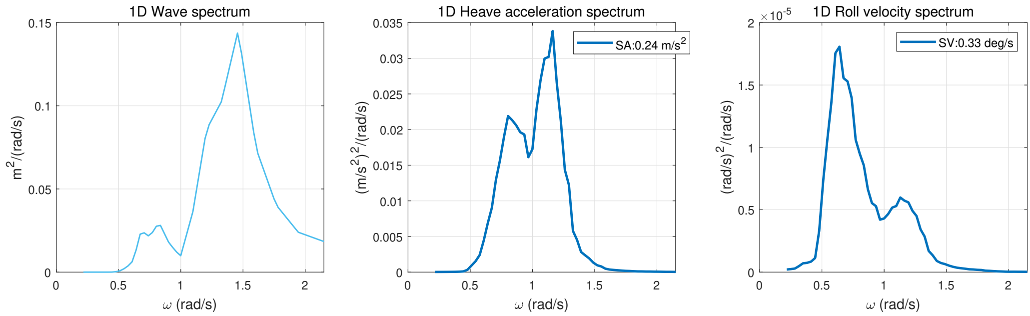

Figure 8.6: 1D wave spectrum and heave and roll response spectra of Measurement event 2 - 17/10/2021

From the data of Figures 8.5 and 8.6, the heave acceleration RAO and roll velocity RAO has been identified and are shown in Figures 8.7, 8.10, 8.9 and 8.10. This RAO is referred to as "identified RAO" in this chapter. In the left plot of the figures, the wave spectrum is shown. In the right plot of the figures, the identified RAO is shown as well as the initial RAOs. The initial RAOs are computed with the model and initial parameters, for different wave directions. The identified $F_{heave}(\omega)$ and $F_{roll}(\omega)$ are plotted in Figures 7.6, 7.7, 7.8 and 7.9 and are indicated in blue. The identified heave and roll RAO followed from multiplying $F(\omega)$ by $D(\phi)$ (Equation 5.3) and is indicated in orange.

At low frequencies (below $\omega = 0.55$ rad/s), where little wave energy was predicted, but in which the vessel actually had measured response energy, the identified RAO shoot up to remarkably high values. Those value were unrealistic and not useful. The cause of those high values was probably because there was actually more wave energy at those frequencies than was predicted. Those extremely high RAO amplitude values have been neglected since they do not add value to the purpose of the RAO identification. Therefore, the identified RAO starts around $\omega = 0.5$ rad/s. The identified RAOs in orange are given for the wave direction of 220 degrees.

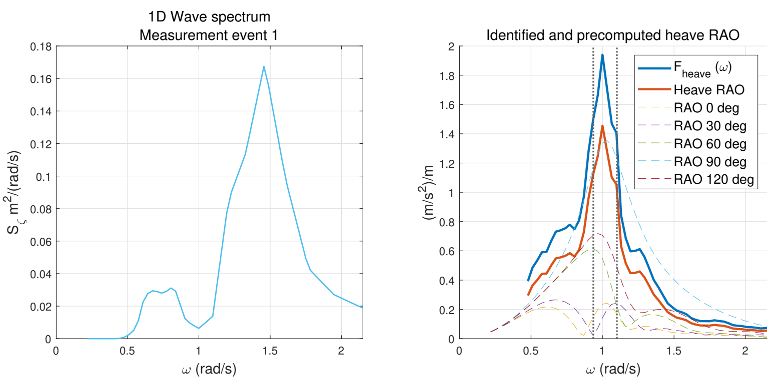

Figure 8.7: 1D wave spectrum and identified and precomputed heave acceleration RAO for Measurement event 1 - 17/10/2021

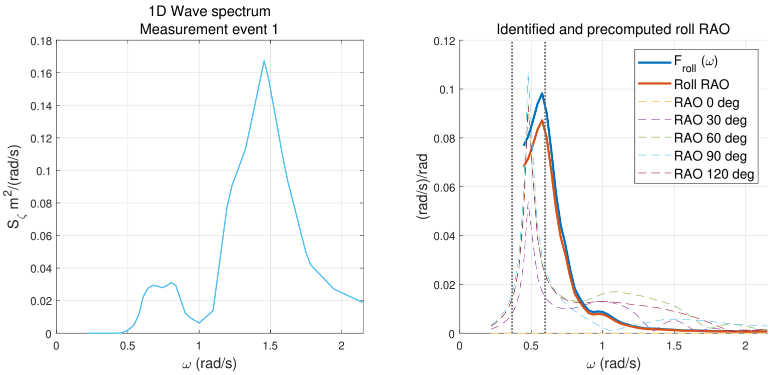

Figure 8.8: 1D wave spectrum and identified and precomputed roll velocity RAO for Measurement event 1 - 17/10/2021

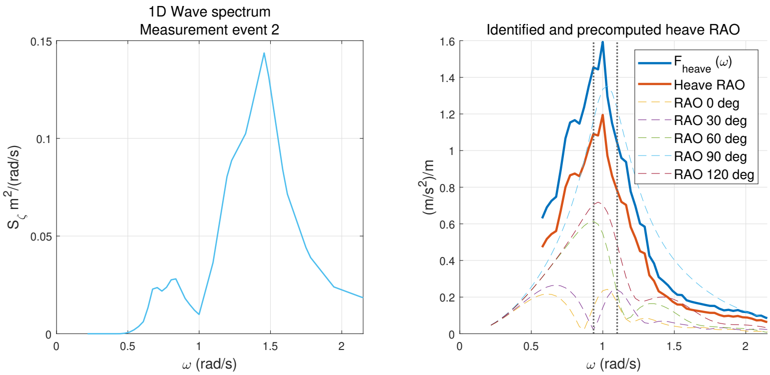

Figure 8.9: 1D wave spectrum and identified and precomputed heave acceleration RAO for Measurement event 2 - 17/10/2021

8

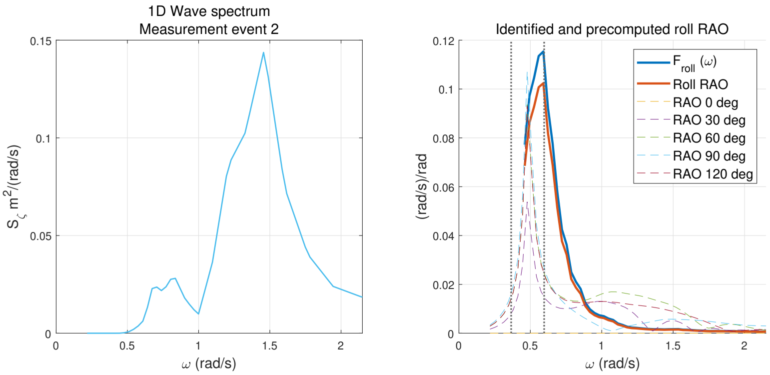

Figure 8.10: 1D wave spectrum and identified and precomputed roll velocity RAO for Measurement event 2 - 17/10/2021

NATURAL FREQUENCIES

The natural heave and roll frequencies are determined from the identified RAOs. A search range was determined in Section 5.6.1 in which the heave and roll natural frequencies are expected to be found. The frequency with belongs to a maximum of the identified RAO in the established search range will be associated to the identified natural frequency. This range is depicted with a dashed line in Figures 8.7, 8.10, 8.9 and 8.10. The natural frequencies belonging to the observed peaks for all Measurement events and the mean among all the events are depicted in Table 8.3. The final natural roll and heave frequency are derived by the mean of all the observed natural frequencies among the events.

	ω_{n3}	ω_{n4}	Unit
Measurement event 1	0.999	0.591	$\frac{rad}{s}$
Measurement event 2	1.03	0.576	$\frac{rad}{s}$
Measurement event 3	1.03	0.543	$\frac{rad}{s}$
Measurement event 4	0.999	0.576	$\frac{rad}{s}$
Mean 1-4	**1.01**	**0.571**	$\frac{rad}{s}$

Table 8.3: Observed heave natural frequency

DISPLACEMENT DETERMINATION

The displacement is determined according to Equation 7.1. The input parameters of the Equation are listed in Table 8.4, as well as the resulting displacement identification. The observed natural heave frequency resulted from the analysis of previous Section. The final natural heave and roll frequency are derived by the mean of the observed natural frequencies among all the events. For this frequency, the corresponding added mass coefficient $a_{3,3}$ is found.

Parameter	Value	Unit
Waterplane area	1406	m^2
Added mass $a_{3,3}$	7302	tonnes
Observed ω_{n3}	1.01	$\frac{rad}{s}$
Initial displacement	6261	tonnes
Identified displacement	**6663**	**tonnes**

Table 8.4: Parameters and identified displacement

8.3.4. OPTIMIZATION RESULTS

The following section presents the results of the optimization algorithm. The objective of the optimization procedure is to identify the parameters k_{xx}, k_{yy}, k_{zz}, GM_t, GM_l and B_{visc}. The parameters are identified in a similar manner as in the previous case study. The displacement determined in the previous section has been utilized for the identification of the remaining parameters.

DOF 4 AND 5 - k_{xx}, k_{yy} GM_t, GM_l AND B_{visc}

For the identification of parameters k_{xx}, GM_t and B_{visc} the measured roll response spectrum is utilized. For the identification of parameters k_{yy} and GM_l the measured pitch response spectrum is utilized.

The GM_t, GM_l and vertical coordinate of the centre of gravity KG are related by Equation 6.6. The input parameters for the Equation followed by the determination of the displacement and are given in Table 8.5.

Parameter	Value	Unit
Identified displacement	6663	tonnes
Draft (T)	5.78	m
C_w	0.87	[-]
C_b	0.69	[-]

Table 8.5: Parameters for calculation GM_t and GM_l

In addition, as described in Section 6.3.2, the radius of gyration roll k_{xx} and GM_t are related by Equation 6.3. If the optimization algorithm modifies the GM_t, the k_{xx} is calculated with Equation 7.2. The input parameters for the Equation are given in Table 8.6.

Parameter	Value	Unit
Identified displacement	6663	tonnes
Added mass $a_{4,4}$	$5.55 \cdot 10^7$	kg$*m^2$
Observed ω_{n4}	0.571	$\frac{rad}{s}$

Table 8.6: Parameters for calculation k_{xx}

Evaluating the optimization algorithm has identified the parameters k_{xx}, k_{yy}, KG, GM_t,

GM_l and B_{visc}. For each Measurement event 1-4, the cost function is evaluated for a certain set of parameters. The parameters belonging to the minimum cost function value and thus the final identified parameters are given in Table 8.7.

	Initial	Identified	Unit
k_{xx}	6.48	5.92	m
k_{yy}	23.35	21.33	m
KG	7.32	6.92	m
GM_t	1.2	1.44	m
GM_l	127	121	m
B_{visc}	5.00	5.7	% of critical damping

Table 8.7: Comparison of initial and identified parameters: k_{xx}, k_{yy}, KG, GM_t, GM_l and B_{visc} for Measurement event 1-4

DOF 6 - k_{zz}

In addition, the parameter k_{zz} is identified by the optimization algorithm using the yaw response spectra. The parameters of the final iterations, and hence the final identified k_{zz} are listed in Table 8.8.

	Initial	Identified	Unit
k_{zz}	23.35	21.90	m

Table 8.8: Comparison of initial and identified parameter: k_{zz} for Measurement event 1-4

8.3.5. COMPUTATION TIME

The time required to run the algorithm has been measured. The algorithm has run for the roll, pitch and yaw motion. The computation time (CPU time) as well as the reason for termination are listed in Table 8.9. The possible reasons for termination were discussed in Section 6.4.1.

8

	CPU time	Reason termination
Roll + pitch	1881 s	XTol satisfied
Yaw	421 s	XTol satisfied

Table 8.9: CPU time and reason for termination of algorithm

8.3.6. FINAL EVALUATION OF COST FUNCTION AND IDENTIFIED PARAMETERS

The results of the parameter identification procedure are given in Table 8.10. The identified displacement is somewhat higher than the initial assumption. The radii of inertia terms are thereby somewhat lower than the initial values, which could be a result of the increase of displacement.

The initial and final values of the cost function $f(x)$ are depicted Table 8.11. Initially, the sum of cost function of all DOF was 1.33, this improved to 1.09, which is an improvement of 18 %. Especially, the roll and pitch motion prediction yielded an improvement with the identified parameters. The measured, initial and identified response spectra for Measurement events 2 and 3 are shown in Figures 8.11 and 8.12. Here, the measured responses are indicated in blue, the initial predictions with the initial parameter are indicated in green and the results obtained with the identified parameters are indicated in red. From the figures, it can be seen that the identified parameters give a better fit to the measured response spectra compared to the initial parameters, however, there are still some deviations.

Parameter (**p**)	Symbol	Initial	Identified	Unit
Displacement	∇	6274	6663	tonnes
Radii of gyration for roll	k_{xx}	6.48	5.92	m
Radii of gyration for pitch	k_{yy}	23.35	21.33	m
Radii of gyration for yaw	k_{zz}	23.35	21.90	m
Transverse metacentric height	GM_t	1.20	1.44	m
Longitudinal metacentric height	GM_l	127	121	m
Viscous roll damping	B_{visc}	5.0	5.7	% of crit. damping

Table 8.10: Initial and identified parameters values - 17/10/2021

DOF	$f(x)$ Initial	$f(x)$ After identification
Surge	0.34	0.33
Sway	0.21	0.18
Heave	0.12	0.11
Roll	0.25	0.16
Pitch	0.22	0.14
Yaw	0.19	0.17
Total	1.33	1.09

Table 8.11: Initial and final evaluation of cost function

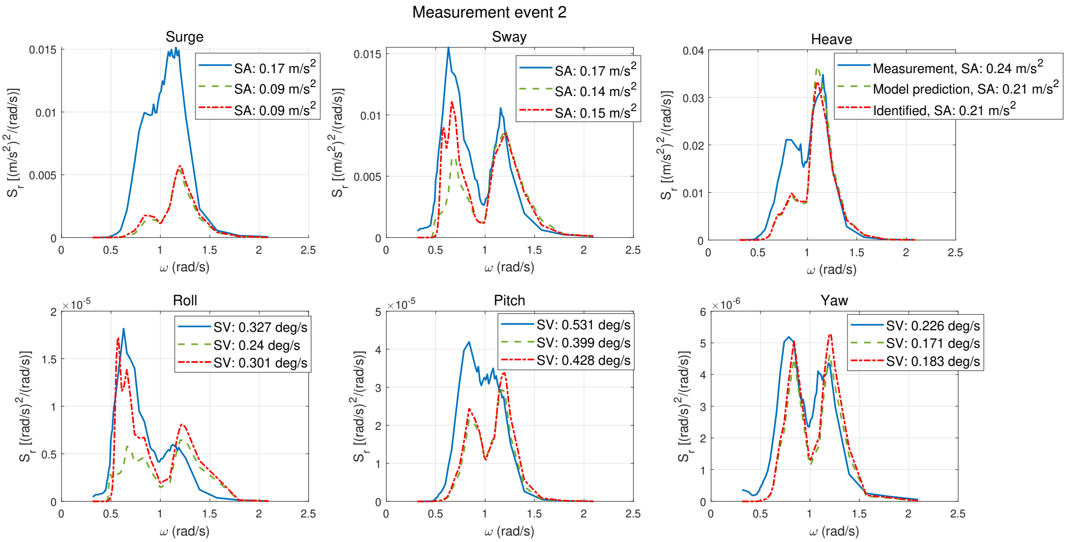

Figure 8.11: Comparison of measured, initial and identified response spectra Measurement event 2 - 17/10/2021

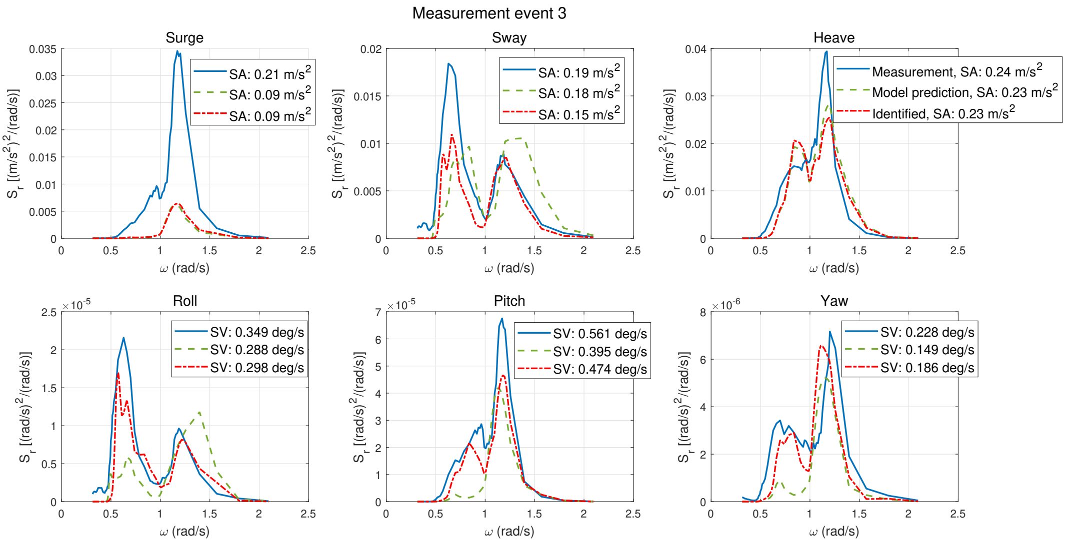

Figure 8.12: Comparison of measured, initial and identified response spectra Measurement event 3 - 17/10/2021

8.4. VERIFICATION

The identified parameters of previous section are obtained from measurements of the 17^{th} of October. In order to verify the identified parameters, a verification test is conducted on another set of measurement data. The data set for the verification step is used to verify how well the identified parameters fit to motions predictions with changed sea conditions.

The verification data is a collection of motion measurements from the 16^{th} of October, the day before the identification day (the 17^{th} of October). The response spectra computed with the identified parameters and the response spectra of the measured verification data set are compared. The measured verification data consists of three "free-floating" events for which the metocean conditions are depicted in Figure 8.13. Those events will be referred to as Verification events 1-3. The initial predictions of the model were obtained by using the metocean conditions of Figure 8.13 as an input and the initial parameter set discussed in Section 8.2.

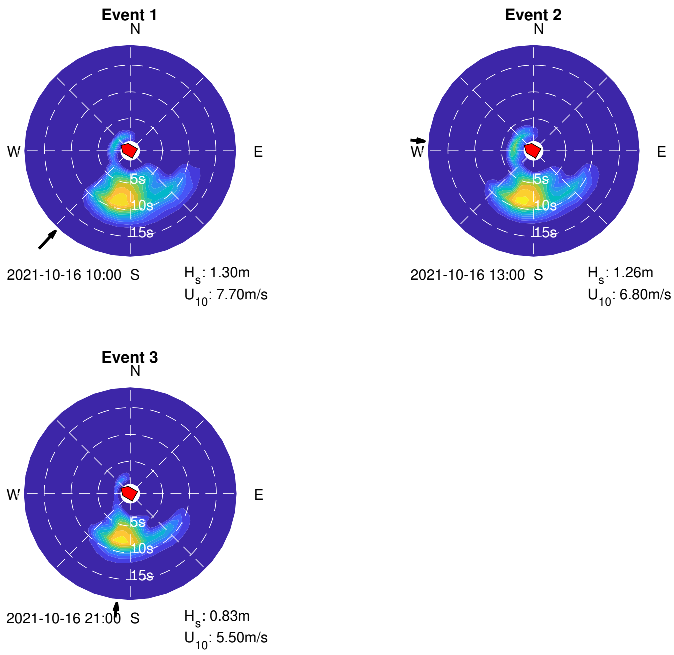

Figure 8.13: 2D wave spectra for free-floating events - 16/10/2021

8.4.1. VERIFICATION RESULTS

Results are acquired by computing RAOs with the identified parameters of previous section. With those RAOs and the wave spectra of the Verification events 1-3 (Figure 8.13), response spectra are computed and compared to the measured response spectra. The results of the verification test are given in Table 8.12. It presents the initial and final values of the cost function $f(x)$ using the initial and identified parameters. Initially, the sum of cost function of all DOF was 1.21, this improved to 1.09. Especially, the sway, roll and pitch motion prediction yielded the most improvements with the identified parameters. In addition, the measured, initial and identified response spectra for Events 1-3 are shown in Figures 8.14, 8.15 and 8.16. The predicted roll response spectrum now give a much better fit to the measured response spectra, mainly at verification events 1 and 2. This indicates that the identified parameters that determine the predicted roll motion have a higher probability of being near the true values than the initial values.

DOF	$f(x)$ Initial	$f(x)$ After identification
Surge	0.25	0.24
Sway	0.16	0.12
Heave	0.30	0.28
Roll	0.16	0.14
Pitch	0.17	0.14
Yaw	0.18	0.17
Total	1.21	1.09

Table 8.12: Initial and final evaluation of cost function

Figures/verification event1DEGup-eps-converted-to.pdf

Figure 8.14: Comparison of the measured, initial prediction and prediction after identification response spectra for Verification event 1 - 16/10/2021

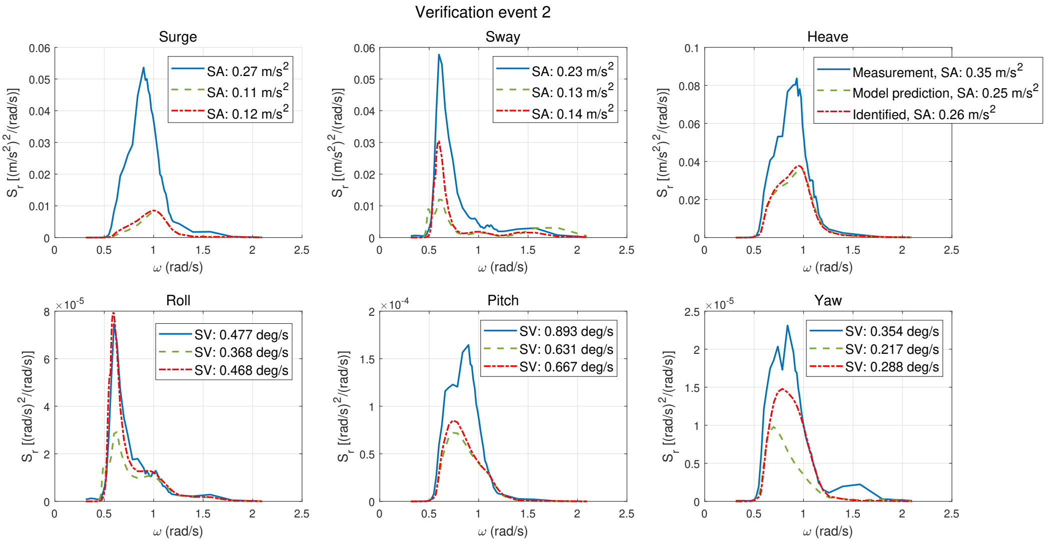

Figure 8.15: Comparison of the measured, initial prediction and prediction after identification response spectra for Verification event 2 - 16/10/2021

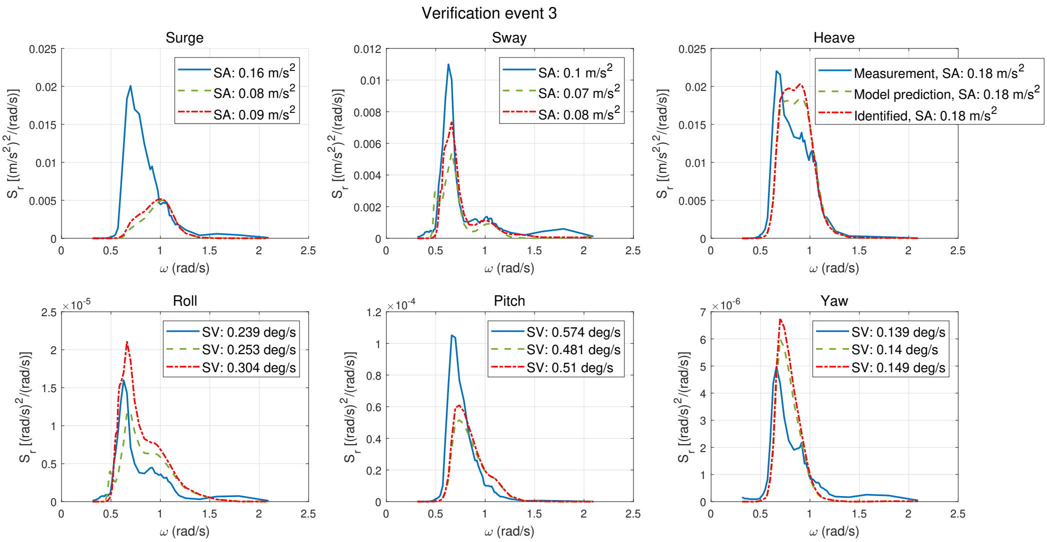

Figure 8.16: Comparison of the measured, initial prediction and prediction after identification response spectra for Verification event 3 - 16/10/2021

8.5. RESULTS - 12/11/2021

This section shows the results of the identification procedure applied to measured data of November 12. The H_s of the 12^{th} of November was twice as high as the H_s of the analysis of prior results. In the past, it was shown that higher H_s (from 2 m) are easier to predict than lower H_s by metocean data providers. Besides, at greater H_s, the ship's excitations are typically larger and easier to quantify. Therefore, the identification procedure is tested on measurements where the H_s was between 1.6-2 m. First, the metocean conditions of the measurement day are presented. Thereafter, the results of the identification process are shown: the identified RAOs, the natural frequencies and the identified parameters.

8.5.1. METOCEAN CONDITIONS

The sea states, in the form of 2D wave spectra, are shown in Figure 8.17. The free-floating events are referred to as Measurement events 1-6.

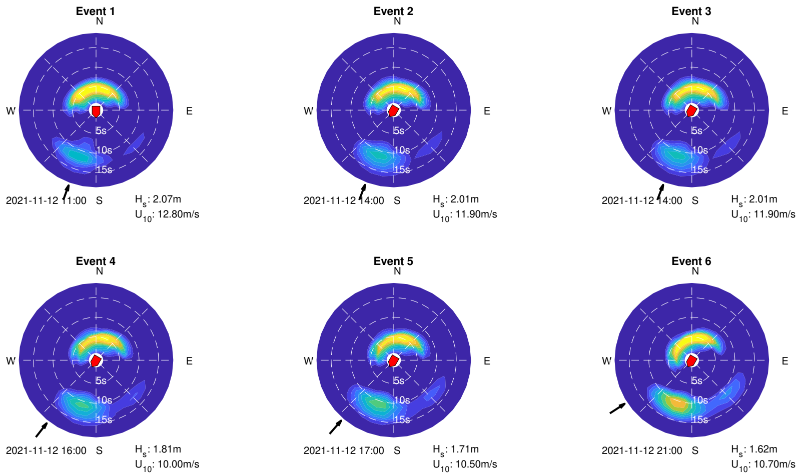

Figure 8.17: 2D wave spectra for Measurement events 1-6 - 12/11/2021

8.5.2. RAO IDENTIFICATION

The RAO identification procedure, described in Chapter 5, has been followed for the heave and roll motion for each of the Measurement events 1-6. The results of Measurement events 2 and 4 are shown in this section. Figures 8.18 and 8.19 show the 1D wave spectrum and the measured heave and roll response spectra for Measurement events 1 and 2.

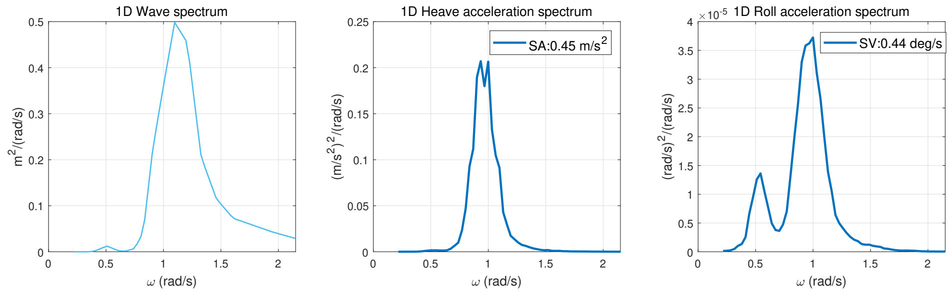

Figure 8.18: 1D wave spectrum and heave and roll response spectra of Measurement event 2 - 12/11/2021

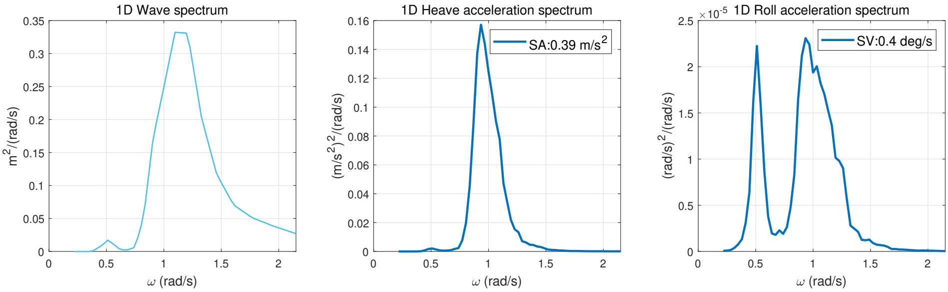

Figure 8.19: 1D wave spectrum and heave and roll response spectra of Measurement event 4 - 12/11/2021

From the data of Figures 8.18 and 8.19, the heave acceleration RAO and roll velocity RAO has been identified. The identified RAOs of Measurement events 2 and 4 are shown in Figures 8.20, 8.21, 8.22 and 8.23. The identified RAOs in orange are given for the wave direction of 220 degrees.

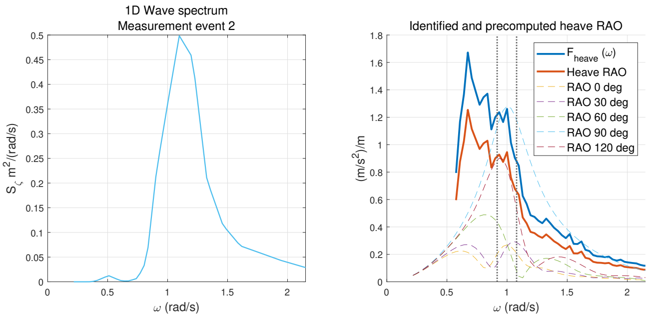

Figure 8.20: 1D wave spectrum and identified and precomputed heave acceleration RAO for Measurement event 2 - 12/11/2021

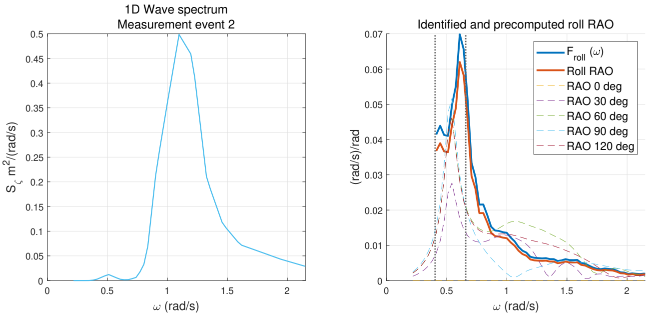

Figure 8.21: 1D wave spectrum and identified and precomputed roll velocity RAO for Measurement event 2 - 12/11/2021

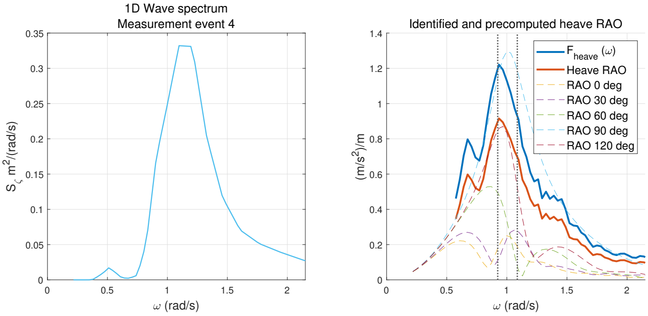

Figure 8.22: 1D wave spectrum and identified and precomputed heave acceleration RAO for Measurement event 4 - 12/11/2021

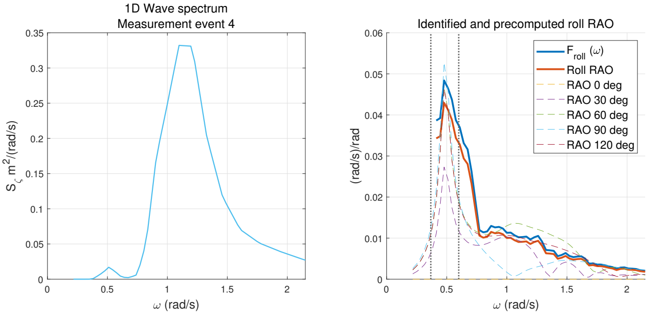

Figure 8.23: 1D wave spectrum and identified and precomputed roll velocity RAO for Measurement event 4 - 12/11/2021

8

NATURAL FREQUENCIES AND DISPLACEMENT IDENTIFICATION

The natural heave and roll frequencies are determined from the identified RAOs. For most of the identified RAOs, a clear maximum was visible. The natural heave and roll frequencies belonging to the observed peaks for all Measurement events and the mean among all the events are depicted in Table 8.13.

The identified heave RAO of Measurement event 2, depicted in Figure 8.20, shows no clear maximum which could be pinpointed to the heave natural frequency. The identified RAO has an irregular and unrealistic shape. This could be due to the presence of more wave energy than was initially predicted at lower frequencies (below 0.7 rad/s). This resulted in measured excitations in that frequency range that were not predicted. This was the case for both days which were assessed. For the RAO identification, this resulted in unreliable identified RAOs with unexpected shapes (Figure 8.20). This made it difficult to pinpoint the natural frequency and highlights the importance of an accurate weather forecast. In those cases, no natural frequency was found, indicated by '-' in Table 8.13. Though, in many other cases the identified RAO's shape approaches the expected one and a clear natural frequency could be found. By taking the average among all the results them seems to give a good representation of the true natural frequency.

	ω_{n3}	ω_{n4}	Unit
Measurement event 1	0.996	-	$\frac{rad}{s}$
Measurement event 2	-	0.608	$\frac{rad}{s}$
Measurement event 3	0.996	0.478	$\frac{rad}{s}$
Measurement event 4	0.967	0.478	$\frac{rad}{s}$
Measurement event 5	0.996	0.543	$\frac{rad}{s}$
Measurement event 6	1.032	0.446	$\frac{rad}{s}$
Mean 1-6	**0.998**	**0.512**	$\frac{rad}{s}$

Table 8.13: Observed heave and roll natural frequency

The displacement is determined according to Equation 7.1 and the observed natural heave frequency. The input parameters of the equation are listed in Table 8.14, as well as the resulting displacement identification.

Parameter	Value	Unit
Waterplane area	1406	m^2
Added mass $a_{3,3}$	7302	tonnes
Observed ω_{n3}	0.998	$\frac{rad}{s}$
Initial displacement	6261	tonnes
Identified displacement	**6805**	**tonnes**

Table 8.14: Parameters and identified displacement

8.5.3. RAO IDENTIFICATION WITH METOCEAN MEASUREMENTS

An additional analysis is executed for the RAO identification for the data from the 12^{th} of November. In the previous analysis of this research, the identification procedure used weather forecasts as input for the wave spectra. As mentioned earlier, it is commonly understood that weather forecasts consist of an amount of uncertainty. Therefore, this analysis compares the previously obtained results of the RAO identification with results obtained with measured wave spectra. Access to measurements of metocean conditions from the 12th of November was provided by NextOcean, which deployed wave buoys at the location of interest to measure the metocean conditions. The measured 1D wave spectra provided by NextOcean as well as the predicted 1D wave spectra provided by Infoplaza of all the Measurement events 1-6 of the 12th of November are depicted in Figure 8.24.

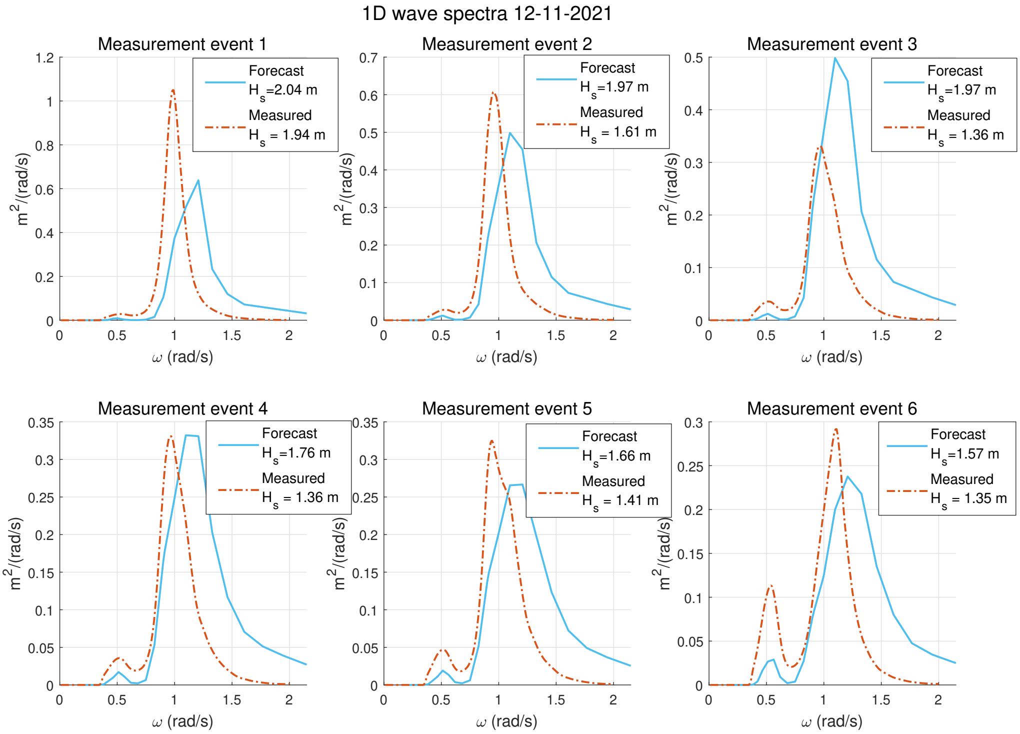

Figure 8.24: 1D wave spectra obtained with measurements and forecasts for Measurement events 1-6 - 12/11/2021

By comparing the 1D wave spectra in Figure 8.24, it can be observed that the 1D spectra obtained with the metocean measurements show a shift in the peak period to the left on the x-axis. Besides, the measured H_s was in all the 6 events was lower than the predicted H_s by the weather forecasts. This is also depicted in the legend of Figure 8.24. In addition, the measured wave spectra show more wave energy at the lower frequencies (below 0.6 rad/s). This was also expected since the identified RAO with the weather forecasts shot to extremely high and unrealistic values for low frequencies, as discussed in Section 8.5.2.

Next, the RAO identification procedure is applied to identify the heave acceleration RAO and roll velocity RAO with the measured 2D wave spectra and the measured vessel motions. The identified RAOs of Measurement events 2 and 4 are shown in Figures 8.27, 8.26, 8.27 and 8.28. The identified $F(\omega)_{roll}$ and RAOs from the metocean forecasts are shown as solid lines in blue and orange, respectively. The identified $F(\omega)_{roll}$ and RAOs from the metocean measurements are shown in the figures as dashed lines in yellow and purple, respectively. The identified $F(\omega)_{roll}$ and identified roll RAO with the metocean forecasts are left out of the graphs in Figure 8.28 to keep the graphs more clear. This was because those graphs had a lot of overlap with the ones obtained with the metocean measurements. Figure 8.23 already showed the identified $F(\omega)_{roll}$ and identified roll RAO obtained with the metocean forecasts. The identified RAOs in orange and purple are given for the wave direction of 220 degrees.

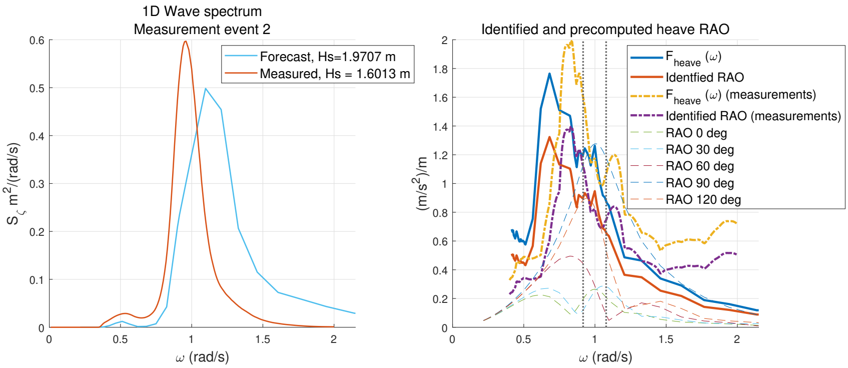

Figure 8.25: 1D wave spectrum and identified (with metocean forecast and metocean measurements) and precomputed heave acceleration RAO for Measurement event 2 - 12/11/2021

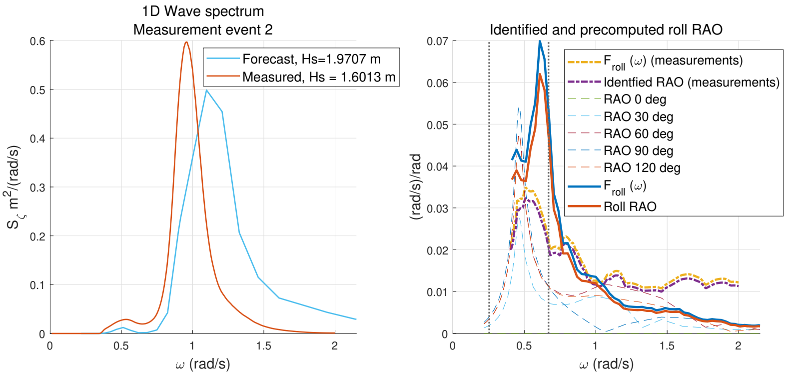

Figure 8.26: 1D wave spectrum and identified (with metocean forecast and metocean measurements) and precomputed roll velocity RAO for Measurement event 2 - 12/11/2021

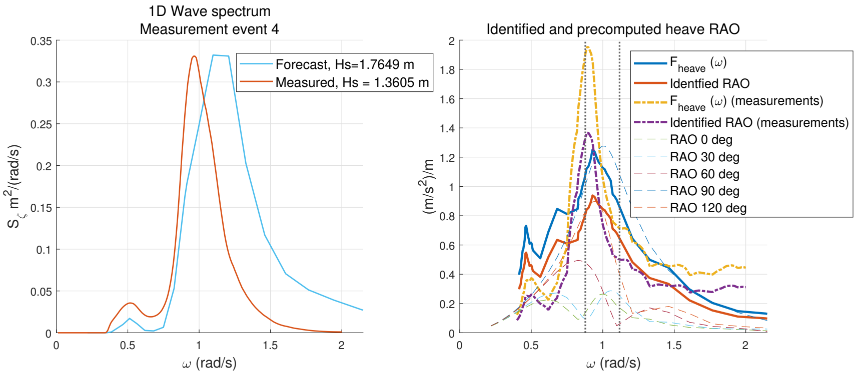

Figure 8.27: 1D wave spectrum and identified (with metocean forecast and metocean measurements) and precomputed heave acceleration RAO for Measurement event 4 - 12/11/2021

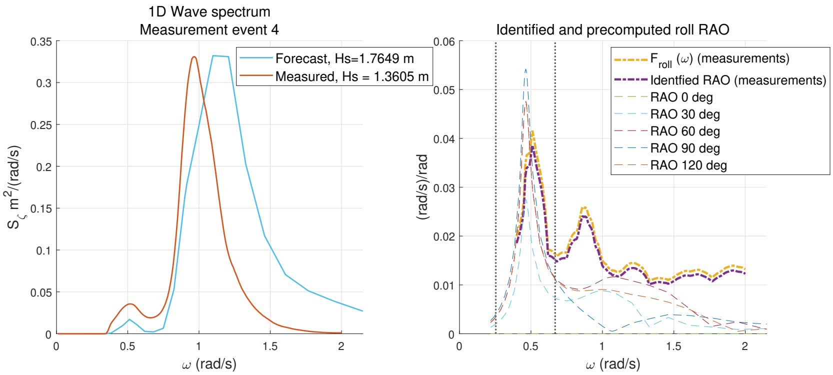

8

Figure 8.28: 1D wave spectrum and identified (with metocean forecast and metocean measurements) and precomputed roll velocity RAO for Measurement event 4 - 12/11/2021

INTERPRETATION RESULTS WITH METOCEAN MEASUREMENTS

The differences in measured metocean conditions compared to the predicted conditions resulted in differences between the identified RAOs. For the analysis with the measured metocean conditions, the peak of the identified RAO shifts to the left and the amplitude is larger compared to the one obtained with the weather forecasts. Besides, at low frequencies, the identified RAO does not shoot to extremely high values. The results of the natural frequencies identification are given in Table 8.15. The second and third column of the table shows the natural frequencies obtained with wave forecast data. The fourth and fifth column gives the identified natural frequencies obtained with measured wave data.

	ω_{n3} (forecast)	ω_{n4} (forecast)	ω_{n3} (measurement)	ω_{n4} (measurement)	Unit
Measurement event 1	0.996	-	0.910	-	$\frac{rad}{s}$
Measurement event 2	-	0.608	-	0.510	$\frac{rad}{s}$
Measurement event 3	0.996	0.478	0.910	0.510	$\frac{rad}{s}$
Measurement event 4	0.967	0.478	0.910	0.510	$\frac{rad}{s}$
Measurement event 5	0.996	0.543	0.910	0.510	$\frac{rad}{s}$
Measurement event 6	1.032	0.446	0.910	0.500	$\frac{rad}{s}$
Mean 1-6	**0.998**	**0.512**	**0.910**	**0.510**	$\frac{rad}{s}$

Table 8.15: Observed heave and roll natural frequency with measured en predicted metocean conditions

The natural frequencies obtained with the metocean measurements are more constant among the all the steady state events compared to the ones obtained with the metocean forecasts. The final identified heave natural frequency obtained with the metocean measurements is 0.910 rad/s, where the final identified heave natural frequency obtained with the metocean forecasts is 0.998 rad/s. Therefore, they differ slightly due to different wave spectra input. On the other hand, the identified roll natural frequencies obtained with the measured and forecast wave spectrum are both around 0.51 rad/s. This could indicate that by taking the mean among multiple events provides a more reliable estimation.

This analysis and especially Figure 8.24 showed that the weather forecasts are subjected to inaccuracies. The results of the parameter identification rely on the accuracy of the weather forecasts and therefore one should be aware of the possible additional uncertainties in the weather forecasts. Still, the identification procedure continues with using weather forecasts as metocean input in further stages of this research. In next section, the results of the optimization algorithm for the measurements of the 12^{th} of November are discussed.

8.5.4. OPTIMIZATION

Evaluating the optimization algorithm has identified the remaining parameters k_{xx}, k_{yy}, k_{zz}, GM_t, GM_l and B_{visc}. The parameters values belonging to the minimum cost function value and thus the final identified parameters are given in Table 8.16. In addition, the initial and final values of the cost function $f(x)$ are depicted Table 8.17.
Initially, the sum of cost function of all DOF was 1.34, this improved to 0.81, which is a total improvement of 39 %. The sway, roll and pitch motion prediction yielded the most improvement with the identified parameters.

RESPONSE SPECTRA

In addition, to visualize the obtained results with the identified parameters, some response spectra are shown of the measured events of 12/11/2021. The measured, initial and identified response spectra for Measurement events 2 and 4 of 12/11/2021 are shown in Figures 8.29 and 8.30. Here, the measured responses are indicated in blue, the

Parameter (**p**)	Symbol	Initial	Identified	Unit
Displacement	∇	6274	6805	tonnes
Radii of gyration for roll	k_{xx}	6.48	6.80	m
Radii of gyration for pitch	k_{yy}	23.35	26.02	m
Radii of gyration for yaw	k_{zz}	23.35	23.60	m
Transverse metacentric height	GM_t	1.20	1.44	m
Longitudinal metacentric height	GM_l	127	118	m
Viscous roll damping	B_{visc}	5.0	7.35	% of crit. damping

Table 8.16: Initial and identified parameters values - 12/11/2021

DOF	$f(x)$ Initial	$f(x)$ After identification
Surge	0.20	0.14
Sway	0.29	0.18
Heave	0.07	0.04
Roll	0.46	0.20
Pitch	0.17	0.09
Yaw	0.15	0.14
Total	1.34	0.81

Table 8.17: Initial and final evaluation of cost function

initial predictions with the initial parameter are indicated in green and the results with the identified parameters are indicated in red.

From the figures, it can be seen that the predicted heave spectrum yielded a lot of improvement with the identified parameters. This indicates that the identified displacement approaches the true value more than the initial value. Besides, the sway and roll motion prediction improved as well. The identified parameters caused more damping to the predicted roll and pitch response spectra, leading to more agreement with the measured response spectra. The peak frequency of the pitch response spectrum agrees more with the measured one, using the identified parameters. However, the predicted pitch spectrum still underestimates the amount of energy, indicating that there was actually more wave energy present than predicted. This finding was also supported by the RAO identification process. Finally, it is observed that the yaw motion yields the least improvement. This was because the peak of the spectrum was at a different frequency than predicted. Modifying the yaw radii of inertia term k_{zz} had no effect on shifting the energy to other frequency sections; it only changed the amount of the predicted energy, which logically follows from the RAO equation as well.

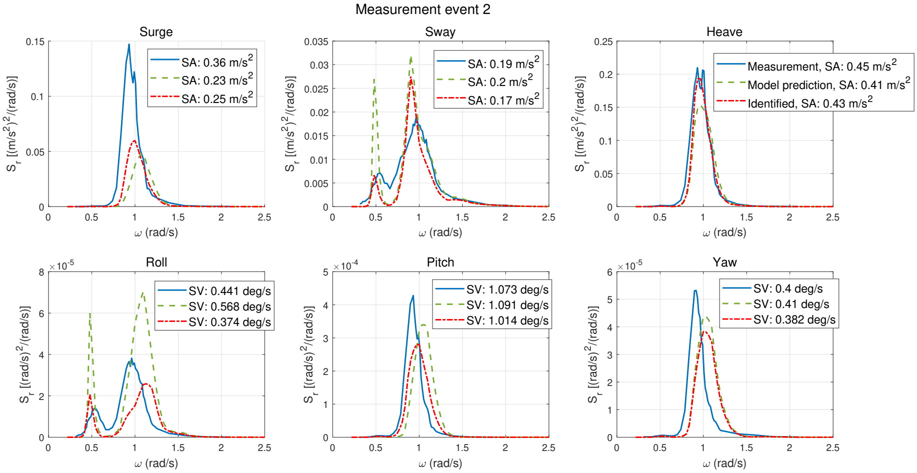

Figure 8.29: Comparison of measured, initial and identified response spectra Measurement event 2 - 12/11/2021

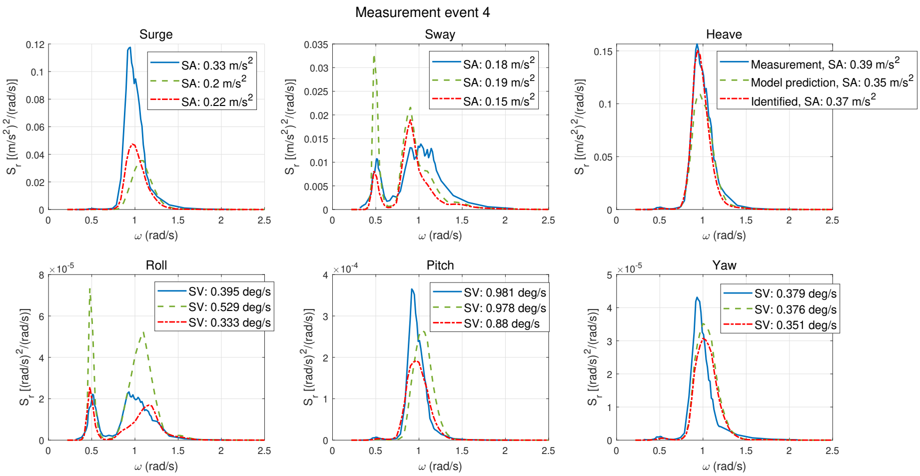

Figure 8.30: Comparison of measured, initial and identified response spectra Measurement event 3 - 12/11/2021

8.6. INTERPRETATION RESULTS

- The resulting identified natural frequencies from both days differ a little. The heave natural frequency identified from the measurements on October 17 and November 12 was 1.01 and 0.998 rad/s, respectively. The roll natural frequency identified from the measurements on October 17 and November 12 was 0.571 and

0.512 rad/s, respectively. The differences are likely due to a different loading condition of the vessel on those days, i.e., the displacement of the vessel was probably higher and differently distributed on November 12.

- The predicted response spectra of the November 12 with the initial parameters already give a better agreement with the measurements than the spectra of October 17. This is probably because the weather report was more accurate on November 12. The identification of the parameters therefore also works better and gives greater improvements and clearer results than the results obtained with the measurements of October 17.

9

Discussion and conclusions

This chapter provides a discussion of the findings and results presented in the report and the conclusions that are derived from them. The results from earlier chapters, as well as their interpretation, have been linked to the initial research objective and assumptions used. This research attempted to work towards the main research objective:

> **Develop a parameter identification strategy to improve vessel motion predictions using nowcast wave spectra and onboard measurement data.**

It was envisioned that a vessel response model, a tool that is useful for decision support of offshore operations, might include an identification module that searches for model parameters using measurements of response. MO4 furnished the required vessel response model for identification.

9.1. Identification procedure

An identification algorithm was developed in Matlab to identify the vessel's RAO with a nowcast wave and response spectrum to find the heave and roll natural frequencies. Furthermore, the procedure includes identification of model parameters by comparing and adjusting prediction results to measured data. An objective function was defined to assess the agreement of the model results with the measured data, by quantifying the output error, i.e., the difference between the measured and predicted response. The model parameters were adjusted to better fit the measurement by minimizing the objective function. A parameter analysis has been conducted to investigate the most influential parameters of the model. The viscous roll damping, stiffness, and mass terms are selected as identification parameters, as they are expected to make a significant contribution to the model's output.

9.2. Case studies

Two case studies were performed to test the identification algorithm and examine the possibilities of parameter identification. Case study 1 was performed with a synthetic data set followed by Case study 2, which was tested with real onboard measurements.

9.2.1. CASE STUDY 1

The optimization procedure was evaluated for two different test cases in Case study 1. The initial parameter values for Test case 1 were highly underestimated where as the initial parameter values of Test case 2 were overestimated, compared to the true parameter values.

The key findings of case study 1 are listed below:

- **RAO and natural frequencies identification**
  The RAO was identified by the measured response, nowcast wave spectrum and a sinusoidal function to describe the directional dependency of the RAO. By using the directional shape function, the identified RAO seems to approach quite well compared to the real RAO's shape. The identified RAOs are quite pragmatic for intended research interest: to observe a maximum around the expected natural frequency. It can be seen that a good agreement between the identified natural frequencies and the real natural frequencies known from the synthetic data set, were found using the identified RAOs. It was demonstrated that the identified roll natural frequency gave consistent results while evaluating multiple wave spectra and vessel headings. The identified heave RAO deviated more among the different sea states and vessel headings.

  Though, the process of evaluating the response at several cases, determining the natural frequency from each of these instances, and then averaging it out throughout all the results yielded the best estimations. This reduces the problem's reliance on a single observation, resulting that the heave natural frequency will be less susceptible to error. As a consequence, the results illustrate the importance of a rich data set. Therefore, it is recommended to assess a large amount of response data in order to derive a valid natural frequency.

- **Displacement identification**
  As the displacement affects the response in each of the six degrees of freedom, it is an important parameter to identify. If the natural heave frequency is not correctly detected, an inaccurate displacement value will be calculated, which will affect the accuracy of identifying the other parameters as well. Though, the identification of the displacement using the natural frequency showed good results for case study 1. The identified displacement parameter approached the true displacement, still some deviation remained. This was because the natural heave frequency differed slightly from the actual frequency. This immediately demonstrates how sensitive the displacement is to an incorrect natural frequency estimation.

- **Identification of mass distribution and damping parameters**
  The identification algorithm successfully identified the parameters k_{xx}, k_{yy}, k_{zz}, GM_t GM_l and B_{visc}, with good agreement to their true values, known from the synthetic data set. The optimization algorithm achieved to minimize the cost function $f(x)$ for each degree of freedom, shown in Table 7.12. Tolerance criteria were set to terminate the algorithm when function improvements or parameter changes were beneath the lower bound. Therefore, the identified parameters for

9

test cases 1 and 2 may differ slightly. With the identified roll natural frequency, the relation between k_{xx} and GM_t was maintained.

Final conclusions Case study 1
Overall, using multiple wave spectra and vessel headings in the identification process led to good results, with the identified parameters approaching to the true values. Therefore, the strategy was applied in to real onboard measurement data, the results of which are discussed in the following section.

9.2.2. CASE STUDY 2

The key findings of case study 2 are listed below:

- **RAO and natural frequencies identification**

  Similar to the RAO and natural frequencies identification of case study 1, maxima in the identified RAO could be found and related to the natural frequency. The identified heave natural frequency was slightly lower than the initial predicted peak period, resulting in modifying the displacement to a higher value.

  At cases where there was little or no wave energy in the zone where actually vessel response energy was measured, it was difficult to derive any information about the RAO in that frequency range. This was because the identified RAO shoot up to extremely high values, which were unrealistic and not useful. Therefore, it is recommended that for cases that do no have wave energy in the zone where actually vessel response energy was measured should be neglected.

- **Identification of mass distribution and damping parameters**
  The identification algorithm was able in determining the parameters values for k_{xx}, k_{yy}, k_{zz}, GM_t GM_l and B_{visc}. The sway, roll, pitch and yaw motion prediction spectra yielded the most improvements with the identified parameters. For the surge and heave, the identified parameters did not cause much change to the predicted response spectra.

  Since the algorithm of each DOF can run simultaneously, the total amount of running time is the time of the longest run. The computation times of the algorithm were given in Table 8.9. It showed that the parameters related to the roll and pitch motion needed the most computation time. Though, the identification is computationally inexpensive since it takes approximately 30 minutes to run and obtain the parameters from the data.

- **Weather uncertainty**
  The study showed that the predicted responses, besides the discussed input parameters, are sensitive to the choice of the wave energy spectrum. In Case study 1, the synthetic measurements and predictions used the same wave input. Therefore, all uncertainty associated with any inconsistency between the measured response spectrum and the corresponding predicted response spectrum could be ascribed to the input parameters of the RAO. From Case study 1, it was shown that

all the correct parameters could be identified and the final predicted responses matched the "measured" responses.

However, in the analysis of Case study 2, weather forecast uncertainties were present. As discussed earlier, part of the underestimated responses could be attributed to an inaccurate weather forecast. For example, if more wave energy was present than initially forecasted by the weather data providers. Therefore, an additional analysis was executed to identify the RAO with measurements of metocean conditions in Section 8.5.3. It was found that the measured wave spectrum differed to the forecasted wave spectrum in terms of peak period and amount of wave energy. This also resulted in differences in the identified RAO and a shift of the peak period, which was link to the natural frequency. The hypothesis that there was actually more wave energy present at the lower frequencies than initially predicted was shown to be correct. If metocean measurements are available it could be to use those instead of forecasts since those give a more accurate representation of the metocean conditions.

- **Identified parameters**
  Given that the true parameters of the vessel during the measured events were unknown, the final computation of the cost function was the only indicator of the identification procedure's performance. This is in contrast to the results of Case Study 1, in which the identified parameters could be directly compared with the actual parameters, which were known from the synthetic data set.

  The parameters have been determined for two distinct days on a number of free-floating events. The parameters found on October 17 differ slightly from those identified on November 12. On both days, the identified displacement exceeded the initial estimate. The identified metacentric heights for both days are comparable. The identified radii of inertia terms on both days varied slightly. This is not unreasonable, since the parameters are operationally dependent. The displacement and weight distribution can vary day by day. Though, it was found that the parameters have a great influence on the output of the vessel response model. Therefore, it is essential to have a thorough understanding of the correct operational parameters for accurate motion prediction.

- **Verification**
  The identified parameters obtained by measurements of October 17 were verified with a verification measured data set of October 16. The vessel response spectra of the verification events were calculated with the identified parameters. A day close to the identifying days was selected to verify the parameters, making it more likely that the operational parameters may remained constant than on an entirely different day of the year. The results show that the identified response spectra approach the measured responses, though some discrepancies remained. Nevertheless, this indicates that the identified parameters are not only valid for the response spectra on which the parameters are fitted, but also for additional data.

- **Model**
  For every model applies the fact that the quality of the output of the model is directly proportional to the quality of the model and input. Besides weather input uncertainty, the remaining discrepancies between measured and response spectrum may be due to model error as well.

- **Final conclusions Case study 2**
  From Case study 2, it was shown that the parameter identification yielded in an improvement, but still some discrepancies remained. Especially when observing the surge spectrum, the predictions underestimated the responses.

9.3. CONDENSED CONCLUSIONS

It is investigated whether combining measured data could result in an improvement in a vessel motion prediction. The research presented in this report shows that the proposed identification framework could serve as additional support to existing vessel motion models. The framework has been tested for a variety of sea states and initial input parameters. This has provided consistent results in terms of convergence and stability, reusable identification parameters and acceptable simulation times. This makes the strategy robust, since it is not limited to any sea states and requires the same computing resources as the existing vessel response model.

The procedure showed to be a versatile solution to identifying the model's parameters and improving the model's output, when uncertainties in wave spectra could be neglected. The application of the identification procedure to real measurements, in which wave spectra uncertainties are included, the resulting parameters improved the model's output by 18 % for the first assessment day and 43 % for the second assessment day but still deviations remained. Therefore, further research for improvement is necessary and discussed in next section.

9.4. RECOMMENDATIONS FOR FURTHER RESEARCH

The developed strategy has shown acceptable results within the intended range of use, although improvement could be achieved while there are still some procedures and tests that have not been carried out. Therefore, additional research has the potential to improve insights, and the most important recommendations are outlined in the following section:

- Wave measurements
  The whole identification strategy should be tested with wave elevation measurements instead of forecasts. Access to both vessel motion measurements and wave amplitude measurements may provide more accurate data regarding the phasing between waves and vessel motion. Since weather forecasts are typically easier to access than real-time wave elevation measurements, it is practical to implement an identification strategy using wave spectra from forecasts. This project was therefore conducted in the frequency domain using predicted wave spectra. Since the time available was limited, only part of the strategy was analysed with

measurements of metocean conditions. This analysis immediately showed that the weather forecasts are subjected to inaccuracies. Therefore, the performance of the whole method with wave measurements should be investigated to validate the strategy and compare the results with those obtained from predicted wave spectra. This could indicate a portion of a strategy error or weather forecast error.

- RAO identification - directional shape
  The RAO has been identified using a directional dependent function described by a simple sinusoidal function. For each frequency, the same function was used. It could be investigated whether a parametric function could describe the directional forms and can be optimized for each frequency. Thereby, this may provide a more precise representation of the directional function than the present sinusoidal method.

- More understanding in parameter change
  Obtain a deeper understanding of the vessel's operating parameters and investigate how often the operating parameters change. This knowledge could be acquired by conducting interviews with seamen. With this information, it may be specified how many times and with how much data the strategy has to run to estimate the operating parameters.

- Anti-roll tank
  The Acta Auriga has an anti-roll tank to control and reduce excessive roll motions. The influence of the anti-roll tank on the roll motion has not been incorporated yet in the vessel response model. Though this has an influence on the results obtained from case study 2, in which real onboard measurements where used. Therefore, modeling of the anti-roll tank should be included in the model and the identification procedure should be retested on real onboard measurements to investigate the performance including the anti-roll tank.

- Validation
  To enhance validation, additional data should be included in future research. Within Case study 1, a wide range of sea conditions was considered. However, for Case study 2, in which real measurements were used, a greater number of samples should be considered for validation purposes.

- Include more vessels
  The identification procedure should be straightforward to implement to any vessel. However, the performance of the identification procedure has only been evaluated on the Acta Auriga in this research. Therefore, it has to be investigated if it is also applicable to other vessels as well.

Bibliography

[1] V. Aanesland, K. Kaasen, and J. Krokstad. “Wave-drift damping of a turret moored ship”. In: *Intl Conf on the Behaviour of Offshore Structures* (1992).

[2] B. Barrass. *Ship stability: notes and examples*. Elsevier, 2000.

[3] A. Biran and R. López-Pulido. *Ship hydrostatics and stability*. Butterworth-Heinemann, 2013.

[4] E. M. Bitner-Gregersen, K. C. Ewans, and M. C. Johnson. “Some uncertainties associated with wind and wave description and their importance for engineering applications”. In: *Ocean Engineering* 86 (2014), pp. 11–25.

[5] S.-P. Breton and G. Moe. “Status, plans and technologies for offshore wind turbines in Europe and North America”. In: *Renewable energy* 34.3 (2009), pp. 646–654.

[6] D. Christie and S. P. Neill. “8.09 - Measuring and Observing the Ocean Renewable Energy Resource”. In: *Comprehensive Renewable Energy (Second Edition)*. Ed. by T. M. Letcher. Second Edition. Oxford: Elsevier, 2022, pp. 149–175. ISBN: 978-0-12-819734-9. DOI: https://doi.org/10.1016/B978-0-12-819727-1.00083-2. URL: https://www.sciencedirect.com/science/article/pii/B9780128197271000832.

[7] S. S. C. Cuadros. *FFT*. [Online; accessed Feb 28, 2022]. 2022. URL: https://www.mathworks.com/matlabcentral/fileexchange/96169-fft.

[8] Y. Dai, L. Liu, and S. Feng. “On the identification of coupled pitch and heave motions using opposition-based particle swarm optimization”. In: *Mathematical Problems in Engineering* 2014 (2014).

[9] R. van Dijk, V. Quiniou-Ramus, and G. Le-Marechal. “Comparison of full-scale measurements with calculated motion characteristics of a West of Africa FPSO”. In: *International Conference on Offshore Mechanics and Arctic Engineering*. Vol. 36819. 2003, pp. 335–339.

[10] G. DNV. “DNV-OS-H101: Marine Operations”. In: *General, Offshore Standard* (2011).

[11] G. DNV. *Marine operations and marine warranty*. Tech. rep. DNVGL-ST, 2016.

[12] M. Drago, A. Del Guzzo, L. Vitali, and R. Bruschi. “Weather Stand-by Assessment in Offshore Operations Using Motion Limit Criteria”. In: *The 27th International Ocean and Polar Engineering Conference*. OnePetro. 2017.

[13] O. Faltinsen. *Sea loads on ships and offshore structures*. Vol. 1. Cambridge university press, 1993.

[14] *fminsearch Algorithm*. [Online; accessed Jul 14, 2022]. 2022. URL: https://nl.mathworks.com/help/optim/ug/fminsearch-algorithm.htmlh.

[15] B. G.A, O. Filatova, C. Mercuri, A. Muntean, M. Peletier, V. Shchetnikava, E. Siero, and I. Zisis. "Identification of a response amplitude operator for ships". In: Jan. 2013.

[16] M. Gasior and J. Gonzalez. *Improving FFT frequency measurement resolution by parabolic and Gaussian spectrum interpolation.* Vol. 732. 1. 2004, pp. 276–285.

[17] A. H. Gjeraker. "Response Amplitude Operator Estimation and Wave Modeling Sensitivity". MA thesis. NTNU, 2021.

[18] M. Grimm, W. Smith, and D. Fortescue. "The influence of roll radius of gyration including the effect of inertia of fluids on motion predictions". In: *RINA, R. Inst. Nav. Archit.-PACIFIC* (2017).

[19] C. Gundegjerde, I. B. Halvorsen, E. E. Halvorsen-Weare, L. M. Hvattum, and L. M. Nonås. "A stochastic fleet size and mix model for maintenance operations at offshore wind farms". In: *Transportation Research Part C: Emerging Technologies* 52 (2015), pp. 74–92.

[20] X. Han, B. J. Leira, and S. Sævik. "Vessel hydrodynamic model tuning by discrete Bayesian updating using simulated onboard sensor data". In: *Ocean Engineering* 220 (2021), p. 108407.

[21] X. Han, B. J. Leira, S. Sævik, and Z. Ren. "Onboard tuning of vessel seakeeping model parameters and sea state characteristics". In: *Marine Structures* 78 (2021), p. 102998.

[22] X. Han, S. Sævik, and B. J. Leira. "A sensitivity study of vessel hydrodynamic model parameters". In: *International Conference on Offshore Mechanics and Arctic Engineering.* Vol. 84317. American Society of Mechanical Engineers. 2020, V001T01A039.

[23] X. Han, S. Sævik, and B. J. Leira. "Tuning of vessel parameters including sea state dependent roll damping". In: *Ocean Engineering* 233 (2021), p. 109084.

[24] T. K. Hareide. *Acta Auriga Final stability booklet.* Feb. 2018.

[25] H. H. Hooyer. *Behavior and handling of ships.* Cornell Maritime Press/Tidewater Publishers, 1983.

[26] Y. Ikeda. "Wave Loads and Propulsive Performance in a Seaway, 1st Marine Dynamics Symposium, The Society of Naval Architecture in Japan". In: *Proceedings of the Ship Motions.* 1984, pp. 241–250.

[27] J. J. Jensen. *Load and global response of ships.* Elsevier, 2001.

[28] D. Jonas, M. Lämmle, D. Theis, S. Schneider, and G. Frey. "Performance modeling of PVT collectors: Implementation, validation and parameter identification approach using TRNSYS". In: *Solar Energy* 193 (2019), pp. 51–64.

[29] J. Journee and W. Massie. "Offshore Hydromechanics. Firs Edition". In: *Delft University of Technology* (2001).

[30] K. E. Kaasen, K. Berget, H. Lie, and R. Bjørkli. "Automatic tuning of vessel models offshore: A feasibility study using high-precision data from model test". In: *Offshore Technology Conference.* OnePetro. 2020.

[31] P. Kaplan. *Lecture notes on nonlinear theory of ship roll motion in a random seaway.* Tech. rep. Webb institute of Naval Architecture Glen Cove NY, 1966.

[32] A. Kirsch et al. *An introduction to the mathematical theory of inverse problems.* Vol. 120. Springer, 2011.

[33] M. Lankarany and A. Rezazade. "Parameter estimation optimization based on genetic algorithm applied to DC motor". In: *2007 International Conference on Electrical Engineering*. IEEE. 2007, pp. 1–6.

[34] H. Le. *smooth.* [Online; accessed Feb 28, 2022]. 2022. URL: https://www.mathworks.com/matlabcentral/fileexchange/274-smooth.

[35] C. Le Cunff, S. Ryu, J.-M. Heurtier, and A. S. Duggal. "Frequency-domain calculations of moored vessel motion including low frequency effect". In: *International Conference on Offshore Mechanics and Arctic Engineering*. Vol. 48180. 2008, pp. 689–696.

[36] L. Þ. Leifsson, H. Sævarsdóttir, S. Þ. Sigurðsson, and A. Vésteinsson. "Grey-box modeling of an ocean vessel for operational optimization". In: *Simulation Modelling Practice and Theory* 16.8 (2008), pp. 923–932.

[37] J. Linder. "Graybox Modelling of Ships Using Indirect Input Measurements". PhD thesis. Linköping University Electronic Press, 2014.

[38] P. A. Lynn. *Onshore and offshore wind energy: an introduction.* John Wiley & Sons, 2011.

[39] A. Marine. *Acta Auriga.* [Online; accessed May 11, 2022]. URL: https://www.actamarine.com/afbeeldingen/_resized/header_auriga_2_w1260_h430_bg.jpg.

[40] Mocean Forecast BV. *MO4 THEORETICAL MANUAL.* Tech. rep. 01. Sept. 2020.

[41] D. J. Murray-Smith. "Methods of system identification, parameter estimation and optimisation applied to problems of modelling and control in engineering and physiology". PhD thesis. University of Glasgow, 2009.

[42] G. C. Ole, J. Aarnes, M. Reistad, Ø. Breivik, A. K. Magnusson, and B. Furevik. "Validation 2D wave spectra-ECMWF". In: (2019). ISSN: 2387-4201.

[43] R. Pascoal, C. Guedes Soares, and A. Sorensen. "Ocean wave spectral estimation using vessel wave frequency motions". In: *International Conference on Offshore Mechanics and Arctic Engineering*. Vol. 41960. 2005, pp. 337–345.

[44] T. Perez and T. I. Fossen. "Practical aspects of frequency-domain identification of dynamic models of marine structures from hydrodynamic data". In: *Ocean Engineering* 38.2-3 (2011), pp. 426–435.

[45] T. Pérez and T. Fossen. "Time-vs. frequency-domain identification of parametric radiation force models for marine structures at zero speed". In: *Modeling, Identification and Control* 29.1 (2008), pp. 1–19.

[46] W. Qiu, J. S. Junior, D. Lee, H. Lie, V. Magarovskii, T. Mikami, J.-M. Rousset, S. Sphaier, L. Tao, and X. Wang. "Uncertainties related to predictions of loads and responses for ocean and offshore structures". In: *Ocean Engineering* 86 (2014), pp. 58–67.

[47] Z. Ren, X. Han, A. S. Verma, J. A. Dirdal, and R. Skjetne. "Sea state estimation based on vessel motion responses: Improved smoothness and robustness using Bézier surface and L1 optimization". In: *Marine Structures* 76 (2021), p. 102904.

[48] R. P. Selvam and S. Bhattacharyya. "System identification of a coupled two DOF moored floating body in random ocean waves". In: (2006).

[49] D. Sen and T. Vinh. "Determination of added mass and inertia moment of marine ships moving in 6 degrees of freedom". In: *International Journal of Transportation Engineering and Technology* 2.1 (2016), pp. 8–14.

[50] S. Singer and J. Nelder. "Nelder-mead algorithm". In: *Scholarpedia* 4.7 (2009), p. 2928.

[51] D. Skandali, E. Lourens, and R. Ogink. "Calibration of response amplitude operators based on measurements of vessel motions and directional wave spectra". In: *Marine Structures* 72 (2020), p. 102774.

[52] J. Taylor. *Introduction to error analysis, the study of uncertainties in physical measurements*. 1997.

[53] E. C. Tupper. *Introduction to naval architecture*. Butterworth-Heinemann, 2013.

[54] M. Vettestad. "Response Amplitude Operator Estimation and Prediction of Heave Motions". In: 2020 (2020).

[55] M. Wu and Z. Gao. "Methodology for developing a response-based correction factor (alpha-factor) for allowable sea state assessment of marine operations considering weather forecast uncertainty". In: *Marine Structures* 79 (Sept. 2021). ISSN: 09518339. DOI: 10.1016/j.marstruc.2021.103050.

List of Appendices

APPENDIX A: FMINSEARCH ALGORITHM

The working principle of the fminsearch algorithm is presented in this appendix and obtained from MathWorks [14]. fminsearch uses the Nelder-Mead simplex algorithm. This algorithm uses a simplex of $n+1$ points for n-dimensional vectors x. The algorithm first makes a simplex around the initial starting point, called x_0, by adding 5% of each component $x_0(i)$ to x_0, and using these n vectors as elements of the simplex in addition to x_0. Then, the algorithm modifies the simplex repeatedly according to the following procedure.

1. Let $x(i)$ denote the list of points in the current simplex, i = 1,...,n + 1.
2. Order the points in the simplex from lowest function value $f(x(1))$ to highest $f(x(n+1))$. At each step in the iteration, the algorithm discards the current worst point $x(n+1)$, and accepts another point into the simplex. Or, in the case of step 7 below, it changes all n points with values above $f(x(1))$.
3. Generate the reflected point
$$r = 2m - x(n+1), \tag{1}$$
where
$$m = \frac{\sum x(i)}{n}, \qquad i = 1 \ldots n, \tag{2}$$
and calculate $f(r)$.
4. If $f(x(1)) f(r) < f(x(n))$, accept r and terminate this iteration. **Reflect**
5. If f(r) < f(x(1)), calculate the expansion point s
$$s = m + 2(m - x(n+1)), \tag{3}$$
and calculate $f(s)$.
   (a) If $f(s) < f(r)$, accept s and terminate the iteration. **Expand**
   (b) Otherwise, accept r and terminate the iteration. **Reflect**
6. If $f(r) f(x(n))$, perform a contraction between m and either $x(n+1)$ or r, depending on which has the lower objective function value.
   (a) If $f(r) < f(x(n+1))$ (that is, r is better than $x(n+1)$), calculate
$$c = m + \frac{r - m}{2} \tag{4}$$
   and calculate $f(c)$. If $f(c) < f(r)$, accept c and terminate the iteration. **Contract outside**
   Otherwise, continue with Step 7 (Shrink).

(b) If $f(r) f(x(n+1))$, calculate

$$cc = m + (x(n+1) - m)/2 \tag{5}$$

and calculate $f(cc)$. If $f(cc) < f(x(n+1))$, accept cc and terminate the iteration. **Contract inside**

Otherwise, continue with Step 7 (Shrink).

7. Calculate the n points

$$v(i) = x(1) + (x(i) - x(1))/2 \tag{6}$$

and calculate $f(v(i))$, $i = 2, \ldots, n+1$. The simplex at the next iteration is $x(1)$, $v(2), \ldots, v(n+1)$. **Shrink**

The iterations proceed until they meet a stopping criterion.

Appendix B: Global minimum check

The parameters which are identified by the algorithm were the radii of inertia terms, the metacentric heights and the viscous roll damping. It is important to ensure that the algorithm find the global minimum of the cost function, independent of the initial starting value of the parameters. Therefore, the optimization algorithm is executed for several initial starting points. The results of each fminsearch run are also shown in Tables 1, 2, 3, 4, 5, 6. The true value, starting value and identified value of the parameters as wel as the final value of the cost function, are given in the tables. The parameters were identified with synthetic created data, generated with different sea states as an input mentioned in 8.2.1.

It was found that the algorithm converged to the same global minimum, independent of the initial starting values. This suggest that the optimization problem is convex.

- k_{xx}

True value	Starting value	Identified value	Final $f(x)$
6.48 m	3.50 m	6.49 m	0.004
6.48 m	5.80 m	6.48 m	0.002
6.48 m	7.50 m	6.48 m	0.002
6.48 m	8.80 m	6.48 m	0.001
6.48 m	10.0 m	6.49 m	0.003

Table 1: Evaluation of optimization algorithm for several starting values of k_{xx}

- k_{yy}

True value	Starting value	Identified value	Final $f(x)$
23.35 m	22.50 m	23.34 m	0.004
23.35 m	23.00 m	23.35 m	0.002
23.35 m	23.50 m	23.36 m	0.001
23.35 m	24.00 m	23.35 m	0.001
23.35 m	24.50 m	23.34 m	0.003

Table 2: Evaluation of optimization algorithm for several starting values of k_{yy}

- k_{zz}

True value	Starting value	Identified value	Final $f(x)$
23.35 m	22.50 m	23.34 m	0.002
23.35 m	23.00 m	23.34 m	0.002
23.35 m	23.50 m	23.35 m	0
23.35 m	24.0 m	23.35 m	0
23.35 m	24.50 m	23.34 m	0.002

Table 3: Evaluation of optimization algorithm for several starting values of k_{zz}

- GM_t

True value	Starting value	Identified value	Final $f(x)$
1.20 m	0.50 m	1.20 m	0.004
1.20 m	1.00 m	1.20 m	0.002
1.20 m	1.50 m	1.20 m	0.002
1.20 m	2.00 m	1.20 m	0.001
1.20 m	2.50 m	1.20 m	0.003

Table 4: Evaluation of optimization algorithm for several starting values of GM_t

- GM_l

True value	Starting value	Identified value	Final $f(x)$
127 m	126.0 m	126.9 m	0.004
127 m	126.5 m	126.9 m	0.002
127 m	127.0 m	126.9 m	0.002
127 m	127.5 m	126.9 m	0.001
127 m	128.0 m	126.9 m	0.003

Table 5: Evaluation of optimization algorithm for several starting values of GM_l

- B_{visc}

True value	Starting value	Identified value	Final $f(x)$
5 %	3 %	5.1 %	0.004
5 %	4 %	5.0 %	0.002
5 %	5 %	5.1 %	0.002
5 %	6 %	5.0 %	0.001
5 %	7 %	5.0 %	0.003

Table 6: Evaluation of optimization algorithm for several starting values of B_{visc} (where B_{visc} is a percentage % of the critical damping